APPLICATION OF AGISOFT PHOTOSCAN AND SEDIMENT TRANSPORT MODELING FOR THE ANALYSIS OF SEDIMENT WAVE PROPAGATION SUCCEEDING GRAVEL AUGMENTATION, OAK GROVE FORK OF THE CLACKAMAS RIVER, OREGON

By

Mindi Lea Curran

A Thesis Presented to

The Faculty of Humboldt State University

In Partial Fulfillment of the Requirements for the Degree

Master of Science in Environmental Systems: Geology

Committee Membership

Dr. Melanie Michalak, Committee Chair

PG. Geoff Hales, Committee Member

Dr. Jasper Oshun, Committee Member

Dr. Thomas Lisle, Committee Member

Dr. Margaret Lang, Program Graduate Coordinator

December 2017

ABSTRACT

APPLICATION OF AGISOFT PHOTOSCAN AND SEDIMENT TRANSPORT MODELING FOR THE ANALYSIS OF SEDIMENT WAVE PROPAGATION SUCCEEDING GRAVEL AUGMENTATION, OAK GROVE FORK OF THE CLACKAMAS RIVER, OREGON

Mindi Lea Curran

Physical features in alluvial rivers such as riffles, gravel bars, pools, and side channels provide refugia, nutrients, and spawning and rearing habitat for anadromous fish and other aquatic organisms. The downstream transport of gravels that continuously replenish these features is prevented by dams, and often leads to a coarsened channel bed condition and other geomorphic changes that have negative impacts on aquatic organisms. Geomorphic change in rivers can be challenging to capture in high resolution, making the propagation and distribution of sediment difficult to quantify, especially if the deposition occurs in small quantities or thin layers. One solution for replenishing physical features that have been cut off from gravel supply downstream of dams is gravel augmentation. This thesis uses two independent methods to investigate the transport and storage of augmented gravels as they route downstream: 1) topographic change detection using photogrammetry and differencing of Digital Terrain Models (DTMs), and 2) a 1D sediment transport model created in HEC-RAS (Hydrologic Engineering Centers River Analysis System) to model flow and sediment scenarios. Together, these methods are used to investigate sediment wave propagation and channel response to augmented

gravels. The location of study is the Oak Grove Fork (OGF), one of the largest tributaries of the Clackamas River, located in northwestern Oregon. The Lake Harriet Dam and diversion were built on the OGF in 1924 as part of a hydroelectric development project by Portland General Electric. Decreased flow and sediment supply downstream of Lake Harriet Dam has resulted in geomorphic and biological changes (including reduced salmonid habitat), leading to a mandated gravel augmentation program that began in September of 2016, which introduced 250 tons of gravel into the river. High resolution DTMs, generated using photogrammetry, captured topographic change at sites on the order of tenths of feet, with vertical accuracy also on the order of tenths of feet. All change detected at photogrammetry sites within one year of augmentation was determined to be a record of typical, natural year-to-year change and is not attributed to transport and deposition of augmented gravels. The 1D sediment transport model suggests that peak flows, exceeding 1,200 cfs, are the primary driving factors of sediment transport, and that higher peak flows exceeding those seen in 2016 and 2017 will be required to transport the augmented gravels downstream 0.81 miles, past a naturally occurring fish barrier waterfall to where anadromous fish habitat begins. A storage capacity estimate calculation suggests that up to 600 tons of gravel could fill interstitial spaces between existing boulders and cobbles as gravel routes downstream, past Barrier Falls, and into accessible habitat.

ACKNOWLEDGEMENTS

I thank the thesis committee: Geoff Hales, Melanie Michalak, Tom Lisle and Jasper Oshun, for their contributions to this thesis and overall advising and editing effort. I specifically thank Geoff and Melanie, the primary advisors of this thesis, who contributed greatly to the overall merit of this work, as well as field data collection efforts, field training, and technical writing assistance. I also thank Geoff and Melanie for contributing to presentations for both the American Geophysical Union and the Salmonid Restoration Federation.

I thank Portland General Electric for showing enthusiasm for this work and allowing me to complete a thesis as part of one of their larger projects. I also thank them for providing field housing and funding.

I thank Scott and Rebecca McBain for creating a graduate student position and for the training, equipment, and transportation they provided. I thank Fred Meyer, Brian Powell, and Ben Snyder for their technical support with AutoCAD and HEC-RAS.

I thank the HSU Geology Department for providing Agisoft Photoscan, the ESRI software suite, and Adobe Illustrator, and for providing the materials needed to present at the afore mentioned conferences. I thank Steve Tillinghast and Laurie Marx for their technical support.

I thank Don Ashton for his help and support in data collection during the field efforts on the OGF. I also thank Hector Flores, Jasper Oshun, and Andre Lehre for their help collecting data for the Redwood Creek Trial Runs.

TABLE OF CONTENTS

LIST OF TABLES

LIST OF FIGURES

LIST OF APPENDICES

INTRODUCTION

Restoration Downstream of Dams

Impact of Dams on Downstream Physical Processes

Water is an essential component for successful and diverse ecosystems on Earth. Throughout the 20th century, accelerated population growth and an increasingly modernized lifestyle required humans to access water for construction of communities, irrigation, reservoir development, and hydroelectricity; this has led to the construction of 75,000 dams nationwide (e. g., Graf, 1999). It wasn't until the latter part of the 20th century that changes to downstream physical and biological processes caused by dams would be acknowledged as major environmental impacts (Ligon et al., 1995; Pess et al., 2008; Duda et al., 2008). Since then, dam operators, government agencies, Native American tribes, and consumers have been working toward finding a balance between preserving and restoring river resources while continuing to consume the natural resources and additional ecosystem services that they provide (Graf, 1999). Restoring river resources requires an understanding of river processes in the pre-dam condition and how the post-dam condition has altered those processes (e.g., Beechie et al., 2010). Therefore, restoration plans that rely on the natural processes of a river require an understanding of the physical and biological changes created by a dam.

Dams can significantly impair three major processes in a river system: (1) they can drastically change the hydraulic and sediment regimes downstream, (2) they increase

water temperatures and affect water quality, and (3) they prevent the upstream and downstream migration of aquatic organisms (Poff, 2002). Stream flow, sediment dynamics, and slope are the primary drivers for the physical characteristics of an alluvial river, including channel geometry (cross section form), sorting of the bed framework, the formation of bedforms such as riffles and pools, and the general channel morphology (Magilligan & Nislow, 2005). Channel morphology and the flow regime influence the success of aquatic lifeforms, which evolve to thrive on specific conditions, and suffer if only small changes occur (Ward & Stanford 1995; McCormick et al., 2009; McCluney et al., 2014).

Dams can also significantly change downstream hydraulic regimes by controlling the timing, magnitude, frequency, and duration of flows (Magilligan & Nislow, 2005). The magnitude and duration of flows are important drivers of geomorphic work: transporting sediment, lateral and vertical channel migration, and the building of side channels and flood plains. The magnitude of flows is also important for reaching sediment mobility thresholds resulting in incipient particle motion. The timing and frequency of high flows maintain water quality and aquatic species temperature thresholds by recycling and flushing nutrients and ensuring that stream temperatures remain within aquatic organisms survival thresholds. High flows also maintain a healthy riparian vegetation corridor; too few high flows can result in vegetation encroachment and channel area loss, but high flows released prematurely can result in drowning of new seedlings (Magilligan & Nislow, 2005). For these reasons, the careful management of

released flows downstream of dams is a crucial component for successful restoration plans.

Sediment transport is important for both physical and biological processes and is integrally linked to hydraulic regime. Particle entrainment and bedload transport require a shear stress capable of mobilizing the particles on the bed, and decreasing the magnitude and duration of high flows limits the shear stress acting on the bed, therefore limiting the size of particles and volumes streams are capable of transporting (Leopold et al., 1964). Shear stress is the relationship of driving forces (hydraulic forces) versus resisting forces (forces on the channel bed) that are acting on the channel bed (Yager et al., 2007a; Parker et al., 2011; Petit et al., 2015). Calculating critical shear stress values to determine incipient motion of a particular grain size is often used to estimate the magnitude of flows needed to mobilize varying populations of grain sizes and how varying populations of grain sizes interact (Yager et al., 2007b; Yager et al., 2012). This is useful for determining if flows released downstream of dams will be sufficient for maintaining sediment transport and physical features.

Dams commonly reduce stream flow to downstream reaches, resulting in reduced stream power, a coarsened bed surface, or a bed completely scoured of sediment altogether. Dams also trap the bedload delivered from upstream, reducing and eliminating finer material that would offset bed coarsening (Ligon et al., 1995; Kondolf et al., 2014a). A highly armored bed is typically less biologically productive because large grain sizes are unusable by fish and more difficult for vegetation to colonize. A bed devoid of sediment (bedrock) is also unsuitable for anadromous fish spawning.

Current Restoration Practices Downstream of Dams

For the past seventy or more years, damming rivers for the production of hydroelectricity has been an important, yet ecologically controversial topic. The necessity to store water and generate electricity has historically been prioritized over preservation of downstream physical processes and habitat (Hart et al. 2002; Duda et al., 2008). However, a recent shift in thinking amongst researchers and restoration-based consulting firms has brought about "process-based restoration," or restoration efforts governed around restoring the natural physical processes, setting the stage for biological and ecological processes to restore themselves (Beechie et al., 2010). A primary focus of process-based restoration is to provide flows that mimic the natural hydrograph and sediment inputs that meet the transport capabilities of the river, so the river can maintain its physical features such as side channels, floodplains, alcoves, and bedforms. Aquatic organisms and riparian vegetation are reliant on the habitat provided by these physical features. When the physical processes are well maintained, the ecological processes thrive.

Efforts to restore physical processes downstream of dams vary in scale depending on the size, lifetime, and degree of changes caused by the dam. The idea of dam removal is popular, yet often infeasible both economically and politically (Hart et al., 2002). The removal of dams causes intense short-term disruption to downstream habitats, but may eventually restore all pre-dam functioning of the stream both physically and biologically. Problems associated with dam removal include cost of removal, flooding to downstream communities, water quality and contamination issues, and the release of large volumes of

accumulated sediments (Hart et al. 2002; Duda et al., 2008). Although short-term, these factors can have a large impact on the river network, often resulting in many changes to channel form as the river rebalances changes to flow and sediment regimes.

Other and more routinely used options for restoring physical processes downstream of dams include releasing flows downstream that mimic the natural flow regime, introducing sediment downstream (gravel augmentation), and reconnecting side channels and floodplains. Implementing these options commonly improves habitat by providing cold water for aquatic organisms, gravels for fish and benthic macroinvertebrates, and diversifying habitat area for both aquatic and terrestrial species. Restoration efforts specifically aimed at improving biological processes include improving structures to allow aquatic organisms to migrate upstream and downstream of dams (e.g., building or improving fish passage structures, building new or improving, existing instream habitat, and removing other physical barriers).

Gravel augmentation as a restoration effort is the focus of this project. Introducing gravel downstream of dams has two immediate goals: 1) to replenish the gravel supply downstream so physical processes may resume, and 2) to replenish the gravel supply so fish habitat quality is improved. Adding supplemental gravel is targeted to improve physical processes by rebuilding geomorphic features such as pools, point bars, and riffles, improving interactions with side channels and flood plains to prevent deep main-channel incision, and resuming the natural sorting of the riverbed framework (Figure 1) (CALFED 2005). Restoring these physical processes will lead to improvements in habitat quality such as increased holding areas for adult fish, rearing and refugia areas for

juvenile fish, and increased primary and secondary food production in the channel and on floodplains (CALFED 2005). Previous studies that have focused on gravel augmentation suggest that there are habitat benefits associated with implementing this technique (Zeug, et al. 2013; Gaeuman, et al. 2014; Ock, et al. 2015), however there is still a lack of ability to track the augmented gravels at a resolution high enough to quantify how the sediment wave is propagating downstream. This thesis sets out to provide a new methodology for tracking augmented gravels at a resolution capable of measuring both small and large changes in sediment storage and to be able to characterize the movement of the sediment wave.

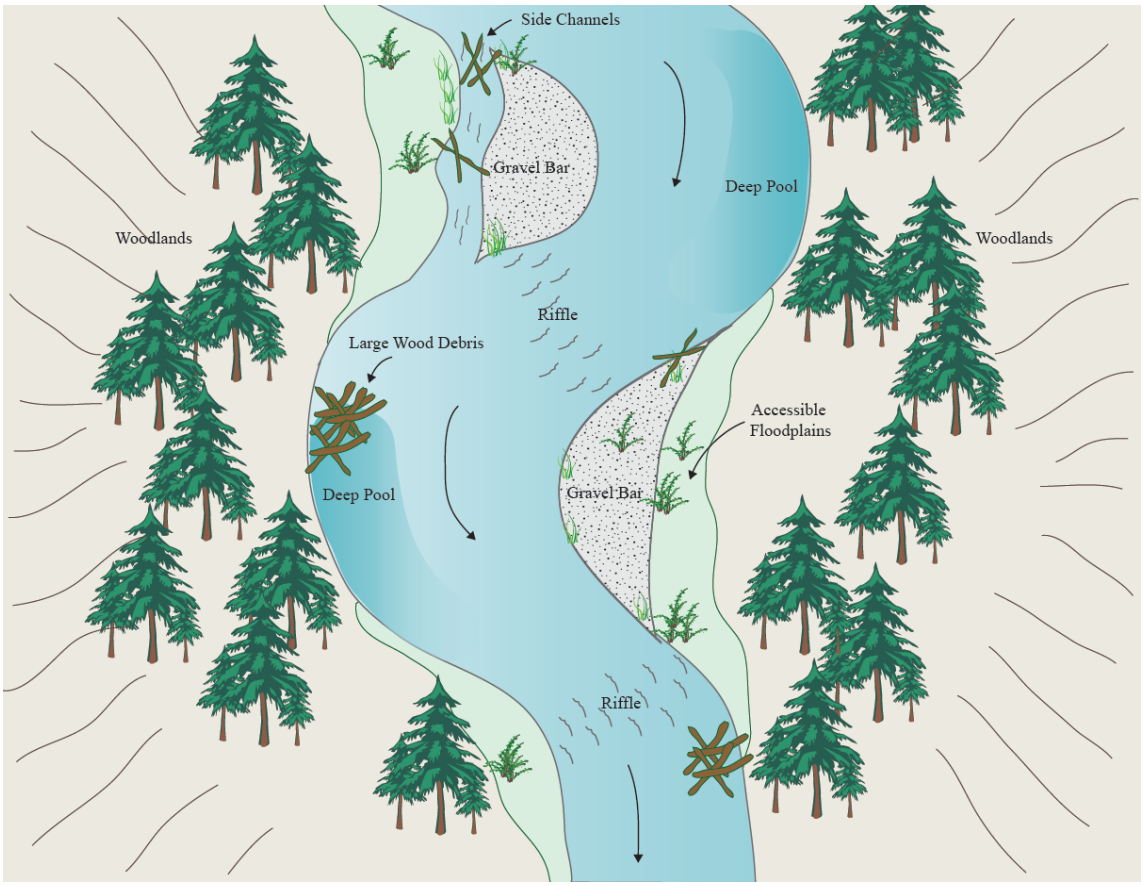

Figure 1. Typical habitat and physical features necessary to support fish and other organisms, such as deep pools and large wood debris that provide refugia, riffles for spawning, and accessible floodplains that introduce nutrients.

Study Area

The Oak Grove Fork (OGF) of the Clackamas River is one of the largest tributaries to the Clackamas River before its confluence with the Willamette River in northern Oregon. The Willamette watershed contains the majority of the state of Oregon's population, including its capital, Salem, and most populated city, Portland. The OGF begins at Timothy Lake and ends at its confluence with the mainstem Clackamas near the unincorporated community of Ripplebrook (Figure 2). The study reach, less than

1 mile of the entire OGF, has a channel morphology defined by steep bedrock canyon walls, adjacent high terraces, a moderate to steep gradient, and is semi-alluvial (McBain & Trush 2004). A more detailed description of the physical setting is provided in the Regional History section.

Lake Harriet is the second of two reservoirs along the OGF, and includes a pipeline that diverts water for the production of electricity (Figure 3). These facilities are owned and operated by Portland General Electric (PGE). In 2010 the Federal Energy Regulatory Commission (FERC) granted the operational relicensing of PGE's hydroelectric facilities on the OGF and on the mainstem Clackamas River (McBain Associates & PGE 2013). As part of license approval, PGE agreed to certain mitigation measures, including improving the quality of anadromous fish habitat downstream of Lake Harriet Dam. PGE is presently (2017) providing improvements on the OGF below Lake Harriet by increasing flows downstream, implementing gravel augmentation, constructing new side channels, and improving instream habitat.

The OGF has a coarse channel surface made of cobbles and boulders and very little fine sediment. In multiple locations, the channel bed is composed entirely of bedrock sheets, and valley confinement prevents the formation of floodplains and terraces. Because of the high stream energy during floods, the natural alluvial storage in the channel is low (McBain & Trush 2004). A sediment yield analysis was completed on the OGF to estimate the long-term average rates of sediment production based on reservoir sedimentation data (McBain & Trush, April, 2002). The purpose of the sediment yield analysis was to estimate how much sediment historically routed through

the OGF watershed and to help understand how downstream sediment transport has been impacted by Harriet and Timothy Lake Dams. This analysis reported that the OGF watershed annual unit sediment yield is naturally (and exceptionally) low at 2.2 tons per square mile (approximately 0.8 tons per square kilometer). This equates to a basin-wide average of 290 tons per year of sediment. The sediment yield is so low because of the young and permeable volcanic rocks that characterize the geology of the region. A more detailed geologic description can be found in the Regional History section. However, even with a naturally low sediment yield, the 93-year damming history on the OGF has caused a coarsening of the channel bed and depletion of gravels used by aquatic organisms.

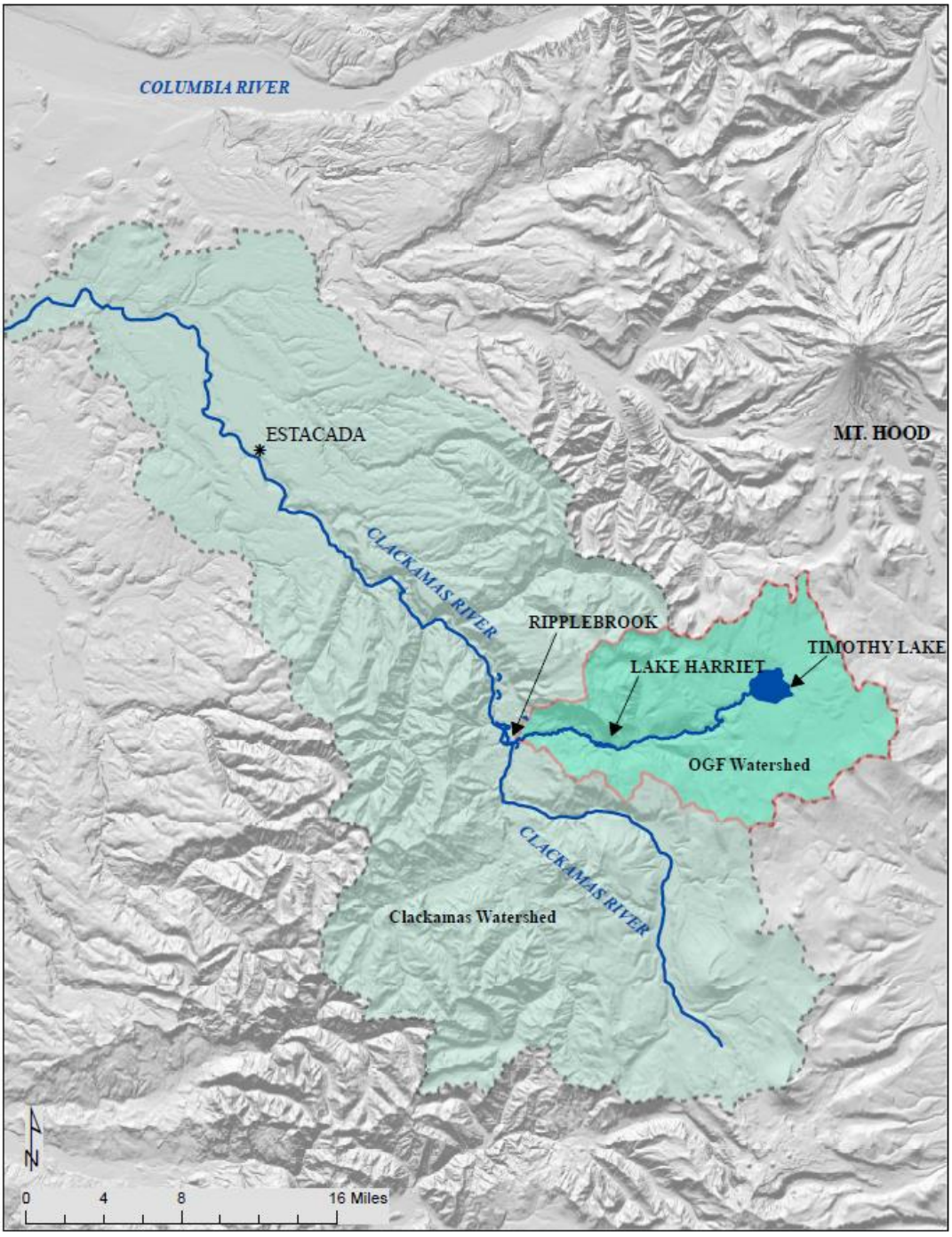

Figure 2. The OGF watershed (red outline) nested within the greater Clackamas River watershed (grey outline), with notable features and places (Map DEM, hillshade, and watershed boundaries from Oregon Geospatial Data Clearing House).

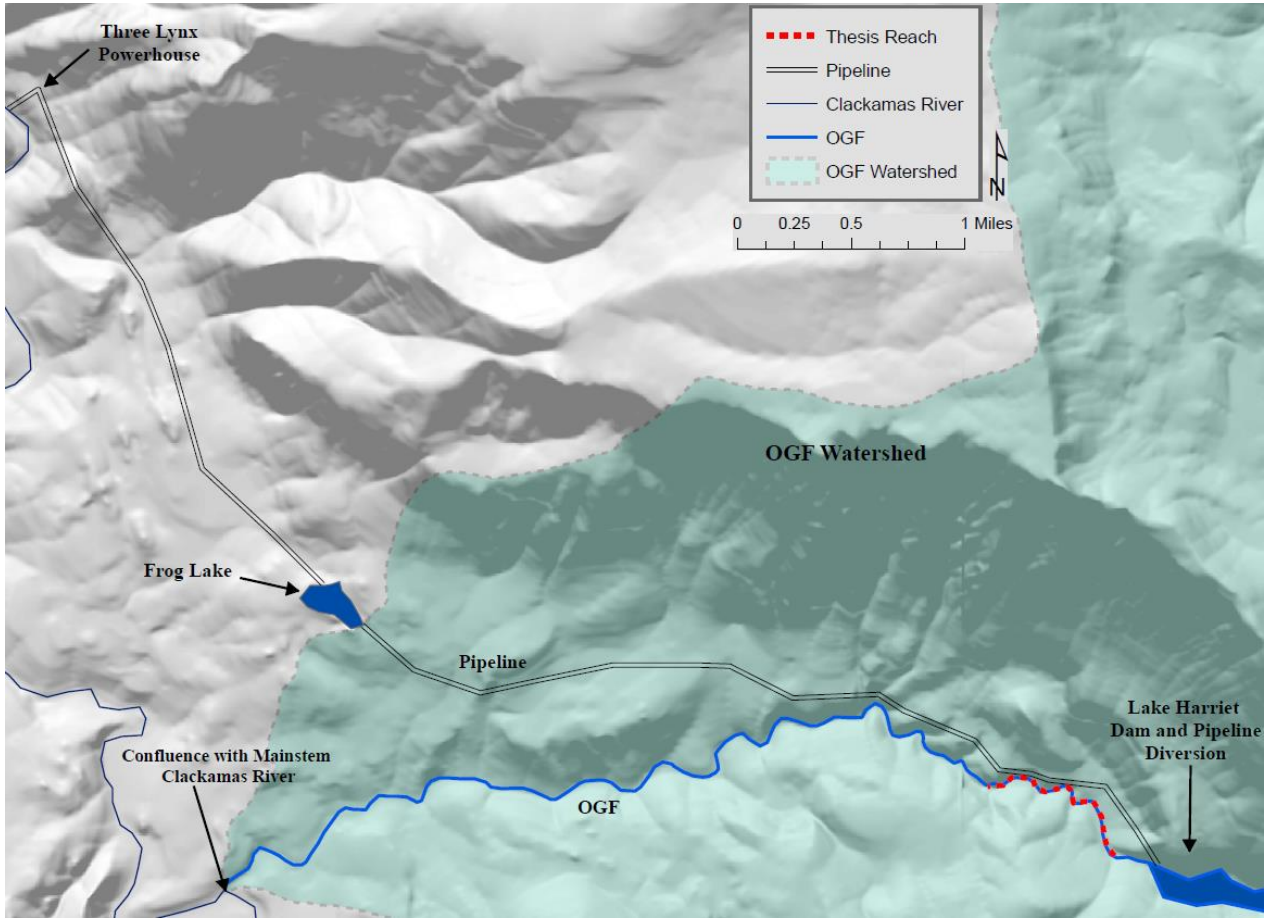

Figure 3. A close view of the OGF, highlighting important features such as Lake Harriet, the pipeline diversion (approximate), and the Three Lynx Powerhouse (approximate). (Map DEM, hillshade, and watershed boundaries from Oregon Geospatial Data Clearing House).

Gravel introduction is presently occurring at two locations on the OGF, one 1,500 ft downstream of Lake Harriet Dam (the focus of this project) and one near the confluence with the Clackamas River. The upstream augmentation location is the focus of this study, and is located approximately 1,500 ft downstream of Lake Harriet Dam at a location known as Crack in the Ground (CG). PGE is adding approximately 1,850 tons of gravel at this location over a five-year period, beginning with 250 tons introduced in September of 2016, followed by 400 tons annually from 2017-2020. Because the objective of gravel augmentation is to improve physical stream processes while also benefiting anadromous salmonids, the gravel composition is made of round rocks of fluvial origin that are sized to fit both the habitat needs and transport capabilities of the OGF.

The reach extends for approximately 4,200 ft downstream from CG and ends directly downstream of the Barrier Falls, a 25 ft tall waterfall that serves as a natural fish barrier. Because of limited road access, the gravel introduction site had to be located upstream of these falls. Until the gravel routes downstream of Barrier Falls it will not provide any direct benefit to anadromous fish. As part of PGE's license, it must be demonstrated that augmented gravels are transporting downstream of the falls within five years of the initial placement, or exploration for a new introduction site must occur, which is not a cost-effective option (McBain Associates & PGE 2013). Therefore, ability to monitor transport and storage of the gravel as it routes downstream is crucial to the success of the project.

Thesis Question

Lisle et al. (2001) define sediment waves as being transient zones of sediment accumulation in channels that are created by sediment inputs, and do not owe their existence solely to variations in channel topography. One of the major issues of studying sediment waves has been the inability to measure elevation changes of the bed and bars at the resolution necessary to track sediment transport (Lisle, 1997). The primary question of this thesis is: How is the gravel augmentation sediment wave propagating and distributing as it routes through the channel, and what is the channel response? To evaluate this question, this study 1) evaluates the movement and transport of the sediment wave as either translational or stationary, 2) estimates the volume of available void space on the existing bed that augmented gravels may fill as they transport downstream, and 3) estimates the time scale over which full dispersal (disappearance of pile) of the initial 250 tons of this material can be expected. Focusing on these objectives, we are also able to estimate the time period over which gravel will need to be added before it routes over Barrier Falls. It is important to note that the methods developed in this thesis do not directly measure sediment transport, instead they infer sediment transport through the observation of topographic change. The topographic change recorded is then interpreted as either having been induced through geomorphic processes or as having other origins such as anthropogenic change.

Previous studies have described and quantified sediment waves that propagate as stationary waves (dispersion waves) and translational waves (Lisle, 1997; Lisle et al., 2001; Cui et al., 2005); other studies have built on this concept and studied this

propagation as a response to gravel augmentation (Sklar et al., 2009; Venditti et al., 2010; Sims & Rutherford, 2017). In translational waves, the body of the wave translates downstream and disperses as it goes, unlike a stationary wave where the trailing edge of the wave stays fixed and dispersion of material occurs as the leading edge of the wave propagates downstream (Lisle, 1997). Translational waves tend to occur most often in channels where Froude numbers (the ratio of velocity to the square root of depth, times gravitational acceleration) are less much less than 1, but in upland channels, where the gradient is typically steeper and Froude numbers approach 1, sediment waves tend to propagate as stationary waves (Lisle, 1997). Stationary waves are also likely to occur when fine sediments are introduced onto an armored bed; these fine sediments promote the tail of the wave to propagate downstream. This thesis uses high resolution photogrammetry and a one-dimensional (1D) sediment transport model to attempt to capture geomorphic changes in high enough resolution to study sediment wave propagation.

Photogrammetry provides a cost-effective method for studying geomorphic change at an equal to, or better, resolution than aerial LiDAR (Bird et al., 2010; Wheaton et al., 2010; Westoby et al., 2012; Fonstad et al., 2013; Javernick et al., 2014; Dietrich, 2016). Photogrammetry, at very fine resolution (0.1 ft), was chosen for this study to investigate the spatial and temporal movement of gravel as it routes downstream. This high-resolution method resulted in the detailed analysis needed to help understand if the gravel will indeed route past Barrier Falls in the five-year timeframe. The amount of gravel introduced in the first year of augmentation (250 tons) is relatively small

compared to the size and storage capacity of the OGF. The current stream bed condition on the OGF is also coarse compared to the material being introduced. For these reasons, it is expected that in the first few years much of the augmented gravel will be stored in interstitial spaces, close to the augmentation site, satisfying the storage capacity, before any significant volume of gravel is routed downstream. Therefore, it is critical the monitoring method can capture small-scale, high-resolution changes in storage.

In addition to photogrammetry, a 1D sediment transport model created in the Hydrologic Engineering Centers River Analysis System (HEC-RAS) was used as an independent method to make predictions on gravel storage and transport that could be tested by photogrammetry results. This model uses measured channel geometry, flow, and sediment inputs to simulate the transport and storage of augmented gravels. This model provided a timeline for full dispersal of the initial 250 tons of gravels and predicts areas within the reach where deposition and erosion can be expected.

Conventional Monitoring and Survey Methods

To evaluate the success of restoration efforts, there are many conventional methods that are used to monitor physical change in river systems. Projects that focus on sediment transport downstream of dams require monitoring efforts that not only capture changes in overall channel morphology but also changes across a range of scales. It is also important to capture subtle changes in equilibrium adjustments such as small changes in width, depth, slope, lateral migration, and position of bedforms (Kondolf & Piegay, 2016b).

Typical channel geometry monitoring methods include surveying cross sections, thalweg profiles, and longitudinal profiles, which are taken periodically to capture changes in channel shape and form. These survey efforts require spatial accuracy, which is achieved by establishing site coordinate control, such as Ground Control Points (GCPs), and surveying them with tools such as Real Time Kinematic (RTK) satellite navigation systems, and then incorporating these spatially accurate points into the ground survey. The ground survey is conducted with either an auto level or total station. The accuracy and resolution of these surveys is dependent on the density of points surveyed. Measuring points for a densely-populated survey is a very time-consuming task.

Particle size analysis of the streambed and gravel bars is useful for understanding sediment transport and gravel storage and can be measured using a variety of techniques. Facies mapping and pebble counts are frequently used for measuring the size of surface particles within a given area (Potyondy & Hardy, 1994; Buffington & Montgomery, 1999; Kondolf et al., 2003; Daniels & McCusker, 2010). Recurring pebble count surveys and facies mapping measure the fining or coarsening of a riverbed through time. Facies mapping defines textural populations on the riverbed and pebble counts provide a statistical size distribution of populations. Tracers are also commonly used as indicators of sediment transport and these can be rocks of an exotic lithology, painted gravels, magnetic materials, or even Passive Integrated Transponders (PIT tags), all of which are collected downstream after transportation (Kondolf & Lisle, 2016).

Current PGE Monitoring Efforts

As part of their gravel augmentation program on the OGF, PGE is monitoring gravel transport and downstream deposition using more conventional monitoring efforts. PGE's monitoring program includes using tracer gravels, conducting recurring longitudinal thalweg profile surveys, and annual photo monitoring. These methods are limited in their resolution, and thus do not capture subtle changes that will likely occur as the augmented gravel transports downstream. For example, a thin layer of small gravels that deposit in between large gravels and boulders is unlikely to be detected using methods such as longitudinal profiles and topographic surveys. However, photogrammetry at this scale and resolution is capable of capturing this level of detail.

Regional History

Geologic History

The Oak Grove Fork sits within the volcanic and volcaniclastic rocks of the Cascade Range, an active subduction-related volcanic arc extending north-south from California to British Columbia (e.g., Sherrod & Scott, 1995). This arc-related Cenozoic volcanism has resulted in two principle geologic groups in this area, the older Western Cascade Group and the younger High Cascade Group. The High Cascades depositionally overlie the Western Cascades (Sherrod & Scott, 1995).

In the Willamette Valley region, the Western Cascades are 10 to 40 Ma old and form the steep western slopes that extend from the range crest westward into the valley (Peck et al., 1964). The Western Cascades primarily comprise partially altered flows and

pyroclastic volcanic rocks. These volcanics are deeply weathered and altered, and are prone to mass wasting events such as landslides and earthflows (Peck et al., 1964).

The High Cascades represent the active volcanism that has occurred during the last 10 Ma, which is responsible for building the crest and eastern slope of the range. These volcanic forms are the familiar, conically shaped stratovolcanoes (such as Mt. Hood), and cinder cones that are visible along the skyline (Peck et al., 1964). The High Cascades form steep terrain, and slope instability usually results in large slump blocks, rockfalls or mudflows during volcanic events (Peck et al., 1964). The majority of the OGF upper watershed sits within the High Cascades and transitions into the Western Cascades near Lake Harriet (similar to the transition between the biogeoclimatic zones). The low erosion rates of the High Cascades and volcanic lithology are responsible for the exceptionally low sediment yield of the upper OGF watershed.

Another principal rock type in this area is the Columbia River Flood Basalts that erupted effusively, flowing across the landscape between 13 and 16 million years ago (Hammond et al., 1980). Not related to arc volcanism, the flood basalts are regionally extensive and are up to 1,800 ft thick within the Clackamas River Valley (Hammond et al., 1980).

The two primary units exposed along the Oak Grove Fork are the basaltic andesite of the Oak Grove Fork and the Columbia River Flood Basalts. The basaltic andesite erupted from local cinder cones and small shield volcanoes that have now either been eroded away or buried by subsequent flows (Sherrod & Scott, 1995). The flood basalts range from columnar to blocky to massive and include calcite veins rich in cinnabar, a

mercury sulfide mineral that is the chief ore of mercury (Brooks, 1963). The cinnabar-bearing calcite veins range in width from six inches to six feet and were mined from within the thesis project area between 1932 and 1943. The 11 years of production generated 173 flasks of mercury and over 900 tons of mercury ore (Brooks, 1963).

Hydrology & Climate

The Oak Grove Fork watershed is 141.5 mi^2 with elevations between 1,300 ft and 5,500 ft. The watershed is largely composed of steep forested terrain but also includes high alpine meadows. The OGF and Clackamas River are within the greater Willamette River Basin, which has been divided into three biogeoclimatic zones (Watershed Network Professionals, 2005). The High Cascades zone, defined as being at elevations above 4,000 ft, the Western Cascades zone between 1,300 ft and 4,000 ft, and the Willamette Valley zone less than 1,300 ft. (Grant, 1997). Biogeoclimatic zones are assigned based on variations in precipitation, ability of the soils and bedrock to route and store water, and ecosystems present in the area. The Oak Grove Fork Watershed above Timothy Lake is within the High Cascades biogeoclimatic zone and transitions into the Western Cascades zone between Timothy Lake and Lake Harriet (McBain & Trush, 2004).

Both the geology and climate have strong controls on the hydrograph in this area. Like all watersheds, climate determines the overall volume, seasonality, and distribution of precipitation, while the geology controls the amount of moisture retained as groundwater and the transmissivity of seepage through dry, summer months (Grant, 1997). The climate of this region is strongly influenced by the Cascade Mountain Range,

which results in large amounts of orographic precipitation (Watershed Professional Network, 2005). The OGF averages 63 in of precipitation annually. The highest peaks of the mountain range receive more than 150 in, most of that stored as snowpack (Watershed Professional Network, 2005).

Streamflow within the Cascades can be characterized by two principle types of hydrographs: a snow dominated hydrograph and a rain-on-snow dominated hydrograph. The snow dominated hydrograph of the High Cascades relies on snow accumulation during the winter months that feeds watershed moisture, followed by a period of rapid melting that rejuvenates the water supply just before the hot, dry summer begins. The rain-on-snow hydrograph of the Western Cascades relies on smaller accumulations of snow that are rapidly melted off throughout the winter by warm rainstorms that move through the region between December and March (Grant, 1997). These warm storms often result in large flood events whose magnitude is largely dependent on the amount of precipitation brought by the storm and the amount of snowpack, which varies by year. The high flow periods of the annual OGF hydrograph are dominated by rain-on-snow events.

The OGF water year 2017 was reflective of a rain-on-snow hydrograph, having fairly irregular flows and no distinctive snowmelt peak (Figure 4). There were several peak flows in the 2016 water year (October 1, 2016 to September 30, 2017), the largest occurring on May 5, 2017 with a peak discharge of 1,080 cfs. There are three distinct periods of high flow present on the hydrograph, 1) a period representing the first high flow events of the water year in February, 2017, 2) a period representing high flow events

at the end of March through early April, 2017 and, 3) the final and largest period of high flow events occurring at the end of April through May, 2017. The first period of high flow events is characterized by two peak events, both of short duration. The second period is characterized by a single, long duration event, where there were a series of peak flows but baseflows overall sustained 400 cfs or greater. The final period is characterized by small events leading up to the short duration 1,080 cfs event, followed by a fairly fast transition into summer baseflows of approximately 100 cfs. This is characteristic of a rain-on-snow hydrograph and not a snowmelt hydrograph. With a typical snowmelt hydrograph, there would be a gradual decline in flow after the peak flow, leading into summer baseflows, instead of a sharp transition. The diversity of character between these three flow periods is important to this study because it provides the opportunity to see if moderate flows with long durations, or high peak flows with short durations, are more effective at transporting gravel.

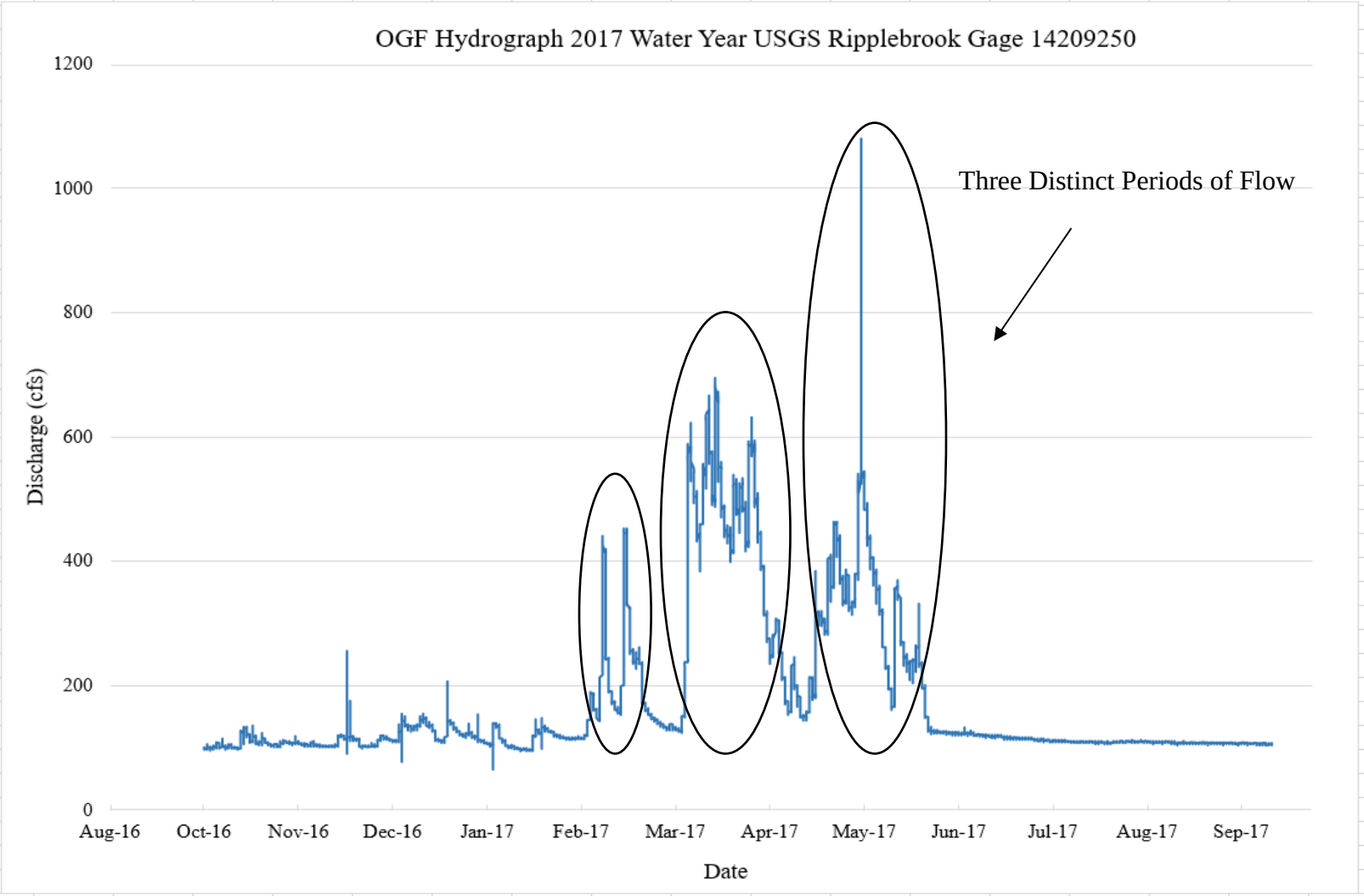

Figure 4. The 2017 water year hydrograph, showing the three distinct periods of high flow.

Oak Grove Fork Salmon and Steelhead History

In the 1800's the Clackamas River was recognized for its abundant salmon and steelhead populations, even though overfishing in the Columbia River was already negatively affecting populations on the Clackamas. Exploration for hatchery development on the Clackamas River began in the mid 1800's by the U.S. Fish Commission and the first hatchery was built in 1877 (Taylor, 1999). After the hatchery was built, millions of native salmon eggs were collected each season for brood stock at the hatchery, greatly contributing to additional decline in native fish populations (Taylor, 1999). Timber harvesting, agriculture, and road building all contributed to habitat degradation throughout the 19th and 20th centuries. The development of dams further restricted fish populations and in some cases completely halted fish access to upper watersheds. It was recognized at the turn of the 20th century that measures needed to be taken to improve fish populations. Because of this people began modifying structures to provide fish passage, drastically reduced the amount of eggs taken at hatcheries, and provided the opportunity for fish populations to rebuild themselves through access to spawning and rearing grounds in upper watersheds (Taylor, 1999). Today, there is an ongoing effort to improve habitat and access for salmonids.

There are five species of Pacific salmon and two species of sea-running trout that are native to North America (Lackey, 2003). The Clackamas River supports runs of spring and fall Chinook salmon (*Oncorhynchus tshawytscha*), two runs of coho salmon (*Oncorhynchus kisutch*), summer and winter steelhead (*Oncorhynchus mykiss*), and cutthroat trout (*Oncorhynchus clarkii*) (PGE Clackamas Fish Runs, 2017).

Historically, the spring Chinook salmon run was one of the largest on the Clackamas River. Spring Chinook migrate in the Clackamas between March and September. Fall Chinook are also native to the Clackamas River and are a wild population not supported by the hatchery. They migrate between August and December and spawn in larger tributaries downstream of River Mill Dam (PGE Clackamas Fish Runs, 2017).

There are two runs of coho salmon, the early run enters in August and the late run in November. The early run is also supported by the hatchery and the late run is endemic to the area. Most coho spawn upstream of North Fork Dam, but natural reproduction does occur in the larger tributaries below the dam (PGE Clackamas Fish Runs, 2017).

Summer steelhead migrate to the Clackamas River between April and November with a peak migration in May through July. Summer steelhead were introduced to the Clackamas in 1970 and have not been passed upstream of North Fork Dam since 1999. There are two runs of winter steelhead, the first run enters the Clackamas beginning in November and the late run enters in January. The early run is supported by the Eagle Creek Fish Hatchery and is released below River Mill Dam so they do not interfere with the native, late run, which spawn primarily upstream of the dam (PGE Clackamas Fish Runs, 2017).

PGE Facilities

PGE currently operates hydroelectric facilities on the mainstem Clackamas River as well as on the OGF. The mainstem Clackamas has three developments: North Fork Dam, the Faraday Development, and River Mill Dam (Watershed Professional Network,

2005).

The first developments built on the OGF were Lake Harriet Dam and the pipeline diversion in 1923. The pipeline diversion that begins at Lake Harriet Dam is capable of diverting up to 660 cfs. Historically, the pipeline diverted all water in the stream channel until 660 cfs was exceeded. This effectively left the channel downstream of Lake Harriet Dam dry during most months, except for tributary accretion and ground water seepage. Now, PGE releases a minimum base flow of between 70 and 110 cfs downstream of Lake Harriet Dam at all times. In 1956, Timothy Lake Dam was built approximately 10 miles upstream of Lake Harriet Dam to provide a larger reservoir. (McBain & Trush, 2004).

From Lake Harriet the water is diverted into a pipeline that carries it 4.1 miles to the Frog Lake forebay and then an additional 2.3 miles to the Three Lynx Powerhouse. After electricity production the water is discharged into the mainstem Clackamas River (PGE, 1999).

Research Approach

Photogrammetry Overview

Photogrammetry is a remote sensing technique that has been used to create topographic maps since the 1930's. Simply speaking, photographs are taken and overlain to produce a three-dimensional representation of an object or surface (Chandler,1999; Westaway et al., 2000; Butler et al., 2002; Chandler et al., 2002; Westaway et al., 2003; Matthews, 2008; Gimenez et al., 2009). Originally, photogrammetry involved using two air photos that overlapped in area, and the offset angles of the photos along with the

overlap generated a three-dimensional (3D) effect in stereoscope view. This method was limited in usefulness because quantitative data such as distances, elevations, areas, and volumes still had to be manually calculated. Today, computer-driven photogrammetry creates three-dimensional objects and surfaces using the same principles as photogrammetry, except that parameters such as camera position, angle, distance, and scale are solved automatically within the software. In this way, elevations, areas and volumes can be quickly calculated over larger areas. Structure from Motion (SfM) is an automated, software-driven version of photogrammetry.

To use software such as SfM, photographs of an object or surface are acquired in the field and are given coordinate control with Ground Control Points (GCPs). GCPs are surveyed monuments that provide real elevation and coordinates (northings and eastings) that the software uses to calculate the position and elevation of all other points within the surface or object (Figure 5). It is important to survey GCPs at a high level of accuracy because the terrain model can only be as accurate as the GCP data. Along with the GCP data, the SfM software requires input of camera parameters such as focal length, pixel size, and resolution. These parameters used in conjunction with the GCP data provide the spatial information needed for the program to create an accurate surface. To build a three-dimensional surface, the software requires 60% overlap between photographs, and the photographs need to be focused and high resolution. Photographs that are blurry, homogenous, or distorted work poorly in the software because they affect pixel size and length, which are used along with coordinate data to calculate the positions of objects in the DTM.

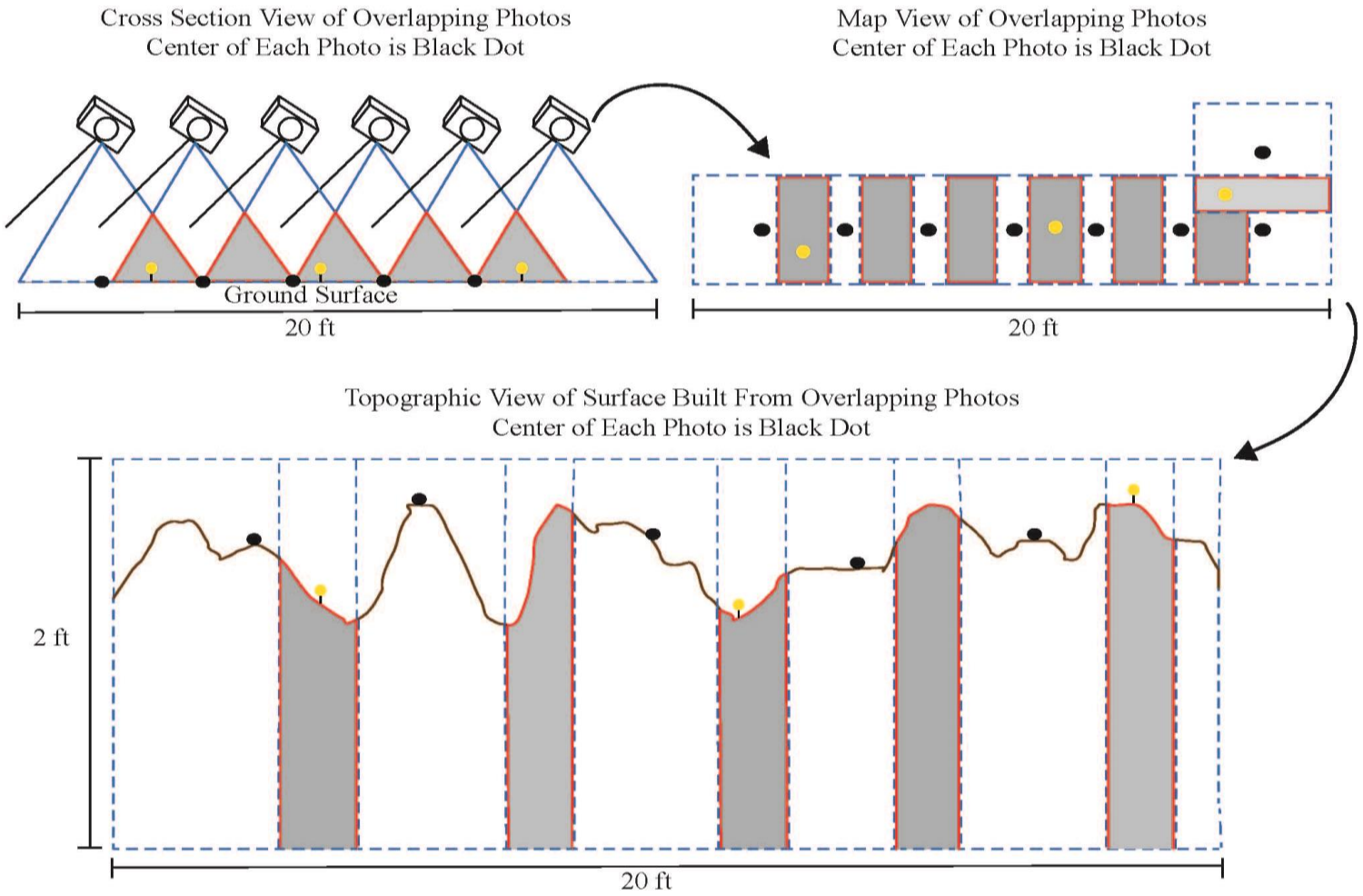

Figure 5. Three schematic cartoons depict a generalized workflow of the photogrammetry process, beginning with taking overlapping photos and then processing to create a topographic surface. GCPs are yellow dots and overlap is shown in grey.

HEC-RAS Overview

One-dimensional (1D) and two-dimensional (2D) hydraulic models are standard tools for studying changes in flow and sediment in rivers. A sediment transport model was incorporated into this project to analyze empirical data and enable field data to be directly applied to make predictions about streambed evolution. In this study, I use HEC-RAS (Hydrologic Engineering Centers River Analysis System), software capable of modeling river systems in 1D or 2D. 2D models can calculate vertical and horizontal variations in flow and shear stress and can estimate the formation and stability of gravel bars (Nelson et al., 2016). Therefore, 2D models are most often used over small areas because they require great detail in topography and bathymetry and are computation intensive. They also require a great deal of survey work for verification of model outputs. On the other hand, 1D models calculate cross-sectionally averaged values in flow, meaning that they are incapable of capturing vertical or horizontal flow variations (Nelson et al., 2016). However, 1D models can predict water surface elevations and estimate areas of deposition or scour throughout the reach. 1D models are frequently used because they require substantially less topographic data input and can be applied on the reach scale. A 1D HEC-RAS model is the best fit for this project because of the relatively long reach length and available topographic data. The 1D model for this study was built and calibrated using measured data (Appendix A) (cross sections, longitudinal profile, water surface elevations, etc.) as well as interpolated cross sections (Figure 6).

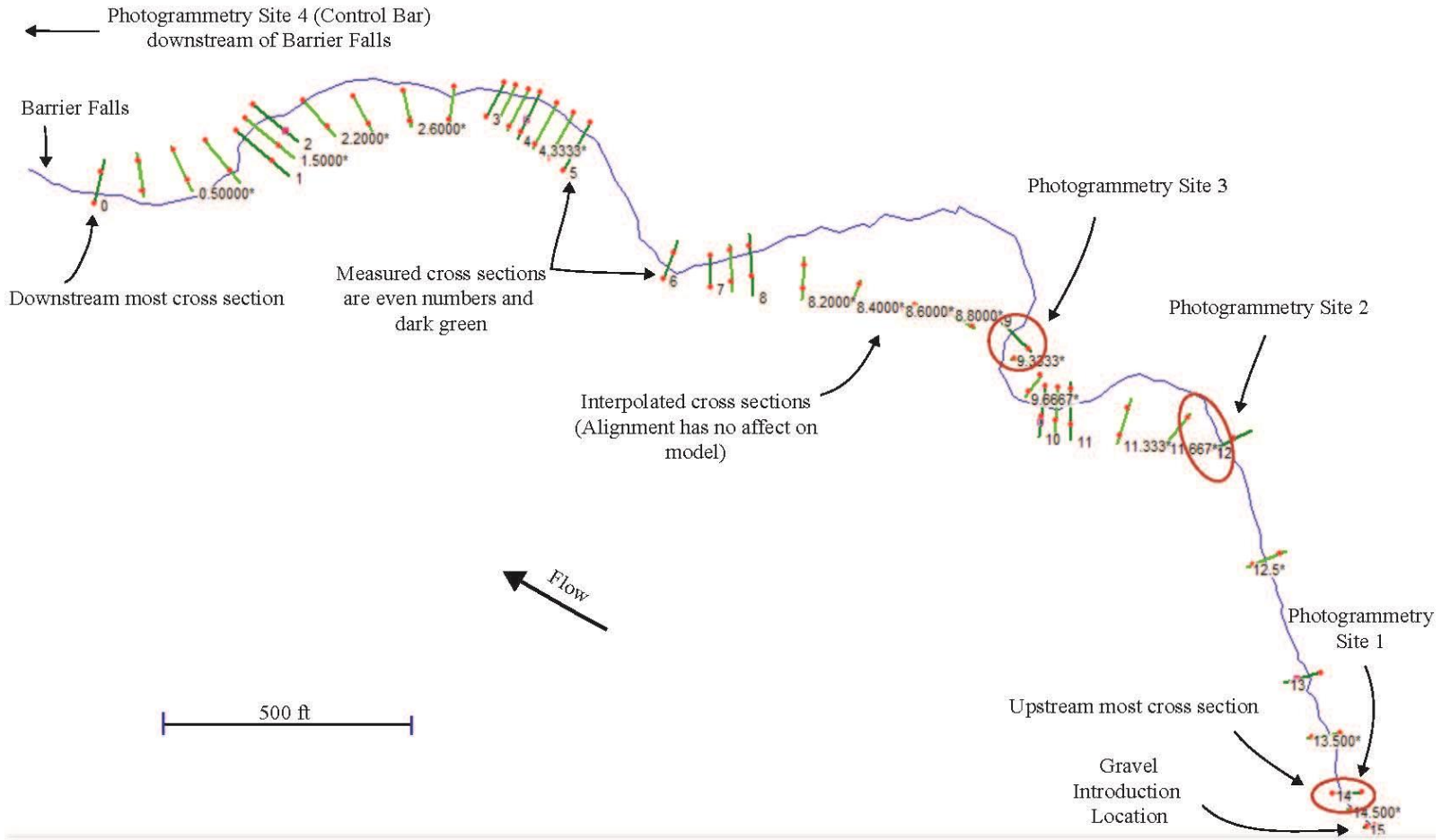

Figure 6. HEC-RAS channel geometry workspace, showing the full reach with measured cross sections (even numbers and dark green) as well as interpolated cross sections (lime green). Red circles indicate photogrammetry sites.

Two Independent Analyses

Incorporating both the photogrammetry SfM methodology and the 1D sediment transport model into this study is complementary because the two methods are independent of each other. Moreover, I can make predictions using the 1D sediment transport model and test those predictions using photogrammetry results. SfM is a new and rapidly evolving technique for studying geomorphic change in rivers, but challenges remain in creating a repeatable workflow and uncertainty in data collection. The 1D sediment transport model offers an additional research approach that supplements the photogrammetry effort. At the end of the study I compare the results of the two methods to see if they report change at the same level of magnitude. This is a valuable comparison because it serves as a confidence check for how well the two independent methods are performing (Figure 7).

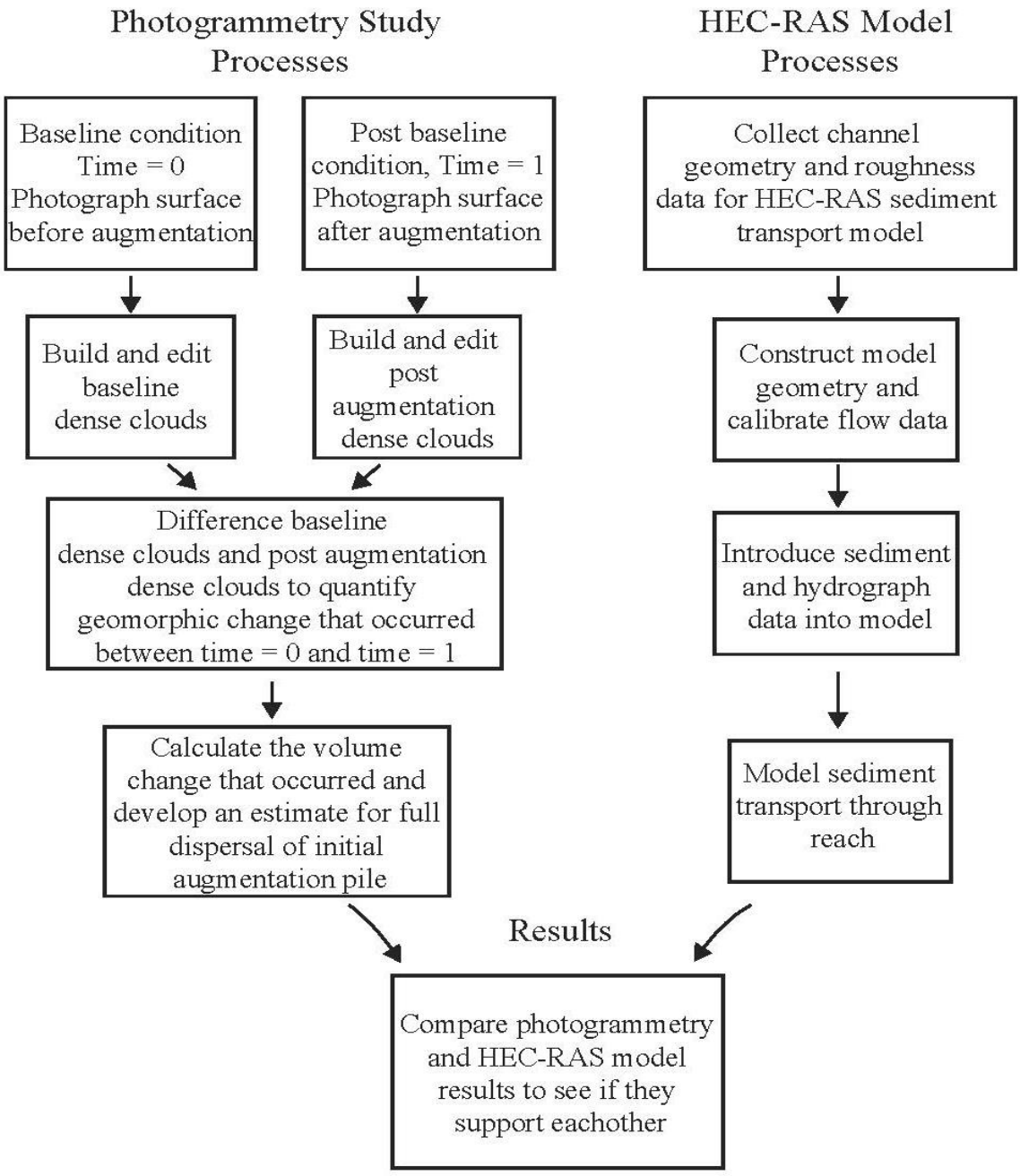

Figure 7. Flow chart that describes the general process of using both photogrammetry and HEC-RAS as independent methods. The results of both methods can later be compared to see if they are reporting change of the same magnitude.

METHODS

Photogrammetry Methods

The photogrammetry methods developed during this project are best described by separating them into two categories: 1) data collection (field work) and 2) data analysis (computer processing). The workflow for data collection included selecting sites that were appropriate for photogrammetry, establishing and surveying Ground Control Points (GCPs) at each site for spatial reference, collecting photographs at each site before augmentation to provide a baseline condition, and collecting photographs after augmentation to capture any geomorphic change that occurred. Site selection is particularly important for a successful photogrammetry project done at this scale; sites need to be as free of vegetation as possible, there must be little turbulence, and light conditions need to vary during the day so shadows and glare on the water surface move positions.

The workflow for data analysis begins by organizing photos and building dense clouds in Agisoft Photoscan using the photographs and GCP data that were collected at each site. Dense clouds for the baseline condition and for each post-augmentation trip are created. The dense clouds are then exported into CloudCompare where vegetation points are removed. If the dense cloud has such a high density of points that the software cannot process efficiently, then the cloud is also thinned in CloudCompare. After editing is complete, the baseline dense cloud and post augmentation dense clouds are aligned and

differenced to calculate the geomorphic change that has occurred. Finally, the differenced cloud is exported to ESRI ArcMap and ArcScene for better visualization and final DTM creation.

Redwood Creek Photogrammetry Pilot Tests

To develop photogrammetry methodology that is suitable for application on the OGF, I conducted a pilot study in a local and controlled environment. Two separate pilot tests were run on Redwood Creek in northern California; one on April 17, 2016, and the other on October 21, 2016. The testing area is a large gravel bar located approximately 0.25 miles upstream from the Highway 101 junction with Lady Bird Johnson Road. The purpose of these pilot tests was to complete the photogrammetric process from start to finish by: 1) selecting a study area representative of a specific geomorphic feature (e.g. point bars, riffle crests, pools, etc.), 2) establishing GCPs, 3) collecting photographs of the site as I found it (representing the baseline condition or time=0), 4) disturbing the site by digging holes, building piles and raking areas, then collecting a second set of photographs (representing a period of time over which geomorphic change occurred, or time=1) 5) creating dense clouds of the site using the photographs and GCP data, 6) differencing the two dense clouds to calculate the geomorphic volume change that occurred, and 7) generating DTMs that visually compare and display the change that occurred.

The first pilot test was conducted on a river bar area that was 150 ft by 80 ft (12,000 ft^2)(Figure 7). Within this area, 25 GCPs were established and surveyed using an auto level. The elevation of the auto level was measured by taking a ground elevation

with a Bad Elf GPS unit (hand-held GPS unit). Different objects were used as GCPs: small orange construction cones, plastic numbers painted red, metal bolts painted red, PVC hexagons painted red, and Agisoft Photoscan "markers" that were printed and glued to cardboard. Distances between the GCPs were measured so their positions could be triangulated. After the GCP setup and survey, I collected 3,500 photographs of the area, each with an overlap of approximately 80%. Time restraints prohibited the disruption of the site so no photographs representing a changed condition were taken. After data collection, the photographs and GCP points were entered into Agisoft Photoscan and a dense cloud of the site was created. This was the first successful dense cloud model created for this thesis (Figure 8). However, I later realized too many photographs had been taken of the area; 3,500 photographs resulted in a processing time of approximately 46 hours, which is an unrealistic and unnecessary processing time when there are multiple sites to process. Photographs with 60% overlap are sufficient and reduces the number of photos so that more sites can be processed in less time.

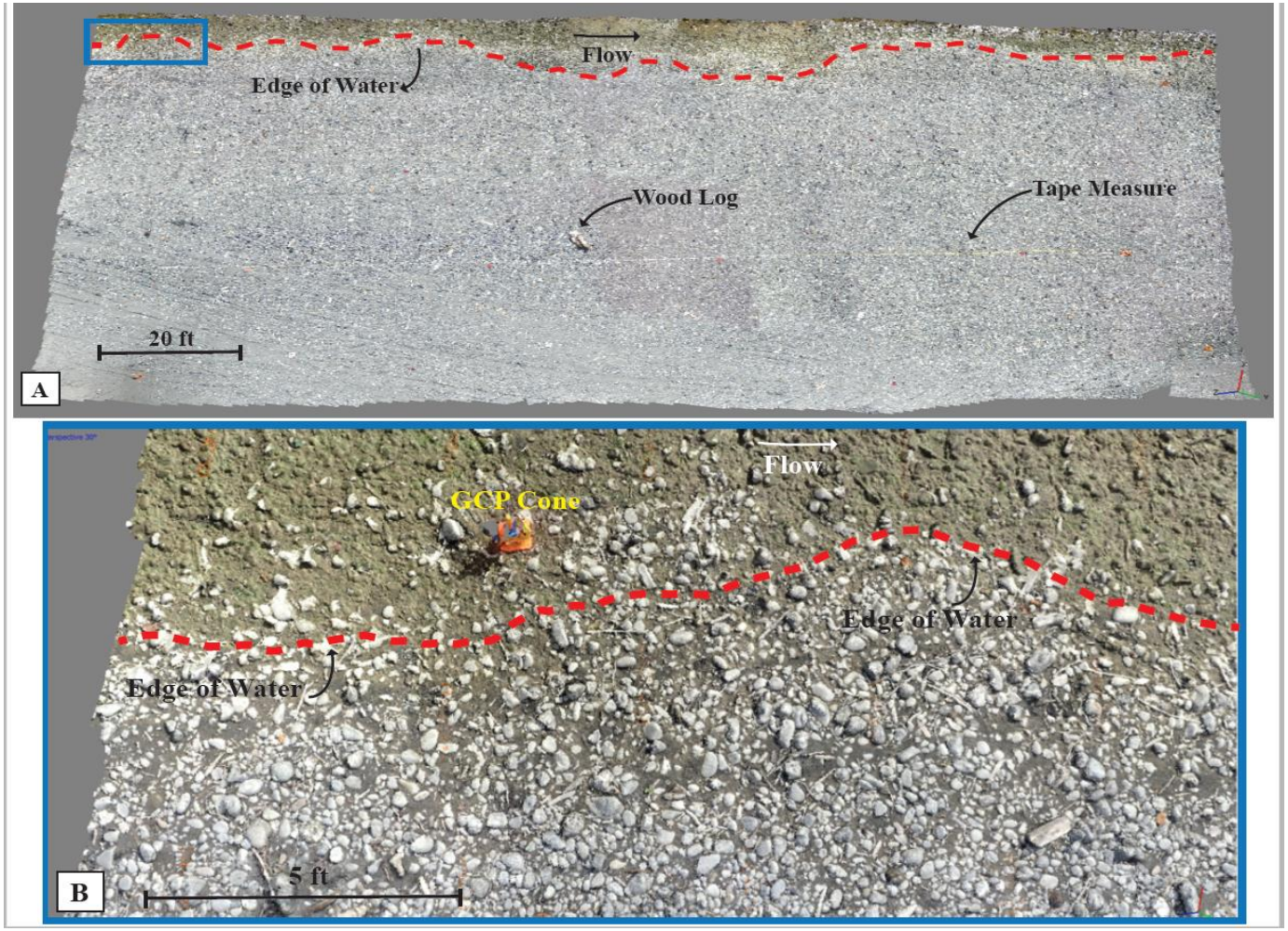

Figure 8. Dense cloud models (not photographs) from the first Redwood Creek trial run. A) view of entire dense cloud. B) close view of dense cloud section, showing the high resolution of the dense cloud (able to see individual grains).

Because the first pilot test could not be used to develop a model that showed geomorphic change detection, and because the density of photographs was too high, a second pilot test was done to address the first test's shortcomings. This second test occurred on the same gravel bar as the first pilot test but was completed over a much smaller area of 50 ft by 50 ft (2,500 ft^2). Like the previous pilot test, the auto level elevation was determined with the Bad Elf GPS unit and four temporary GCPs were surveyed. However, for this test, only 350 photographs of the undisturbed site were collected. The area was then disturbed at 10 locations within the site by digging holes, building piles, and raking. Following disturbance, the site was photographed again so the geomorphic change of the holes and piles could be imaged. After data collection the photographs and GCP data were entered into Agisoft Photoscan and dense clouds were created for the baseline (time=0) model and for the disturbed (time=1) model (Figure 9). The dense clouds were transferred to CloudCompare and differenced using the "direct cloud to cloud" differencing tool (Girardeau-Montaut, 2015). This methodology produced DTMs with resolution better than 0.05 ft. The results of differencing clearly shows the areas that were disturbed and with fine enough resolution that individual grains within piles and raked areas are visible (Figure 10). However, the "direct cloud-to-cloud" differencing tool's results are highly simplified. For example, the tool displays any change detected as a positive value because it does not sense what is topographically up versus what is topographically down, it just reports the absolute value of change. This resulted in change being reported equally for holes and piles. For the OGF models, this tool was replaced with the Multiscale Model to Model Cloud Comparison (MC32) plugin

(Lague et al., 2013), because it reports negative and positive values for change and also reports significant versus insignificant change based on the accuracy of GCP elevations. After the dense clouds were completed they were transferred to ESRI ArcScene so they could be color coded based on elevation and to highlight topographic change (Figure 11).

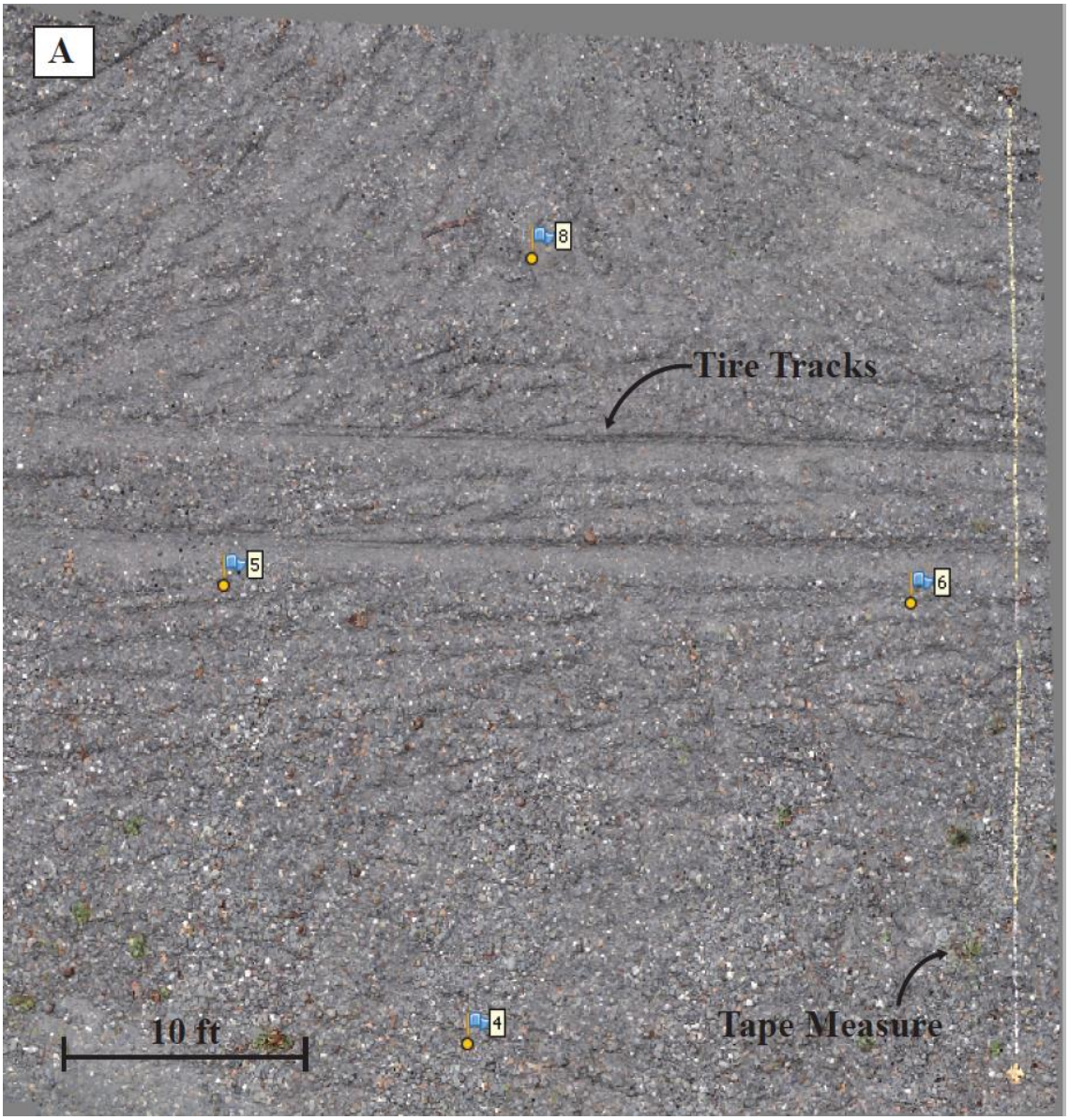
A
8
Tire Tracks
5
6
10 ft
4
Tape Measure

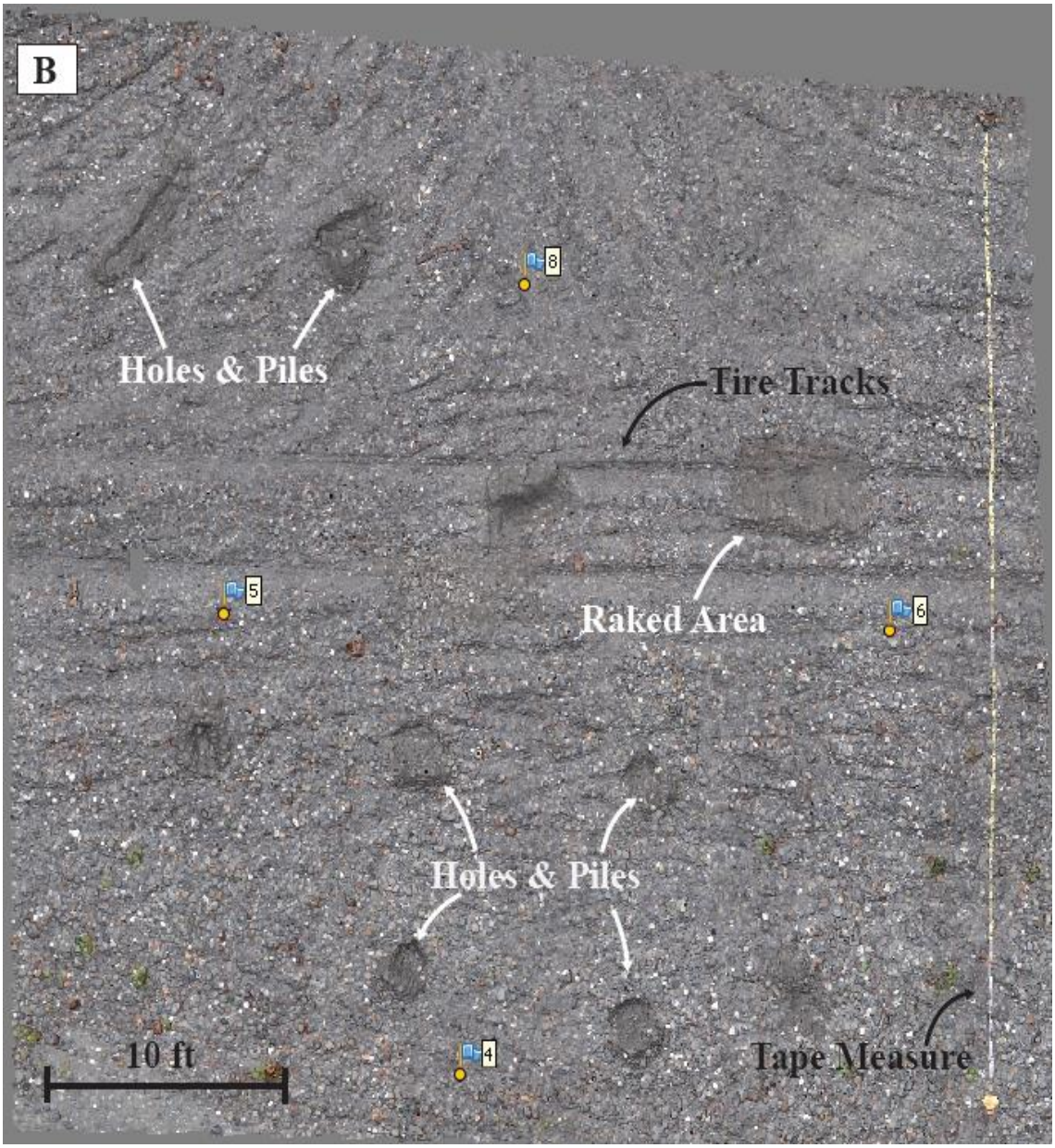

Figure 9. Dense cloud models (not photographs) from Agisoft Photoscan of the second trial run area. A) Dense cloud of the area undisturbed (time=0). B) Dense cloud of the area disturbed (time=1) after the area had holes, piles, and raked sections.

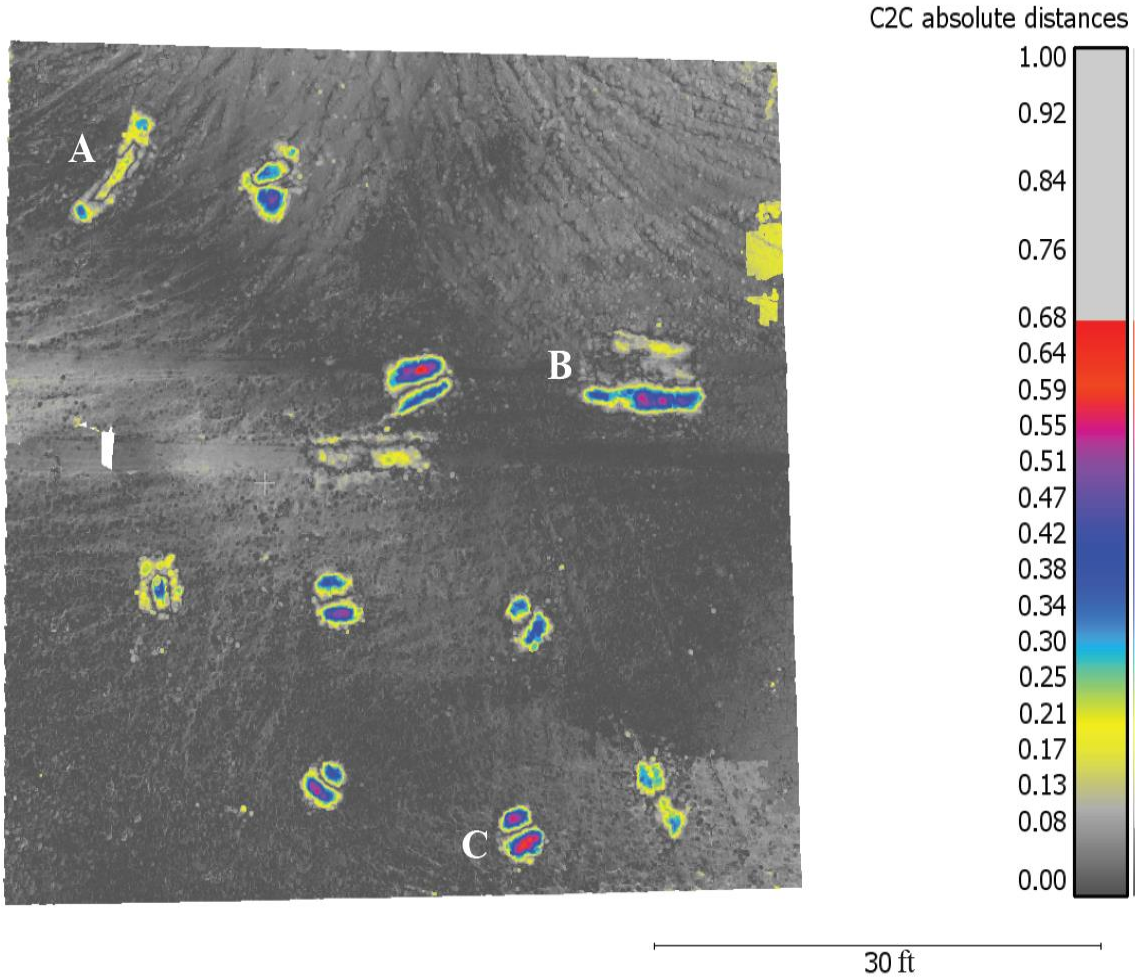
C2C absolute distances
1.00
0.92
0.84
0.76
0.68
0.64
0.59
0.55
0.51
0.47
0.42
0.38
0.34
0.30
0.25
0.21
0.17
0.13
0.08
0.00
A
B
C
30 ft

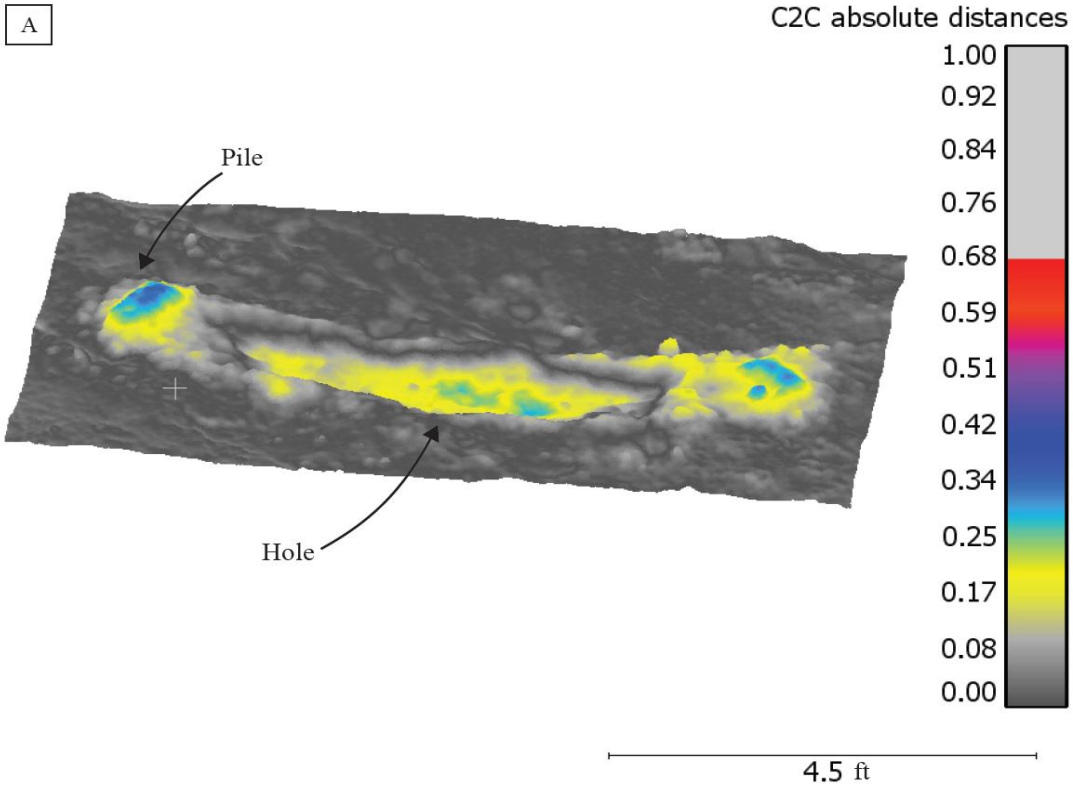
A
C2C absolute distances
1.00
0.92
0.84
0.76
0.68
0.59
0.51
0.42
0.34
0.25
0.17
0.08
0.00
Pile
Hole
4.5 ft

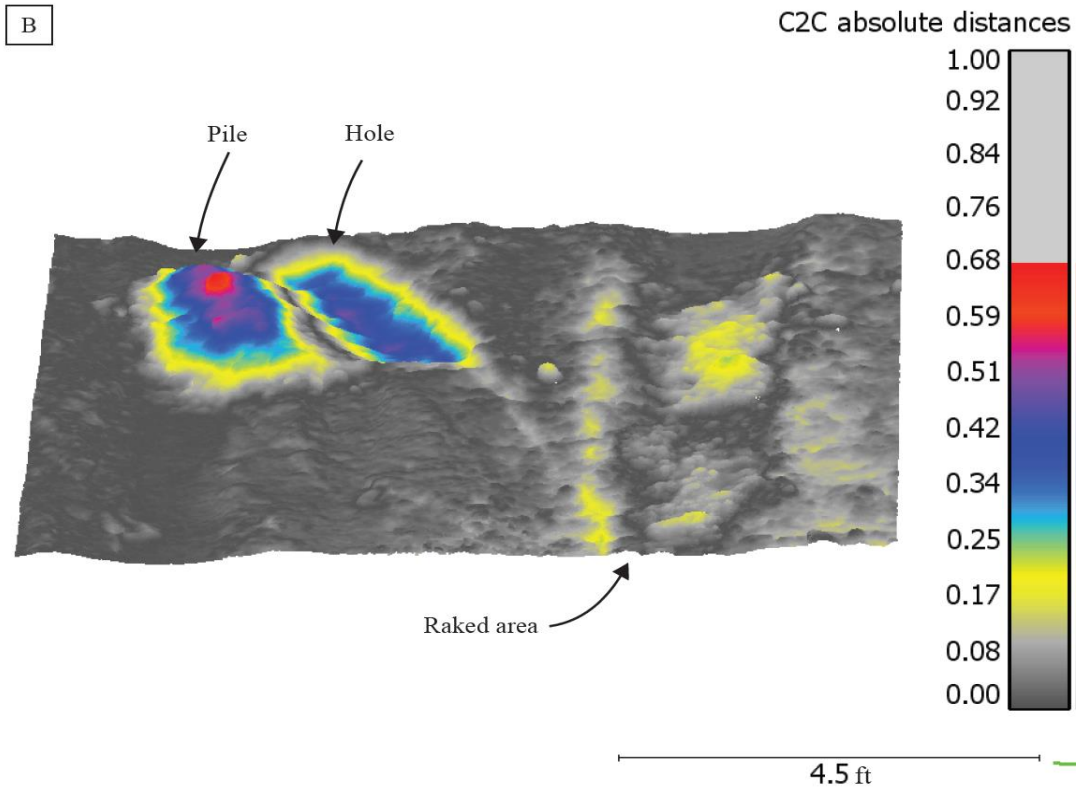
B
C2C absolute distances
1.00
0.92
0.84
0.76
0.68
0.59
0.51
0.42
0.34
0.25
0.17
0.08
0.00
Pile
Hole
Raked area
4.5 ft

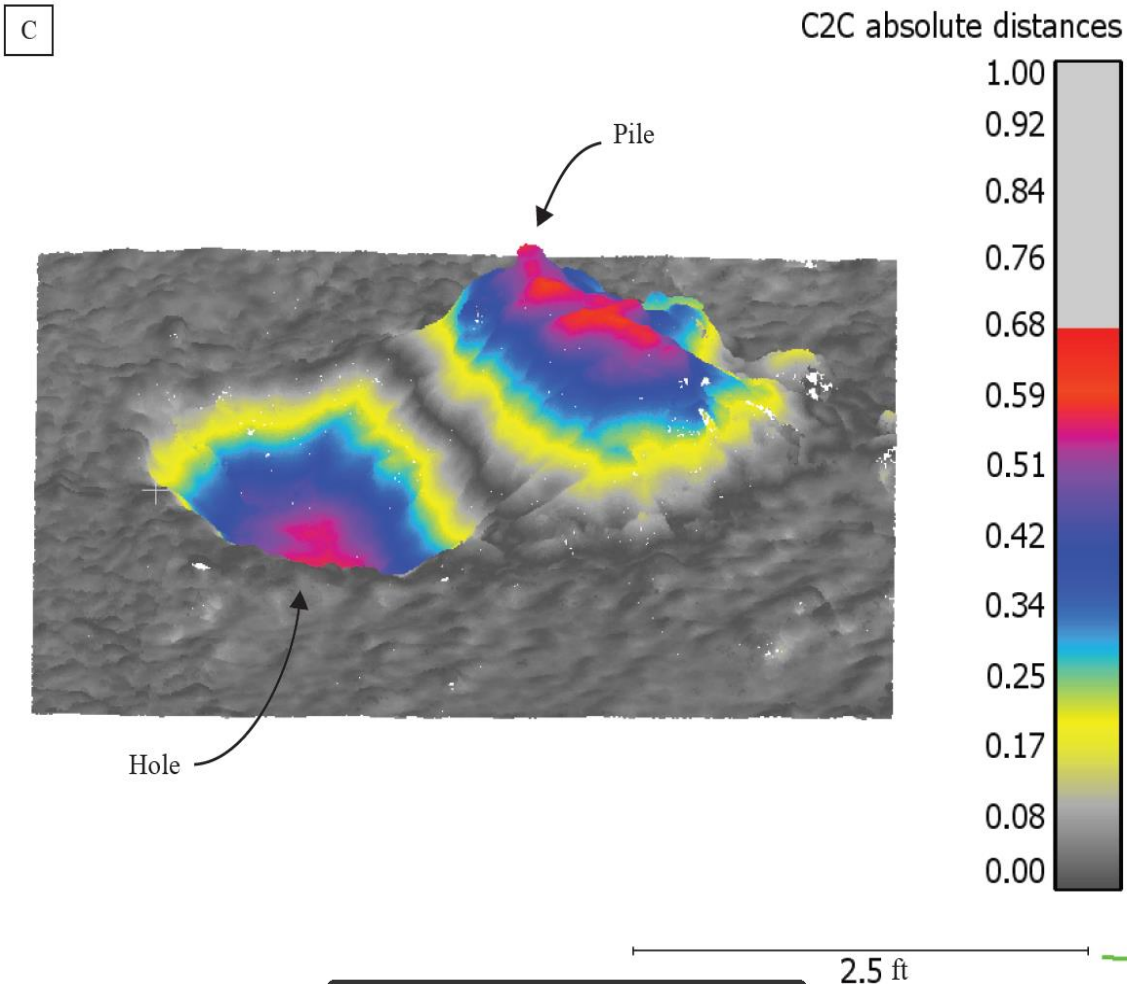

Figure 10. Dense clouds (not photographs) from CloudCompare of the second trial run area, after direct cloud-to-cloud differencing of the time=0 and time=1 clouds. The figure above shows the entire area including the ten locations that were disturbed. The next three images (locations shown above with A, B, and C), are close views of three of the disturbed areas; A) shows a long hole that was dug and two associated piles, B) shows a hole and pile, as well as a raked area, and C) shows a deeper hole and taller pile. Notice that in all three images individual grains are visible. Both scale bar values are feet.

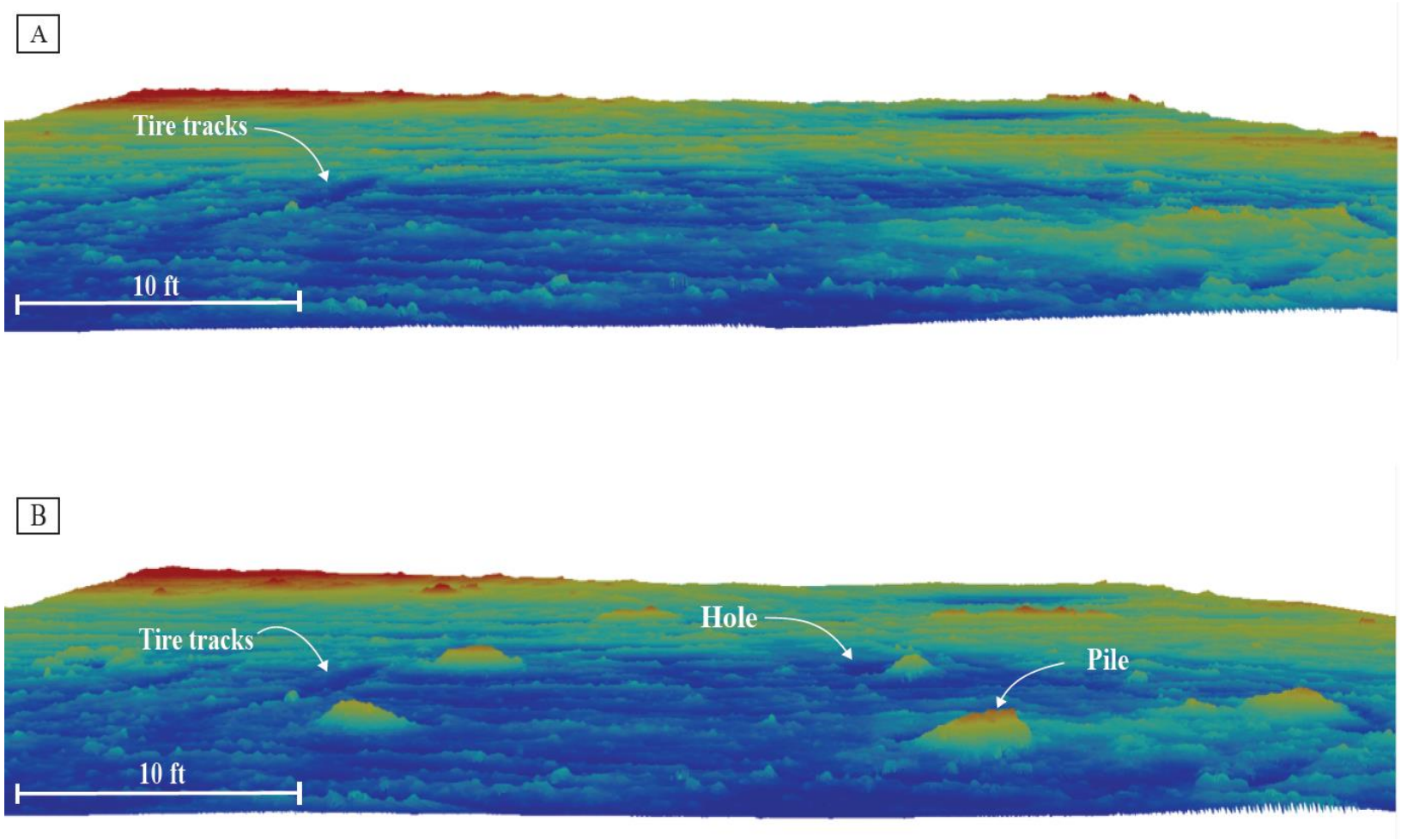

Figure 11. DTMs from ArcScene of the second trial run area: A) cross section view of the area undisturbed, B) cross section view of the area disturbed, C) oblique plan view of the area undisturbed, D) oblique plan view of the area disturbed.

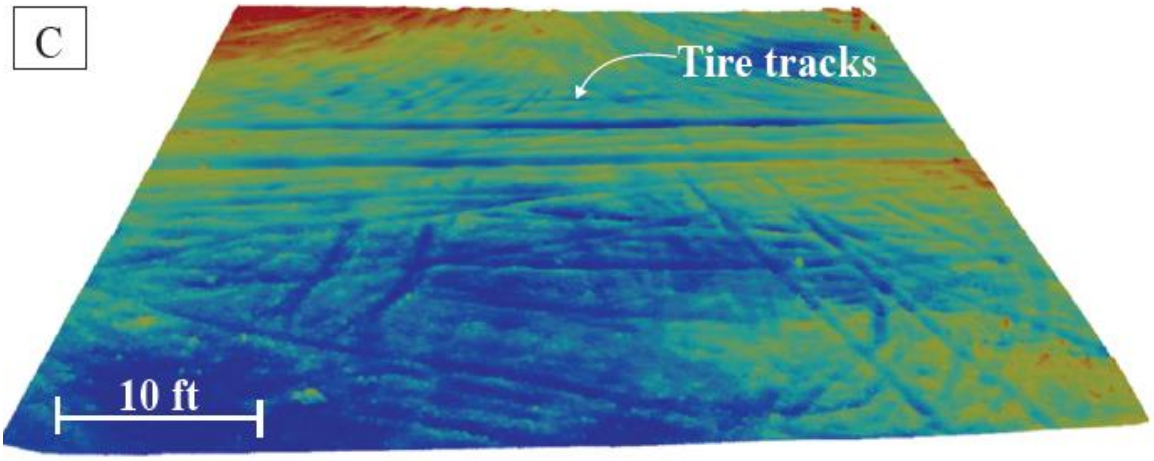

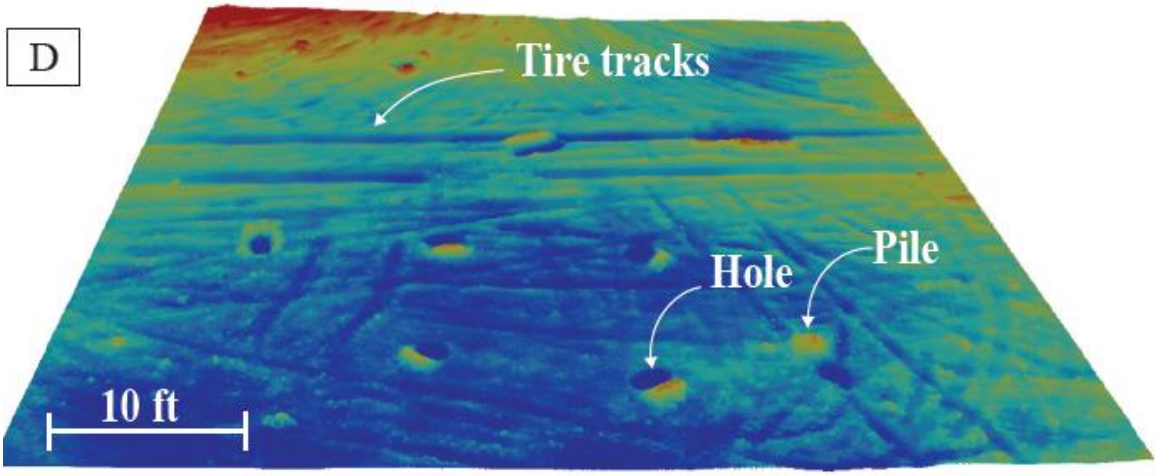

Study Site Selections and Photogrammetry Data Collection

Four sites on the Oak Grove Fork between Crack in the Ground and Barrier Falls were chosen for photogrammetric analysis (Figure 12). These sites were chosen because

they each represent a unique setting within a river channel (i.e. gravel bars, main channel, side channel), which reduces bias that would occur if only studying areas likely to store sediment (i.e. gravel bars). Progressing downstream from Lake Harriet Dam, Site 1 (Approximate Station is 278+63, which is the distance in feet upstream from the confluence with the mainstem Clackamas River) is closest to the augmentation site, and is almost completely underwater during low flows, which required snorkeling to collect photographs. Site 2 (Station 266+15) consists of two large bars separated by a side channel. Site 3 (Station 259+20) is a large bar and associated section of main channel. Site 4 (Approximate Station 320+00) is a small gravel bar that is the farthest downstream from the introduction site and is at the base of Barrier Falls. It is unlikely that the gravel will transport the full 0.81 miles downstream of Crack in the Ground past Barrier Falls within the thesis time frame, so this site serves as a control bar.

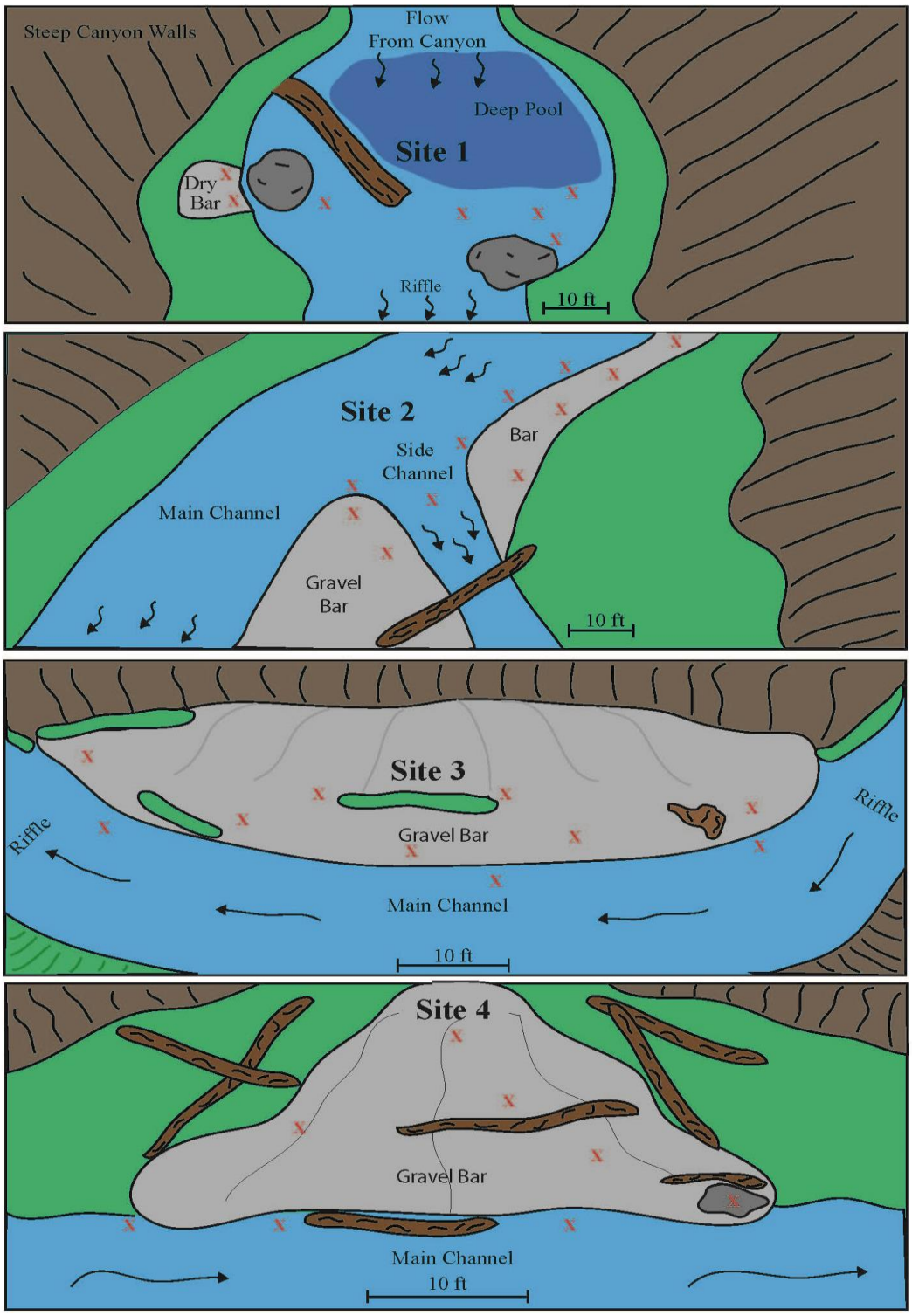

Figure 12. Schematic cartoon showing the general setup of each site. GCPs are red X's.

In July 2016, GCPs were established and surveyed at the four study sites (Appendix B) (Figure 13). Unlike the pilot tests, permanent GCPs were set at the four sites by hammering in a 3 ft rebar stake with a yellow plastic cap for visibility. Care was taken to evenly space the GCPs, and to ensure they would not move during high flows. Setting permanent ground control allows for the sites to be photographed over time and the resulting models can be aligned and differenced to detect geomorphic change. Having permanent GCPs also reduces field survey time because GCPs are surveyed initially and then checked annually, but do not need to be surveyed every time the site is photographed. Each site has 10-13 GCPs, some placed on dry land and some placed within the channel.

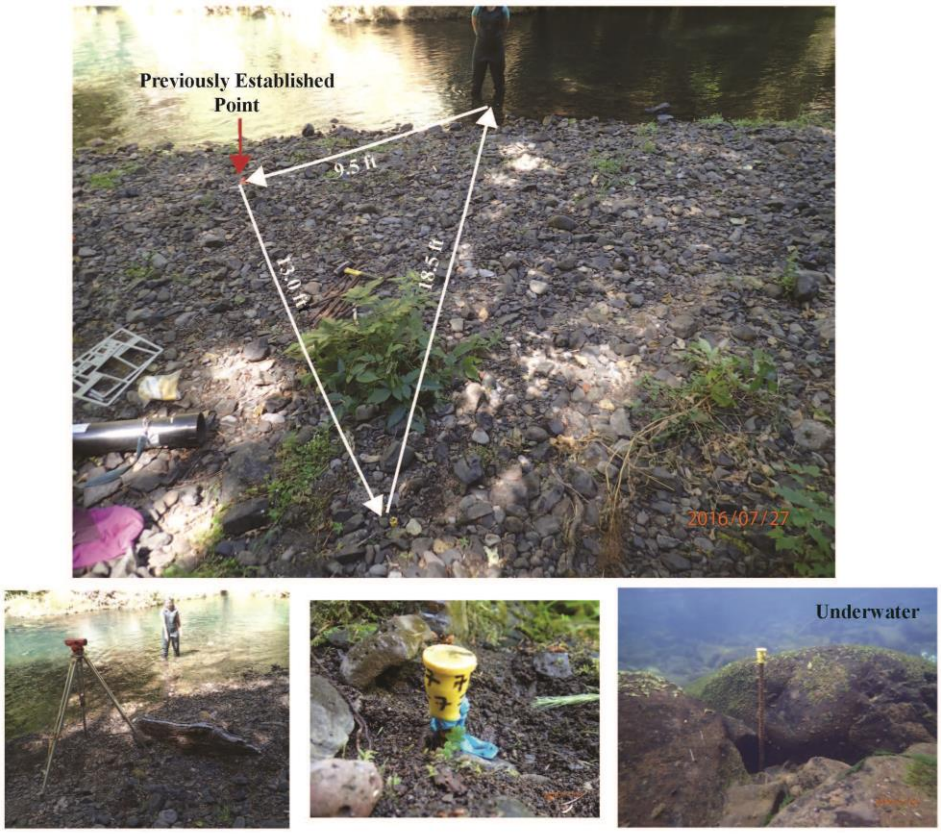

Figure 13. Photos of GCP setup and examples of GCPs above and below water.

The GCPs were surveyed using an autolevel; previous topographic surveys by others provided coordinate control for reference, therefore allowing me to calculate real elevations for my GCPs. Distances between the GCPs and the total station control points were measured using a surveying tape. Later, during data processing, the distances between the GCPs and total station points were used to triangulate the true position (northings and eastings) for each GCP using AutoCAD, so they could be imported into the photogrammetry software (Figure 14).

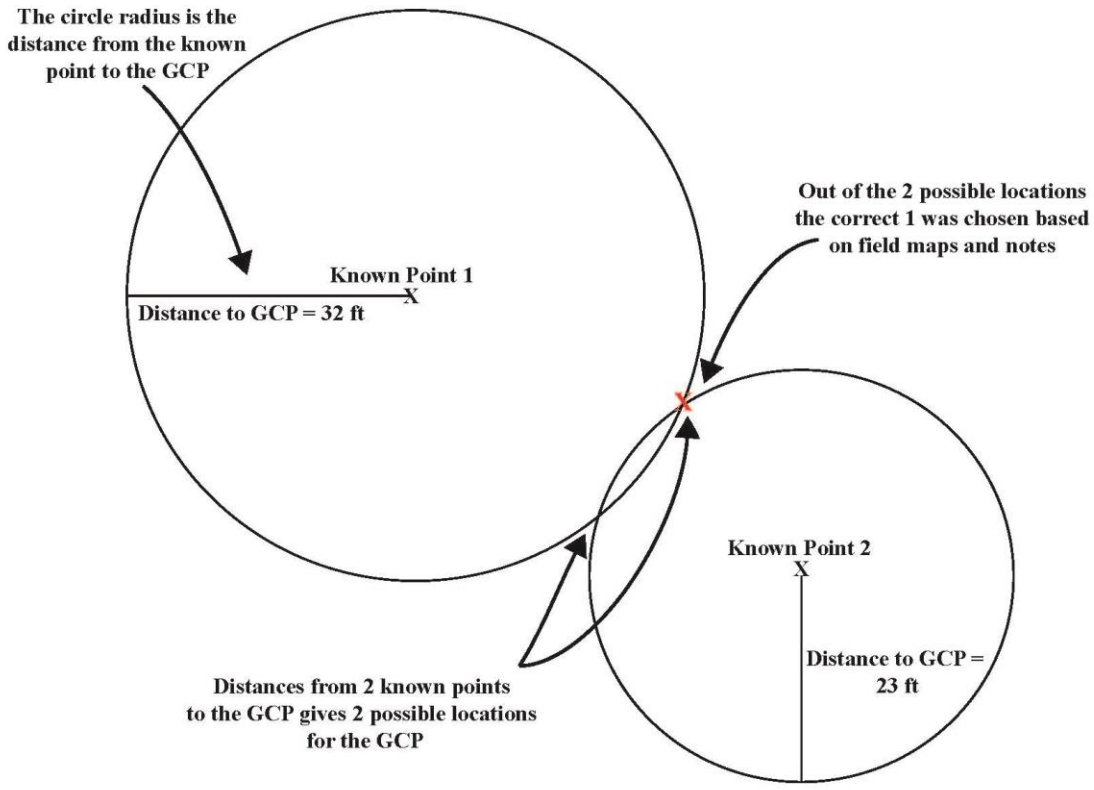

Figure 14. GCP triangulation process in AutoCAD.

After GCP setup and survey, each site was photographed to collect the baseline (pre-augmentation) condition in September, 2016. Site 1 required a snorkeling effort to collect underwater photographs. Sites 2-4 were photographed on foot using a camera and extendable pole that held the camera approximately 10 feet off the ground. In most photogrammetry projects, each individual photograph is geotagged by the camera's GPS system, which makes processing the photographs in Agisoft Photoscan much more time efficient. However, due to poor GPS signal and close distances between photographs, many photographs were geotagged with the same latitude and longitude, causing the

program to produce false results. For this reason, the geotagged latitudes and longitudes on each photograph were not used; this had no effect on the outcome other than increasing processing time.

Gravel augmentation was conducted in late September 2016, by adding 250 tons of gravel immediately downstream of Crack in the Ground. Originally, the first post-augmentation photo collection trip was planned for early spring 2017, after winter flows had receded, but before snowmelt flows began. Flows were monitored by using the USGS real-time flow webpage for the Ripplebrook Gage (USGS Gage # 14209250). Unfortunately, flows were too high for working conditions during the spring, eliminating the possibility of collecting the second photoset before the snowmelt flows began. Therefore, the post-augmentation photoset was collected in June 2017, after the snowmelt flows receded, following the same methods as the first photoset collection. This photoset captured the natural geomorphic change and any change from gravel transport that occurred at the sites during the winter and spring of 2016-2017. In summary, photogrammetry data collection was conducted twice, once pre-augmentation and once post-augmentation, using identical field methods and data processing, described below.

Photogrammetry Data Processing

Agisoft Photoscan processing. There are three primary processing steps for dense cloud creation in Agisoft Photoscan (camera and software specifications in Appendices C & D). First the photographs are imported into the program along with GCP data. Any blurry or distorted photographs are removed and areas with poor lighting conditions

(glare on the water surface, shadows, or areas of high contrast) are clipped from the images using the “Mask” tool.

Aligning the photographs is the first step to creating a point cloud. There are three options for aligning the point cloud: reference based selection, generic selection, and disabled selection. Reference based selection could not be used for this project because it aligns photographs based on the geotag assigned by the camera. Generic selection aligns photographs based on the order that they are entered into the program (i.e., photo 1 is aligned to photo 2, which is aligned to 3, which is aligned to 4, and so on). This option worked well when the photographs shared the appropriate overlap (approximately 60%). Disabled selection aligns photographs by attempting to align each individual photograph with every other photograph, regardless of input order, until a match is found. This is the most time-consuming photo alignment option, but worked the best when photographs did not share enough overlap and the generic selection failed. The result of alignment is called a “sparse cloud”. Sparse clouds are the building blocks for dense clouds, but the GCP data must be entered into the sparse cloud to spatially reference it before the dense cloud can be built. Entering GCP data is most time efficient after photo alignment is complete because the program automatically begins registering GCP locations after they are entered on a small set of photographs.

The second step is generating the dense cloud (Figures 15, 16, & 17). Generating dense clouds produced models with more accurate depths, greater detail in features, and tens of millions more points than the sparse clouds. The options for this step are to process on low, medium, or high intensity. Because of the large number of photographs

for each site it was impossible to process the dense clouds on high, so I used the medium setting. The clouds produced have tens of millions of points, and such fine detail that individual grains are displayed clearly. Dense cloud processing time ranged from six hours to 28 hours depending on the number of photographs and size of the site.

The third step is to correct any distortion within the model by using Agisoft Photoscan's "Gradual Selection" tool. Gradual selection allows the user to mass delete "bad" points based on the reconstruction uncertainty (points that introduce noise because they are found in a low number of photographs) and reprojection error (the error of point placement during the alignment stage) (Sloan and Adams, 2016). Gradual selection is an iterative process that greatly improves the model quality and reduces the Root Mean Square Error (RMSE) of the model by removing points that have low confidence intervals of being placed in the correct locations. Point deletion performed in this manner improves the accuracy of the model, not the aesthetics.

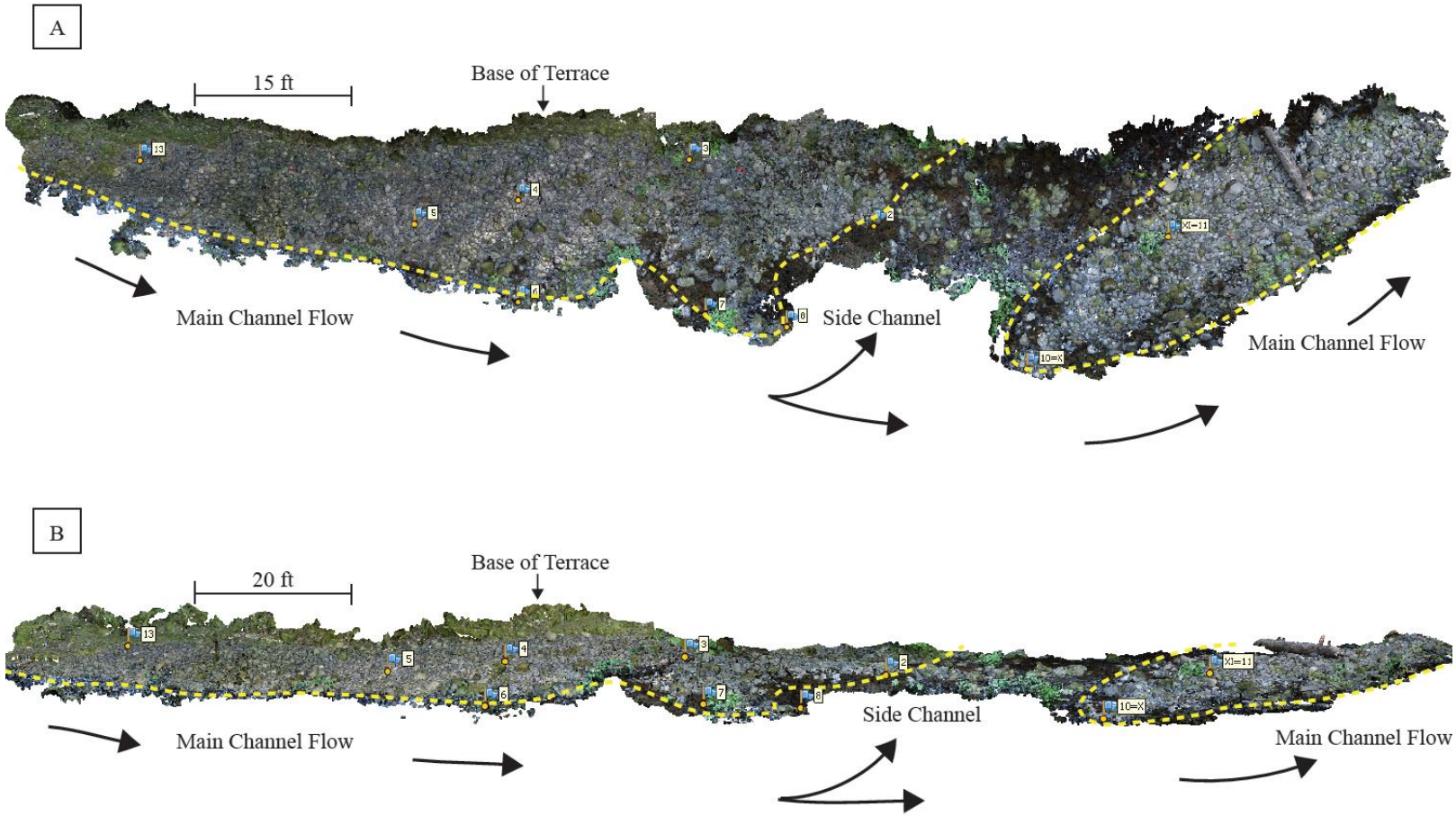

Figure 15. Dense clouds (not photographs) of Site 2: A) planview of the Site 2 dense cloud with GCP locations and flow indicated, B) Oblique view of the Site 2 dense cloud with GCP locations and flow indicated. Dashed line shows approximate edge of water at 100 cfs.

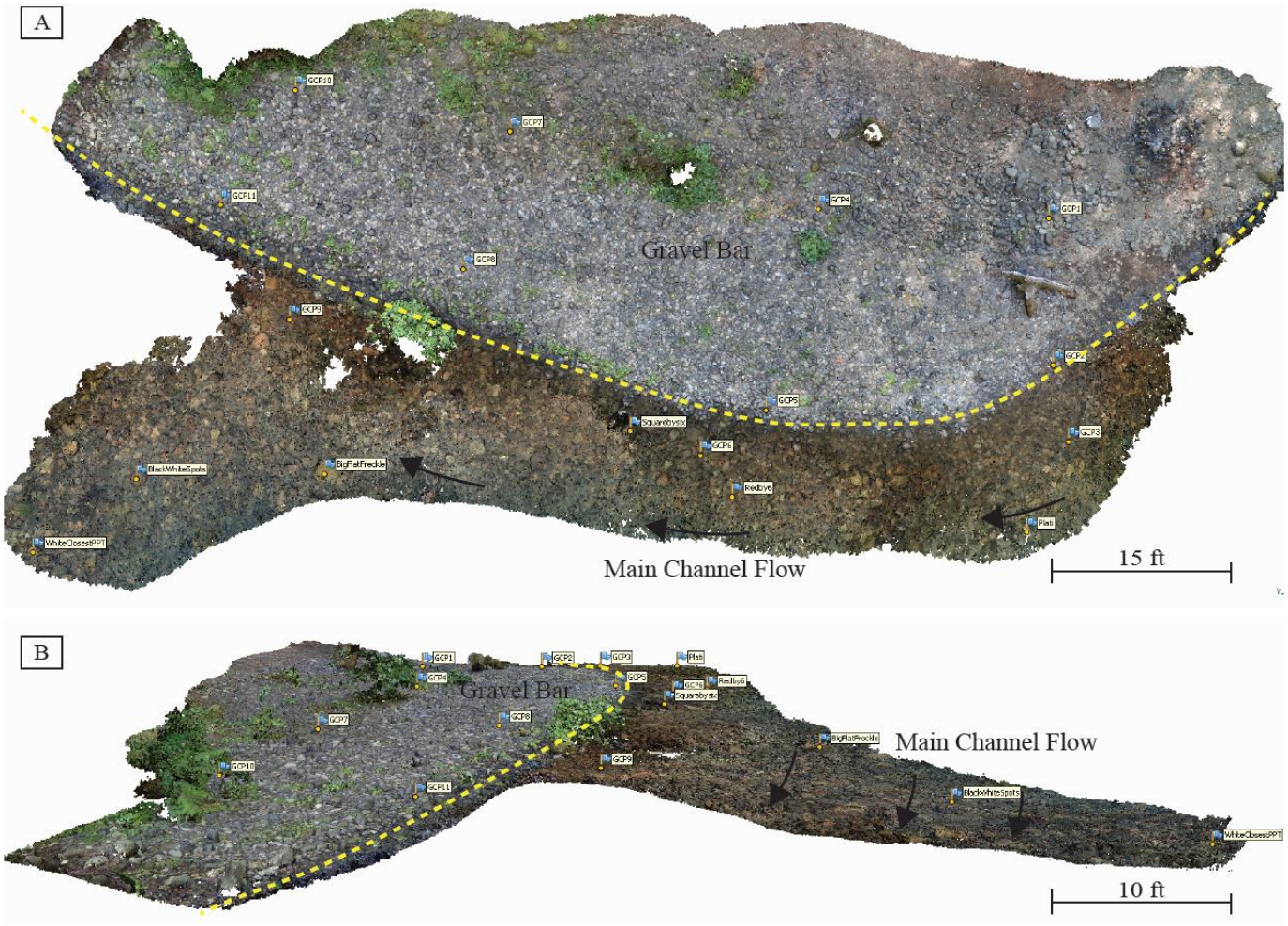

Figure 16. Dense clouds (not photographs) of Site 3: A) planview of Site 3 dense cloud with GCPs and flow indicated, B) Oblique view of Site 3 dense cloud with GCPs and flow indicated. Dashed line shows approximate edge of water at 100 cfs.

Figure 17. Dense clouds (not photographs) of Site 4: A) planview of Site 4 with GCPs and flow indicated, B) Oblique view of Site 4 with GCPs and flow indicated. Dashed line is approximate edge of water at 100 cfs.

CloudCompare processing. After gradual selection is completed in Agisoft, dense clouds are exported into CloudCompare for further editing and differencing. CloudCompare is a cloud editing software created by Daniel Girardeau-Montaut for the purpose of editing LIDAR point clouds. The program has numerous tools and plugins (tools created by other authors and added to CloudCompare) but the vegetation removal tools and differencing tools were used most often in this work.

Two tools were used to remove vegetation and remaining stray points from the models: The Caractérisation de Nuages de Points (Characterization of Clouds of Points) plugin, or CANUPO, was used for mass deleting and the scissors tool was used for manually deleting (Brodu and Lague, 2012). The CANUPO plugin separates vegetation points from ground points after the user trains the program to discriminate between the two. This is done by cropping sections of ground points and assigning them as their own class, and then doing the same for vegetation points. Once the two classes have been constructed, the program statistically measures the difference between the points in the two classes by measuring their 3D relationship to neighboring points, at varying scales assigned by the user, and learns to discriminate between them. It is possible to discriminate between vegetation and ground points by measuring relationships between a single point and its neighbors because groups of vegetation points have a more 3D shape to them compared to the more linear, or flat, shape of the ground surface. During the training process, the program reports a Fischer Discriminant value that informs the user on how separable the classes are and a Balanced Ratio value that informs the user about how well the program is performing. The user can iteratively run the training session,

improving the results until they are satisfactory. The training process produces a file that the user can then apply to the entire cloud to mass discriminate between vegetation and ground points, which allows the user to filter out vegetation and thin the point cloud (Figure 18). The major limitation of using this tool is that point clouds cannot exceed one million points or the program crashes. Thinning point clouds can significantly reduce the resolution of the surface, so when vegetation was minimal it was removed manually with the scissors tool instead of with CANUPO.

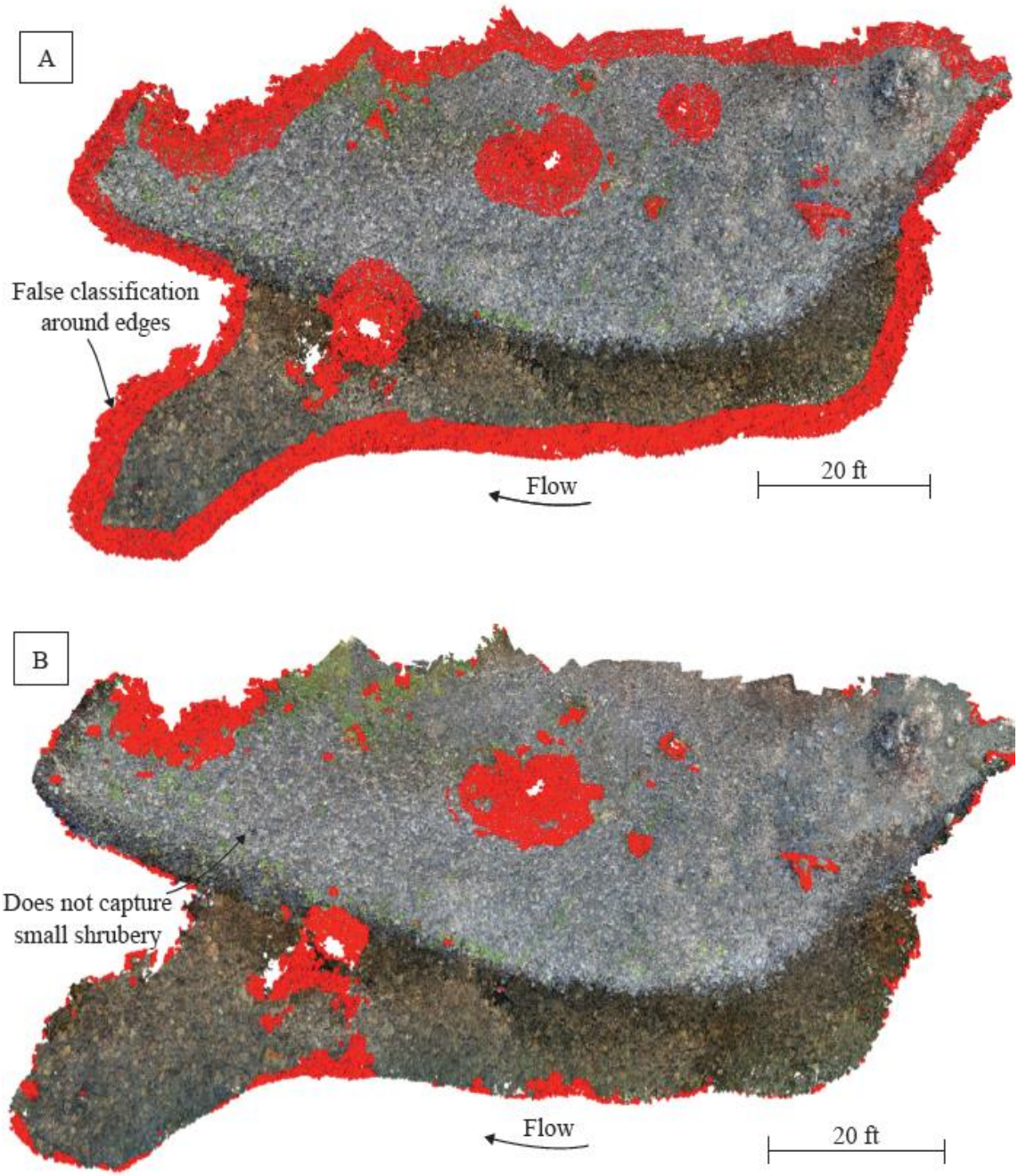

Figure 18. Dense clouds from the CANUPO vegetation classification process (red is classified vegetation): A) first attempt at classifier training resulted in significant false classification in water, B) second attempt resulted in a much more accurate classifier.

The plugin used for differencing clouds, and previously described in the pilot testing methods, is called M3C2. Although originally created for LiDAR point clouds, much like CANUPO, this tool also processes photogrammetric point clouds. Before the clouds can be differenced they must first be aligned. This was completed using the "align by point pairs picking" tool. This tool allows the user to define four points that both clouds share and aligns the clouds based on the position and elevation of those four points. For this study the four points chosen in each cloud were most often GCPs because the elevations were known, which helped assess the accuracy of alignment.

After the clouds have been aligned, M3C2 is used to calculate the topographic difference between the clouds. The first step is to identify the core points that will be used to compare the difference between the clouds. The 2016 clouds represent the baseline condition so they were chosen as the "reference" clouds, which contain the original set of core points, and the 2017 clouds are the "aligned" clouds. The core points can either be a subset of the reference cloud or the entire cloud. After the core points have been chosen, normals are calculated for the core points. Normals are the vectors used to choose the point in the "aligned" cloud that corresponds with the equal core point in the "reference" cloud (Lague et al., 2013). The two clouds can be differenced after normals are computed. The user can also choose to input a registration error reflective of the accuracy of the cloud alignment. This will produce an estimate of significant versus insignificant change (any change caused from poor alignment is insignificant).

ESRI ArcMap and ArcScene processing. The final processing steps after cloud differencing are completed in ESRI ArcMap and ArcScene. To transfer files between

Agisoft, CloudCompare, and ESRI, the files are saved as .LAS files. This file type makes transferring files easy and data is preserved well. After successful transfer, ArcMap is used to create a LAS database so the point clouds can be uploaded into the program; this is completed by using the “create LAS Dataset” tool. After upload, the clouds are color coded based on elevation using the basic symbology adjustments within the layer properties. I found that DTMs retain the most detail when kept as point clouds instead of interpolating a surface (although interpolation is an option). After the LAS database was created in ArcMap the clouds were then transferred into ArcScene for 3D viewing (Figures 19, 20, & 21).

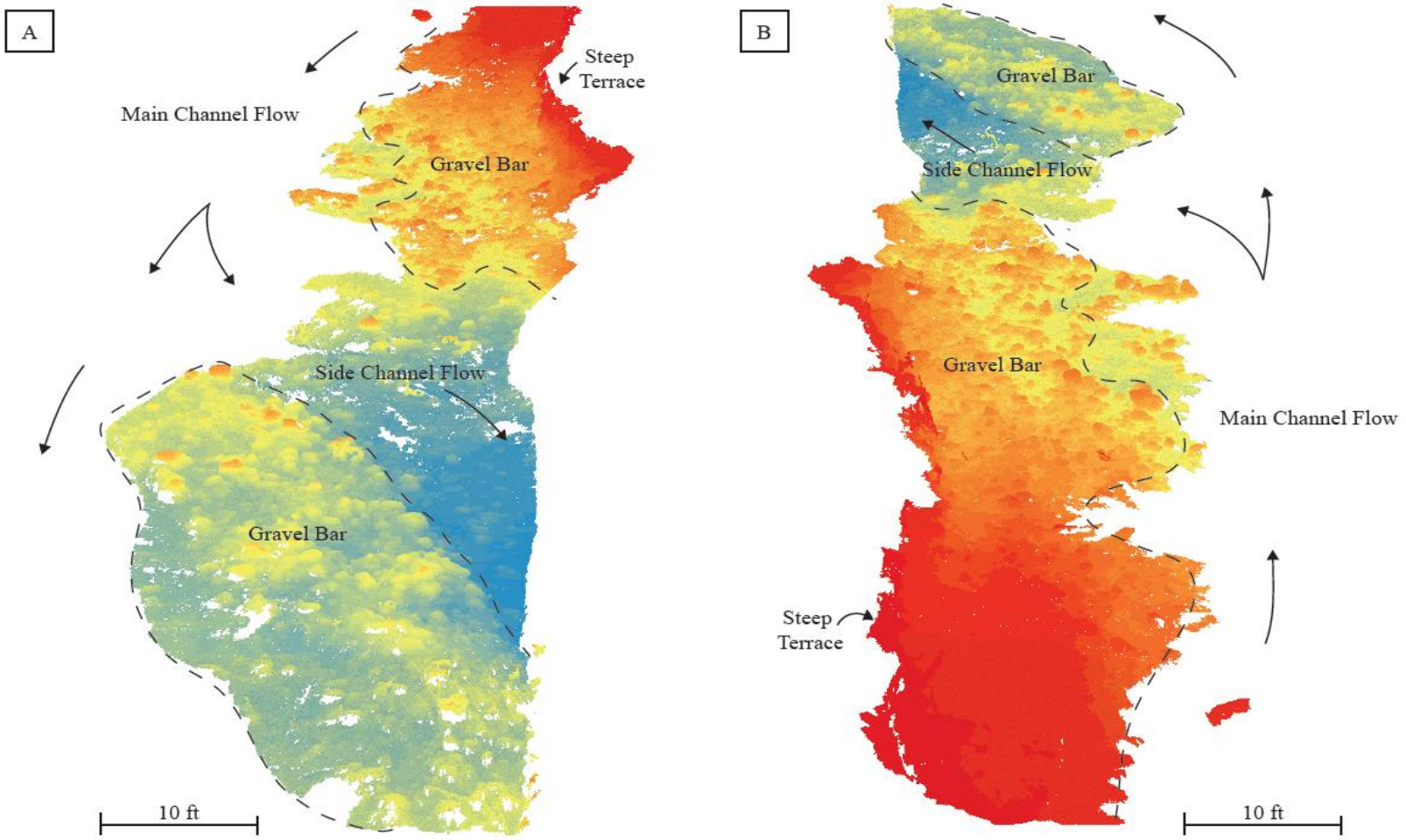

Figure 19. DTMs of Site 2: A) Site 2 looking upstream, B) Site 2 looking downstream. Dashed line is approximate edge of water at 100 cfs. Warm colors are topographically high and cool colors are topographically low.

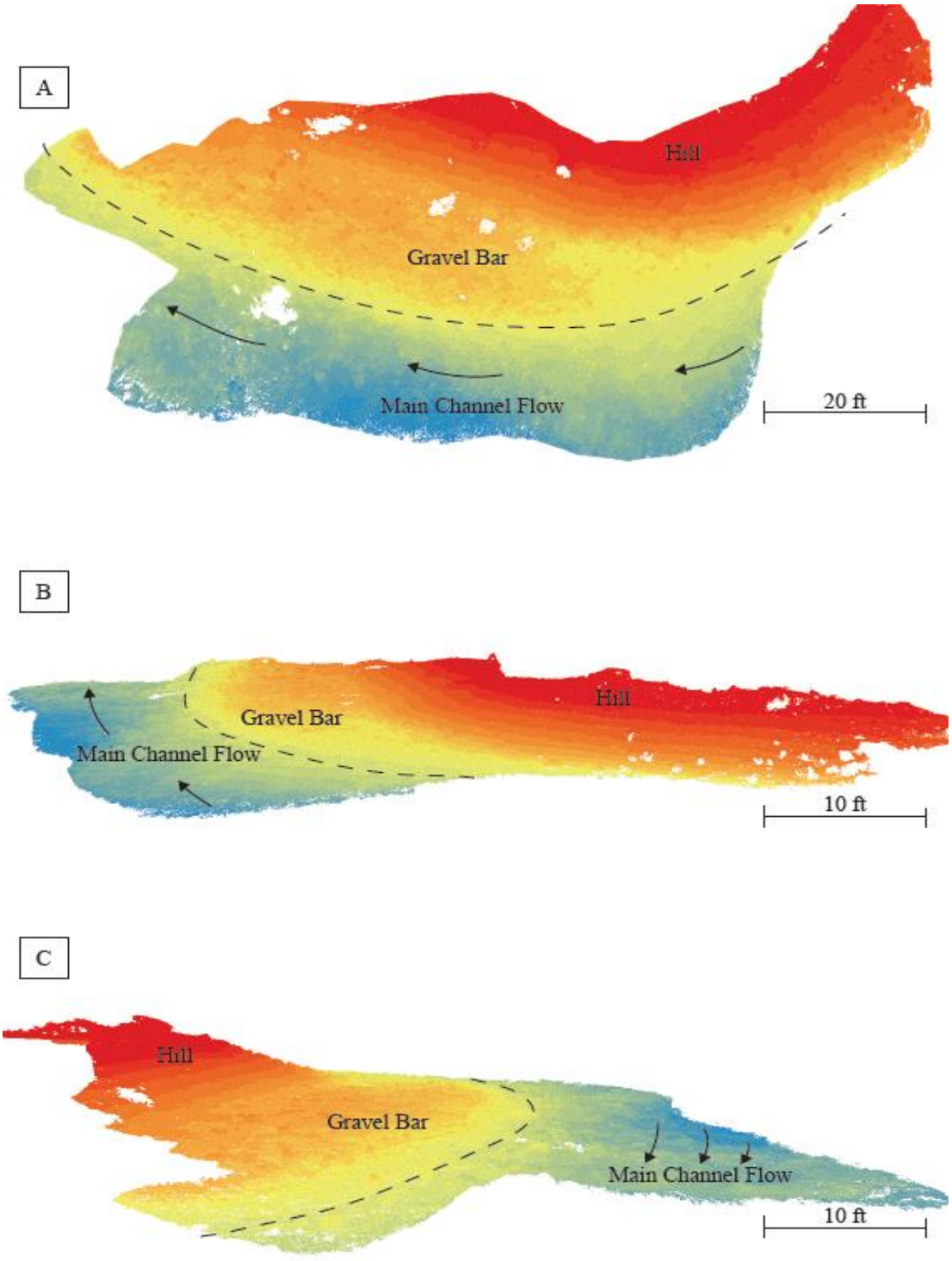

Figure 20. DTMs of Site 3: A) planview of Site 3, B) Site 3 looking downstream, C) Site 3 looking upstream. Dashed line is approximate edge of water at 100 cfs.

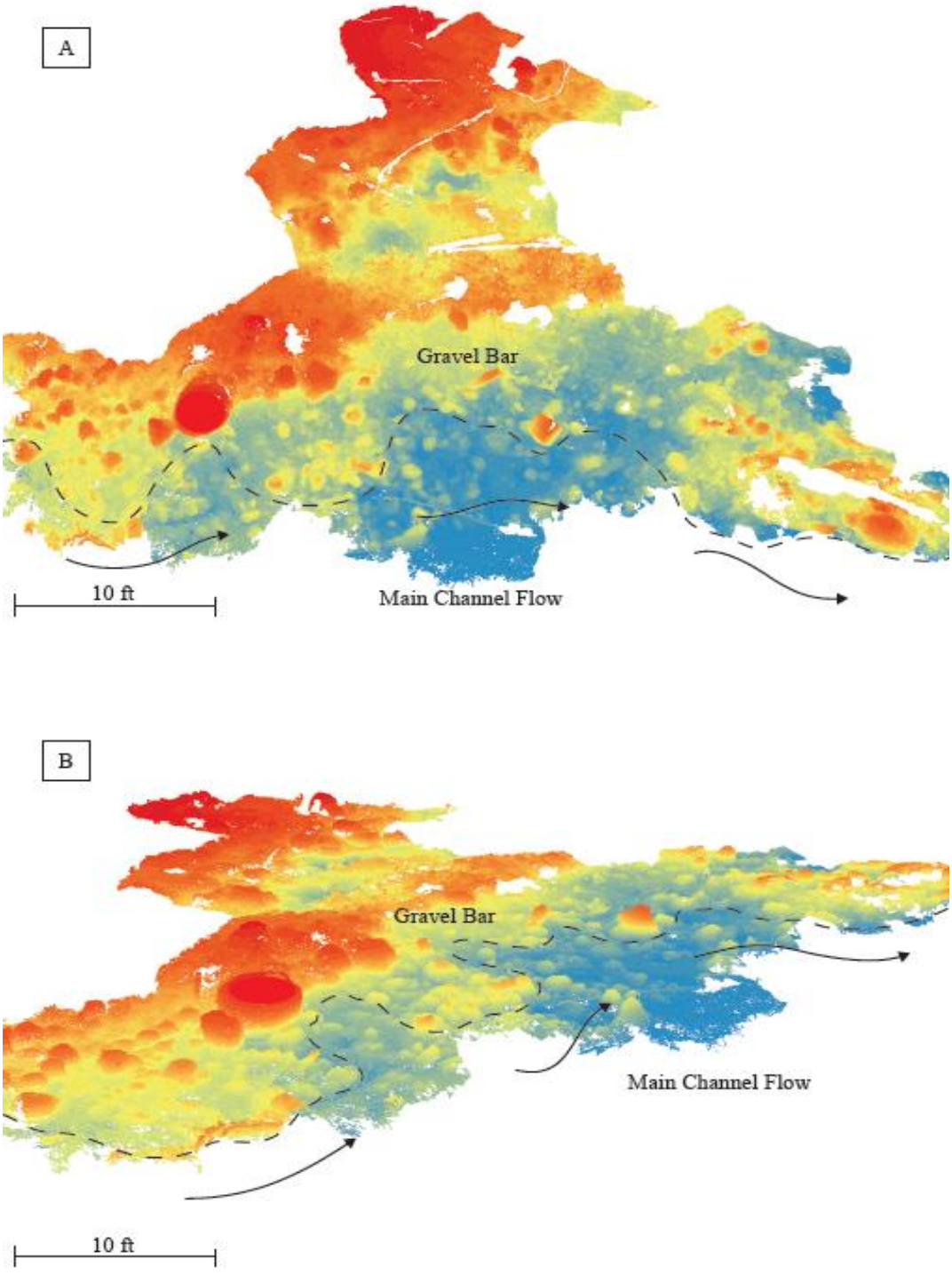

Figure 21. DTMs of Site 4: A) planview of Site 4, B) Site 4 looking downstream. Dashed line is approximate edge of water at 100 cfs.

Dense Cloud Accuracy Assessment

An accuracy assessment was completed for the 2017 dense clouds. This assessment was completely separate from the bundle adjustment and Root Mean Square Error (RMSE) process that was completed in Agisoft Photoscan. This assessment consisted of surveying the elevation of four additional points at Sites 2, 3, and 4 (this assessment was not completed at Site 1). The four surveyed points were not used as GCPs when building the point clouds, instead they were used to check the accuracy of the dense clouds after they were constructed. After the dense clouds were completed the elevations of the four additional points were checked and compared to the measured elevations. This assessment informs us of the spatial accuracy of the completed dense cloud for each site.

Storage Capacity Volume Estimate

A primary objective of using photogrammetry for this thesis is to estimate the volume of gravel that could first be used to fill void space on the existing, coarse channel bed, before completely transporting downstream of Barrier Falls. It is not assumed that this gravel would remain in the void space forever, instead it would fill the void space, which in turn would fine the existing bed, and actually increase transport. It has been observed in armored channels that fining of the channel bed results in increased bedload transport (Lisle & Church, 2002). Therefore, as augmented gravels fine the existing coarse channel bed, there should be an increase in sediment transport through the reach. This storage capacity estimate attempts to provide a rough estimate of the volume of augmented gravels that could fill interstitial spaces between particles on the existing bed.

This estimate should be viewed as an estimate of available space that augmented gravels can fill and not the amount of space that needs to be filled.

Site 2 was chosen as a pilot site for this volume calculation because it has the coarsest particle size distribution of the photogrammetry sites and is the best representation of the alluvial features in the thesis reach. Two raster point clouds were built from the Site 2, 2017 dense cloud in CloudCompare. During the rasterizing process the 2017 dense cloud was turned into a grid at an interval of 0.1 ft^2 (meaning that there is one point per 0.1 ft^2 cell) and two point clouds were created: one point cloud that selected the maximum elevation point within each 0.1 ft^2 cell and one point cloud that selected the minimum elevation point within each 0.1 ft^2 cell (Figure 22). The purpose of this was to have two point clouds that could be differenced, one point cloud representing the minimum elevations of the 2017 point cloud and one representing the maximum elevations of the 2017 point cloud, to estimate the height of available space where augmented gravels can be stored. It should be noted that the distances from minimum elevation points to maximum elevation points within each cell over estimates the actual distance; this is because the points do not sit directly on top of each other, therefore the distances are longer than if the points were stacked (Figure 22). The height applied over the area of the cloud gives us an approximate estimate of the storage capacity volume, which can then be extrapolated over the reach length to estimate how much gravel could go into storage before routing downstream past Barrier Falls.

The process for calculating the volume included creating the two clouds of minimum and maximum point elevations, differencing the two clouds using the M3C2

plugin, exporting the height distances from the differenced product into Excel, finding the mode of the height differences, multiplying the mode by the area of the gravel bar to calculate a volume in yd^3, and then converting the volume to tons using a conversion of 1.35 yd^3 of gravel per 1 ton. Also, the mode of the calculated distances between the two clouds was used instead of the average to try and eliminate skew introduced from having large immobile boulders on the bed that would produce extremely large differences in minimum and maximum elevations. After a volume was established for Site 2, it was extrapolated over the thesis reach. Finally, 25% of the total volume of gravel that could be stored in the thesis reach was subtracted to account for the approximate 25% of the channel that is composed of bedrock that will not store gravel like an alluvial reach.

This calculation is based on several assumptions and it should be taken as an approximate and conservative estimate. The first assumption is that this gravel bar is a good representation of the entire reach and that storage capacity here is representative of storage capacity throughout the reach. The second assumption is that no gravel will be stored in bedrock sections. It should also be noted that the total storage area calculated is an estimate that is based on an average channel width.

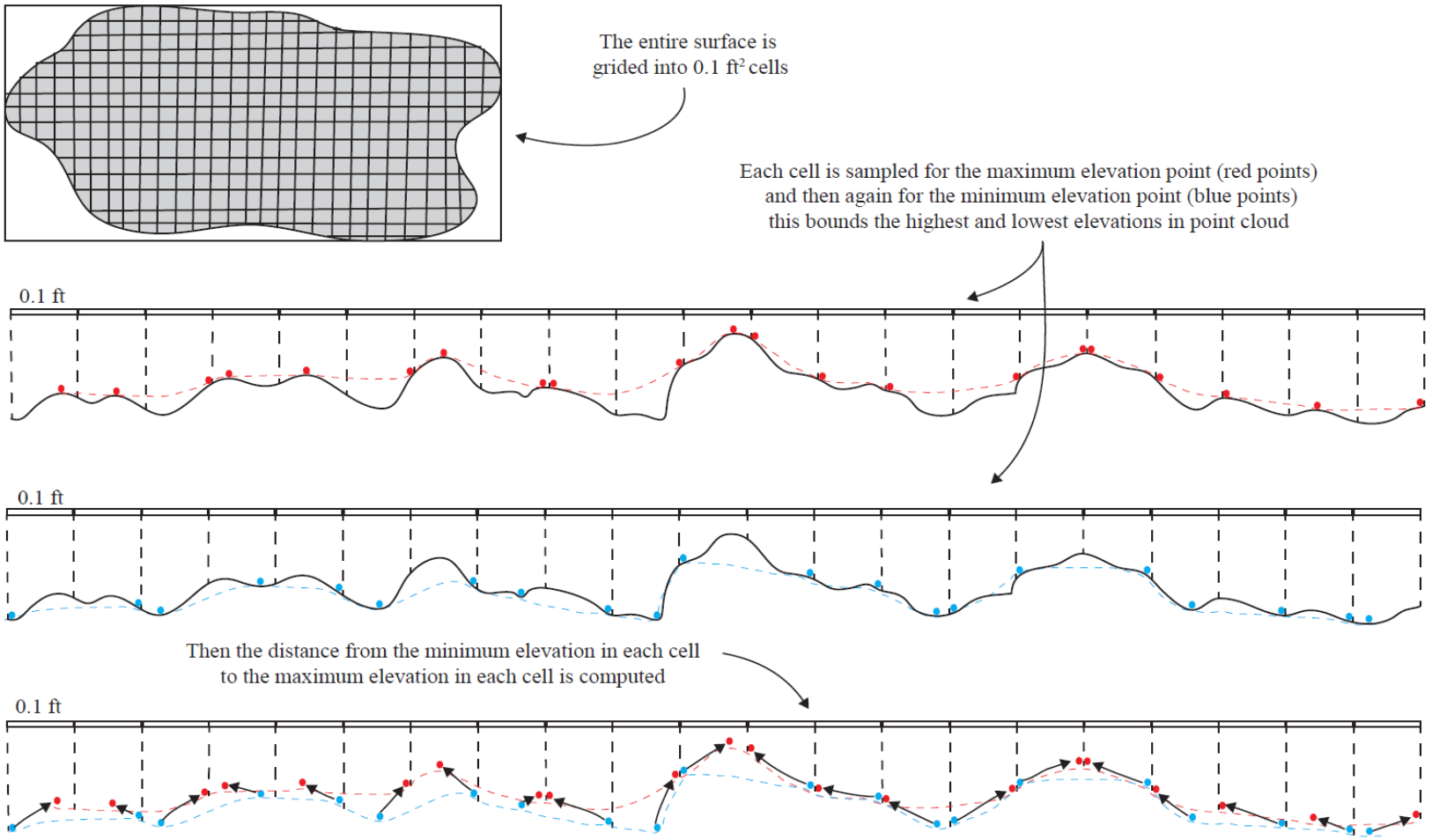

Figure 22. Generalized schematic showing how the distances between the Minimum and Maximum points are calculated to estimate the storage area where augmented gravels could be stored. Dashed lines reflect 0.1 ft areas.

HEC-RAS Methods

To use HEC-RAS as a tool for modeling sediment transport the user must create a geometry file, steady flow file, quasi-steady flow file, and sediment file. Channel geometry and the steady flow file are used to calibrate the hydraulic model so modeled water surface elevations are comparable to measured water surface elevations. This ensures that the channel geometry, flow, roughness, and slope of the model are representative of the actual river. After the steady flow calibration was complete, a quasi-unsteady flow file was created based on flows that commonly occur on the OGF. The quasi-unsteady flow file sets an upstream and downstream boundary condition that controls how flow is modeled through the rest of the system. The upstream boundary condition (the initial condition set at the farthest upstream cross section) is a "flow series." The flow series consists of different magnitude flows that last for specified durations, which creates a hydrograph that the model uses during sediment transport computations. The downstream boundary condition (the initial condition set at the farthest downstream cross section) for this study was developed using a flow rating curve. A flow rating curve is the relationship of water surface elevations (stage) at different magnitudes of flow. The flow rating curve used in the quasi-unsteady flow file was developed by running the steady flow model for a range of flows during the calibration stage. The sediment file requires the user to choose a sediment transport function, input bed gradations for each cross section, input the maximum existing sediment storage within the channel that could be potentially eroded, and the sediment

boundary condition at the farthest upstream cross section. Together, the geometry file, quasi-unsteady flow file, and sediment file are used to model sediment transport through the reach over the course of the input hydrograph.

HEC-RAS Data Collection

The purpose of the HEC-RAS model is to provide predictions about the transport and storage of augmented gravels that can then be tested using the photogrammetry techniques. To build the HEC-RAS model, input parameters are collected in the field including channel geometry (cross section form of the channel), roughness, and the particle size of the bed. After data collection, a spatially accurate replica of the study reach is built in model space, which can then be used to simulate flow and sediment inputs. Data collection for the HEC-RAS model took place the same week in July, 2016 as the photogrammetry GCP setup and survey. During this trip, 15 cross sections were surveyed with an auto level between the augmentation location and Barrier Falls. Similar to the GCP setup, previously established points from prior surveys by others were used to establish real elevations. Each cross section consists of 15 to 25 points, capturing major breaks in channel topography. Pebble counts were collected using a gravelometer at 10 of the 15 cross sections as well as a few adjacent positions. Pebble counts were collected (n=100 each count) for both the baseline condition and post augmentation condition.

Survey data were entered into Excel and then transferred to AutoCAD, and were then used to triangulate the positions of each cross section based on the distances from the cross section to known points. Once the cross section positions were established, the northings and eastings were exported from AutoCAD via .CSV files. The 2015 total

station thalweg survey points were also exported from AutoCAD and used in HEC-RAS to define the thesis reach.

HEC-RAS Data Processing

Geometry file and steady flow analysis. The cross section geometry was input in HEC-RAS to create the model channel geometry (Figure 23). The geometry input variables control important parameters within the model such as the spatial referencing of each cross section (e.g., the spatial referencing of point bars, riffles, pools, cascades, and other important channel characteristics), the channel hydraulic roughness, and the boundaries of main channel versus side channels and overflow areas. There are four variables that must be defined and set for each cross section: 1) the downstream reach lengths (the distance between the cross section and the next cross section downstream), 2) Manning's (n) values (hydraulic roughness), 3) main channel bank stations (the area within a cross section that is defined as being the main channel), and 4) contraction/expansion coefficients (coefficients that signal contraction or expansion of the channel that may cause energy loss between cross sections).

The downstream reach lengths were measured in AutoCAD when the cross section locations were triangulated. The main channel bank stations were defined based on field notes and topographic breaks within the cross sections. The contraction and expansion coefficients were left at default values based on the recommendations listed in the HEC-RAS user manual. Assigning channel roughness was the most difficult variable to input, but has substantial control on computed water surface elevations. Water surface elevations within the model were calibrated iteratively by adjusting the channel

roughness values until the modeled water surface elevations matched surveyed elevations for a known flow of 100 cfs. The first roughness value for the reach was calculated using Manning's equation, which returned a roughness value of 0.043. However, when used in the model during the calibration flows, this value was too low for the study reach, resulting in modeled water surface elevations that differed from measured elevations by more than 0.5 ft. To fix this, roughness values were iteratively adjusted until the modeled water surface elevations were within 0.1 ft of measured water surface elevations. This resulted in roughness values of 0.078 for the main channel and 0.12 for the banks and overflow areas. This adjustment is justified because the equation used to calculate the 0.043 value does not account for densely vegetated areas or large boulders within the channel, which are common on the OGF.

In general, the steady-flow model used for model calibration is based on gradually varied flow and the computation uses a 1D energy equation, which is calculated between cross sections in a step-wise fashion. The energy equation states that at the upstream cross section, the sum of: (1) the main channel invert elevation (thalweg elevation), (2) the flow depth, and (3) the average velocity divided by the gravitational acceleration, will equal the sum of those variables plus the energy head loss, at the downstream cross section (Brunner, 2001). The energy head loss is calculated by summing friction losses, such as roughness (Manning's n) and expansion/contraction of channel geometry. Data for channel geometry, flow, and roughness parameters were collected during field surveys. Cross section surveys provide the channel geometry inputs, thalweg elevations, and water surface elevations. Streamflow on the OGF is obtained from PGE flow release

records and from the USGS Ripplebrook Gage, and cross section velocity is calculated from discharge and cross sectional area. Substrate characterization based on pebble counts and vegetation mapping help identify a range of roughness values to input.

There are three important assumptions made when using the HEC-RAS 1D steady flow simulation: 1) flow is steady, 2) flow is gradually varied between cross sections, and 3) flow is one dimensional, meaning that velocity and depth are cross sectionally averaged (Brunner, 2001).

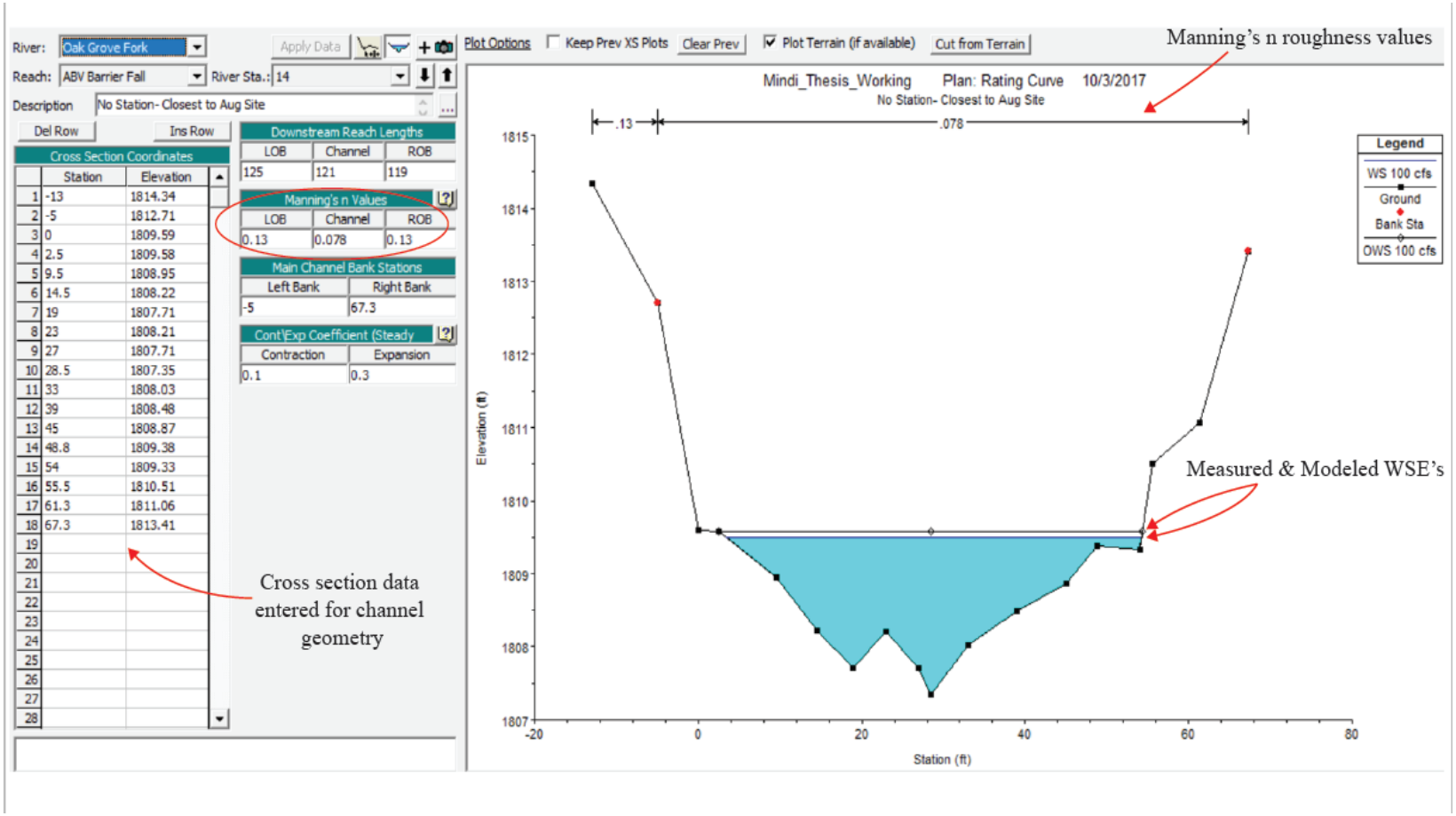

Figure 23. Cross section geometry in HEC-RAS showing that after calibration the measured and modeled water surface elevations only differ slightly. Manning's n roughness values are visible at the top of the cross section.

Quasi-unsteady flow. Quasi-unsteady flow files are used in HEC-RAS to model sediment transport and are based on estimated streamflow hydrographs that assign flow magnitudes and durations to the model (Brunner, 2001). For the quasi-unsteady flow files, flow series were created based on flows that occur on the OGF. Flow series can be created for any length of time ranging from 1 day to several years, which allows the user to make predictions about long term changes in sediment storage. A particularly sensitive input to the flow series data is the "computation increment." This input informs the model about how frequently it should recalculate and rebuild channel geometry as its processing flow data (Brunner, 2001). If the flows are high and sediment transport is occurring, then the computation increment needs to be set at a low increment so channel geometry is updated frequently. Model instabilities such as over estimations of erosion or storage will occur if the channel geometry is not updated frequently enough to keep up with transport. Along with the flow series, a rating curve (the relationship between flow and water surface elevation) was developed to inform the model on how water surface elevations change through the reach as flow varies. The rating curve was created by running the steady flow simulation after the calibration flows, for 100, 200, 500, 750, 1080, 1,200, and 1,500 cfs, and then imported into the quasi-unsteady flow file.

Sediment transport function. In order to perform a sediment transport analysis in HEC-RAS, the user must have a quasi-unsteady flow file, geometry file, and a sediment file. The sediment file defines important parameters such as the gradation of particles on the bed, particles introduced from augmentation, the transport function by which the sediment transport calculations are derived, the depth and width of erodible material on

the existing bed (bedload storage), and a boundary condition set at the upstream most cross section (Brunner, 2001). This model assumed an equilibrium load boundary condition, where the model calculates sediment transport capacity at the upstream cross section and uses this capacity as the sediment inflow transporting downstream (Brunner, 2001).

The transport function is the most critical parameter set in the sediment file. This model explored using both the Wilcock-Crowe and Ackers-White transport functions (Ackers & White, 1973; Wilcock & Crowe, 2003). These transport functions are two of eight possible transport functions in HEC-RAS. They were chosen based on the recommendations of others for sediment transport modeling in alluvial rivers (Snyder, personal communication).

Combining the sediment, flow, and geometry files, the model predicts where aggradation and degradation of sediment might occur both laterally within cross sections, and progressively downstream between cross sections. Simulating a variety of hydrographs, and knowing the recurrence probability of the peak flows within the hydrographs, allows predictions to be made about how long it might take augmented gravels to route past Barrier Falls, and the magnitude and duration of flows that are required.

Hydrograph analysis. Four different hydrographs were chosen to use in the HEC-RAS model for the sediment transport analysis; water years 1996, 2011, 2016, and 2017 (Figure 24). The purpose of choosing four varying hydrographs was to narrow down the flow characteristics needed to model sediment transport through the thesis reach. For this

reason, the sediment and geometry file inputs were held constant for the model runs, leaving the quasi-unsteady flow file as the varying parameter.

The hydrographs were chosen because they varied in flow characteristics. Water year 2017 was chosen because it was the hydrograph that would have influenced transport of the augmented gravels during the thesis lifetime (peak flow of 1,080 cfs), and because it had moderate flows with long durations, which is not present in the other hydrographs (Figure 25). Water year 2016 was chosen because it had a similar maximum peak flow as 2017 (1,220 cfs), but overall the flows occurred mostly as short duration and high magnitude (Figure 25). Water year 2011 was chosen because it had a similar peak flow (1,330 cfs) as 2016 and 2017, but it was the last year before PGE substantially increased baseflows below Lake Harriet (70-100 cfs baseflows) (Figure 25). Therefore, I can evaluate if increased baseflows have any impact on sediment transport (even though it is highly unlikely). Water year 1996 was chosen because it was a major flood year with the second highest flow on record (3,930 cfs) (Figure 25). By choosing these water years to model, I was able to focus on how the magnitude, duration, and baseflows impact sediment transport.

It is also important to understand the recurrence interval of the flows that are present in the hydrographs that were chosen for analysis. The 2017 peak flow of 1,080 cfs has a recurrence interval of 1.2 years, the 2016 peak flow of 1,220 cfs has a recurrence interval of 1.45 years, the 2011 peak flow of 1,330 cfs has a recurrence interval of 1.5 years, and the 1996 peak flow of 3,930 cfs has a recurrence interval of 59 years (McBain Associates, personal communication). All recurrence intervals are based

on post-dam data because of lack of pre-dam data. Knowing the recurrence intervals of the flows is important because it aids in estimating the time frame for the augmented gravels to reach Barrier Falls. If the model suggests that flows with a long recurrence interval are needed to transport the gravel past the falls then it can be determined that the gravel will not pass the falls within the five-year timeframe.

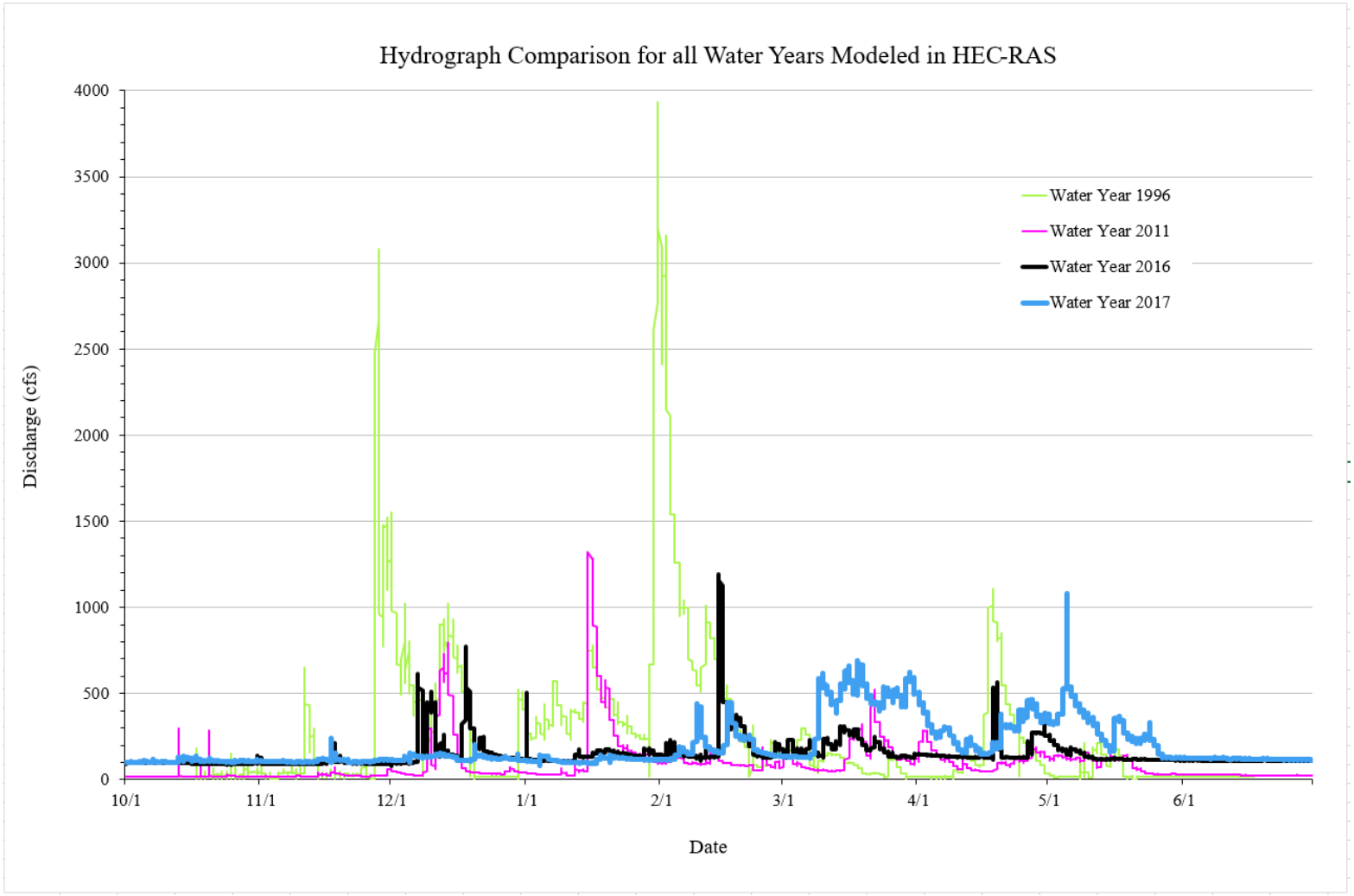

Figure 24. Hydrograph comparison of the four water years chosen for modeling in HEC-RAS.

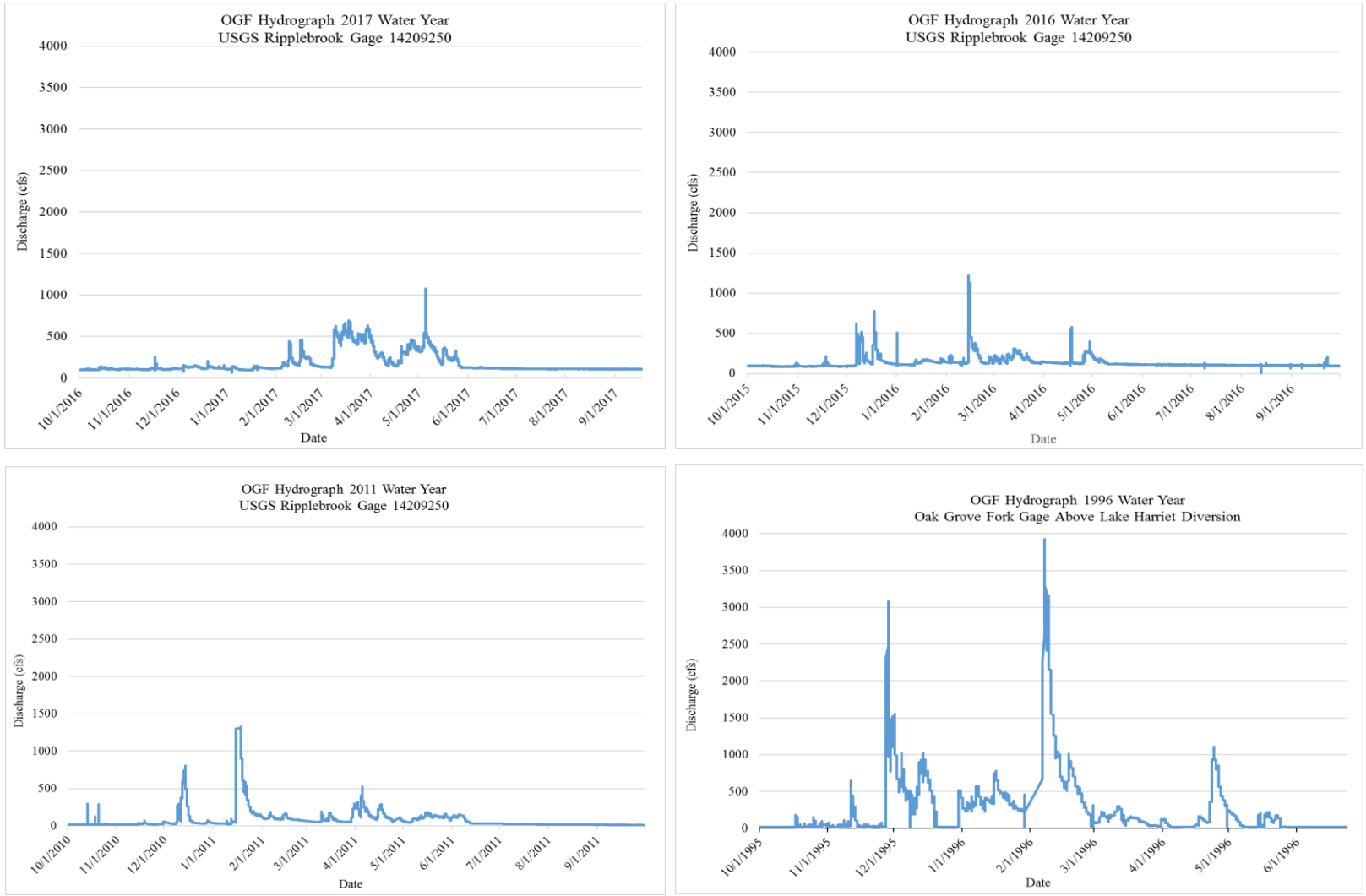

Figure 25. Individual hydrographs of the four water years that were modeled in HEC-RAS.

RESULTS AND DISCUSSION

Photogrammetry Results and Discussion

Individual Site Results

The results of the photogrammetry analysis vary by site and were greatly impacted by lighting condition, water depth, GCP placement, and camera stability. For example, the 2017 snorkeling effort at Site 1, immediately downstream of the augmentation location, revealed that the 250 tons of gravel introduced in September of 2016 did not transport far enough downstream to reach Site 1. The augmented gravel progressed downstream approximately 80 ft from the introduction site, but stopped in the closest pool, on the upstream boundary of Site 1. The pile significantly filled the pool at the upstream boundary of Site 1 and there is a sharp contrast between augmented material and native bed material (Figure 26). For this reason, any change recorded by the photogrammetry analysis, at any site, is attributed to natural geomorphic change unrelated to gravel augmentation.

Below, I report my observations and measurements for each site (i.e., absolute elevation changes), present a check point error analysis for each GCP (including a calculated Root Mean Square Error (RMSE)), followed by a discussion of each result. Success of the photogrammetry results is evaluated and compared between sites; the most successful sites resulted in complete site models, have low RMSE values, and low

alignment errors. All results are reported in English units, which is the convention in geoengineering fields in the United States.

Site 1. Site 1, located closest to the gravel introduction site, was the least successful of the photogrammetry models (Figure 26). Steep canyon walls and a dense tree canopy proved to be obstacles for obtaining good lighting conditions. It was necessary to wait to take photographs until midday, when the sun had completely passed over the canyon, to avoid shadows and contrast between bright and dark areas. However, the shadow created by the canyon walls darkened the channel to such an extent that there was insufficient light within the channel, and the colors of the river bed became homogenized to a point where the software could not align all of the photographs. A second obstacle was that the position of the site at the downstream end of the tightly confined canyon created high water velocities that made collecting stable, focused photographs through a snorkeling effort extremely difficult. Photographs that were blurry or unfocused could not be used and were removed, resulting in poor alignment of the remaining photographs. Changing conditions at the site between 2016 and 2017 also made the analysis of topographic change challenging. In 2016, the pool located at the upstream end of Site 1 was so deep that the bottom was not visible when snorkeling. This prevented GCP establishment in the pool area, resulting in photographs only being taken of the riffle area on the downstream end of Site 1. In 2017, the augmented gravels filled the pool creating shallower water and improved my ability to photograph the bed, but because there were no established GCPs, the 2017 model that captures the augmented gravels is not spatially referenced. The suboptimal lighting and velocity conditions also

resulted in poor alignment of the riffle section at Site 1. Altogether, these conditions resulted in incomplete models of the bed surface for 2016 and 2017 that do not share overlap, and therefore could not be compared.

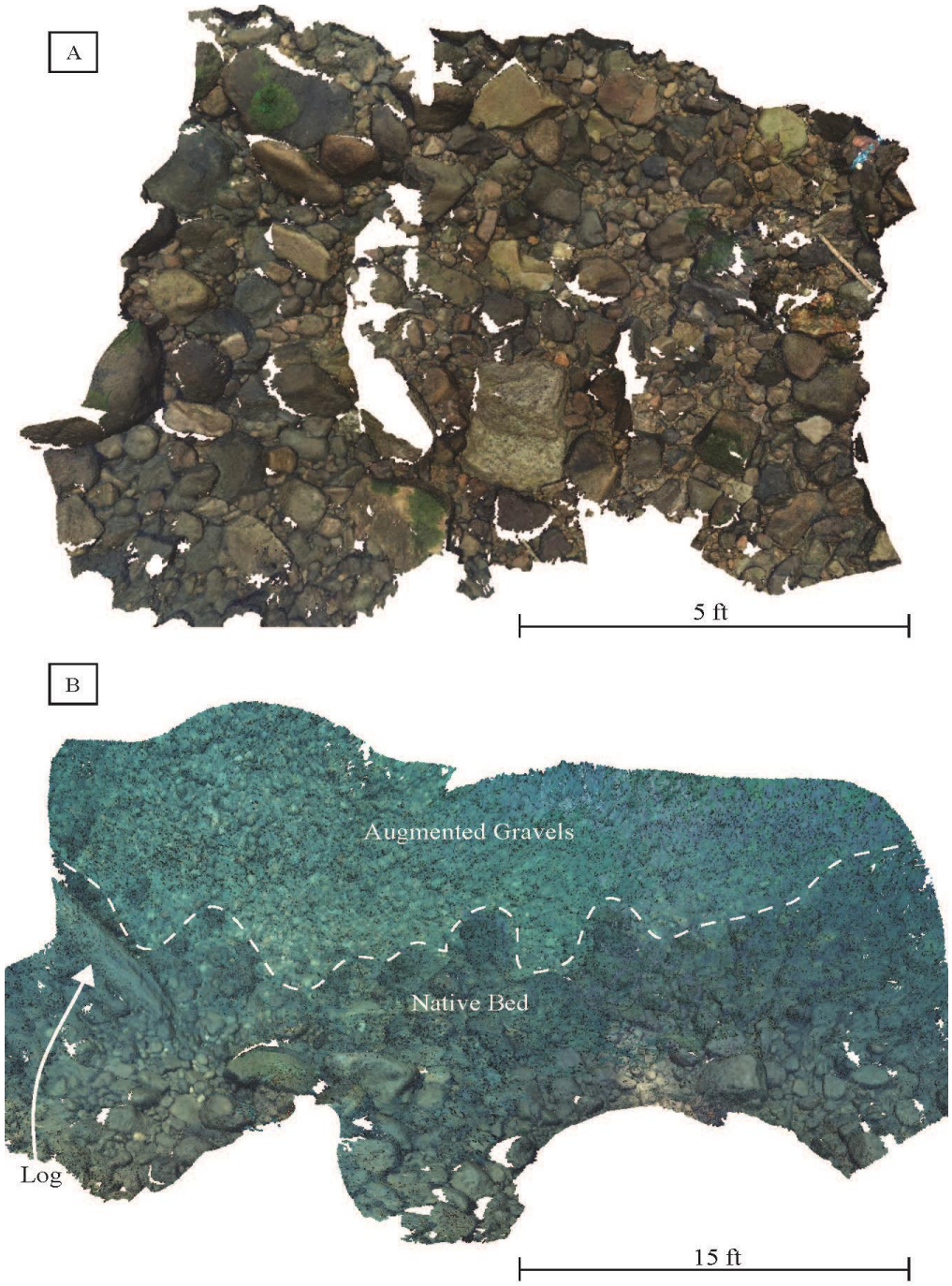

Figure 26. Site 1 dense cloud results: A) best alignment of photos at Site 1 for 2016, B) best alignment of photos at Site 1 for 2017. Dashed line is boundary between native gravels and augmented gravels. The 2016 and 2017 models do not share overlap.

Site 2. The photogrammetry analysis at Site 2 was more successful than Site 1 (Figure 27). Referenced dense clouds were completed at Site 2 for both 2016 and 2017. The accuracy assessment for the 2017 dense cloud returned an RMSE of 0.18 ft for the cloud overall. The highest error is within an area in the center of the cloud, near check point four, where the modeled elevation and measured elevations deviate as much as 0.27 ft (Table 1). This area was a problem area for photo alignment for both the 2016 and 2017 point clouds, resulting in the point cloud having to be processed in two "chunks", and then merged into a single chunk.

Although an accuracy assessment was not done for the 2016 dense clouds, it is assumed that the 2016 cloud also retains error in the same area as the 2017 cloud because elevations of known points differed between the two clouds as much as 0.45 ft for that area. However, even with accepting a vertical elevation error of 0.45 ft in that area, there is still an additional registered change of up to 0.5 ft (Figure 27). The remaining area of the two clouds was thoroughly checked for alignment errors, but GCPs 13, 2, 1, and some immobile boulders all reported correct values for both clouds, indicating that the high error is only isolated to the center region.

Table 1.Check Point Accuracy Assessment for Site 2.

Check Point Name	Measured Elevation	Model Elevation	Difference
Check Point # 4	1794.77 ft a.s.l.	1795.04 ft a.s.l.	0.27 ft
Check Point # 5	1798.11 ft a.s.l.	1798.16 ft a.s.l.	0.05 ft
Check Point # 6	1796.01 ft a.s.l.	1795.78 ft a.s.l.	0.23 ft
Check Point # 8	1795.33 ft a.s.l.	1795.43 ft a.s.l.	0.10 ft
Calculated RMSE			0.18 ft

The area where the 2016 and 2017 cloud elevations aligned most correctly is the side channel and downstream gravel bar, which is one of the more active portions of this site. 2017 high flows inundated the bar, captured by the movement of a large log that was transported approximately 60 ft downstream in early 2017. The downstream gravel bar shows deposition on the upstream end where sediment from the main channel deposited during high flows. There is also a fair amount of area that registered no change, which would be the case for large cobbles and boulders that are generally immobile.

Overall at Site 2, the product of M3C2 tool cloud comparison revealed that scour has occurred at the upstream end of the site near the water's edge and at the upstream end of the side channel (Figure 27). Additionally, approximately 0.5 ft of deposition occurred on the upstream bar and at the upstream end of the downstream bar. The deposition on the upstream bar is attributed to material falling downslope from the adjacent river terrace. The deposition on the upstream end of the downstream bar is most likely from sediment transport during high flows. Approximately 30% of the entire area registered as having no change (Figure 27).

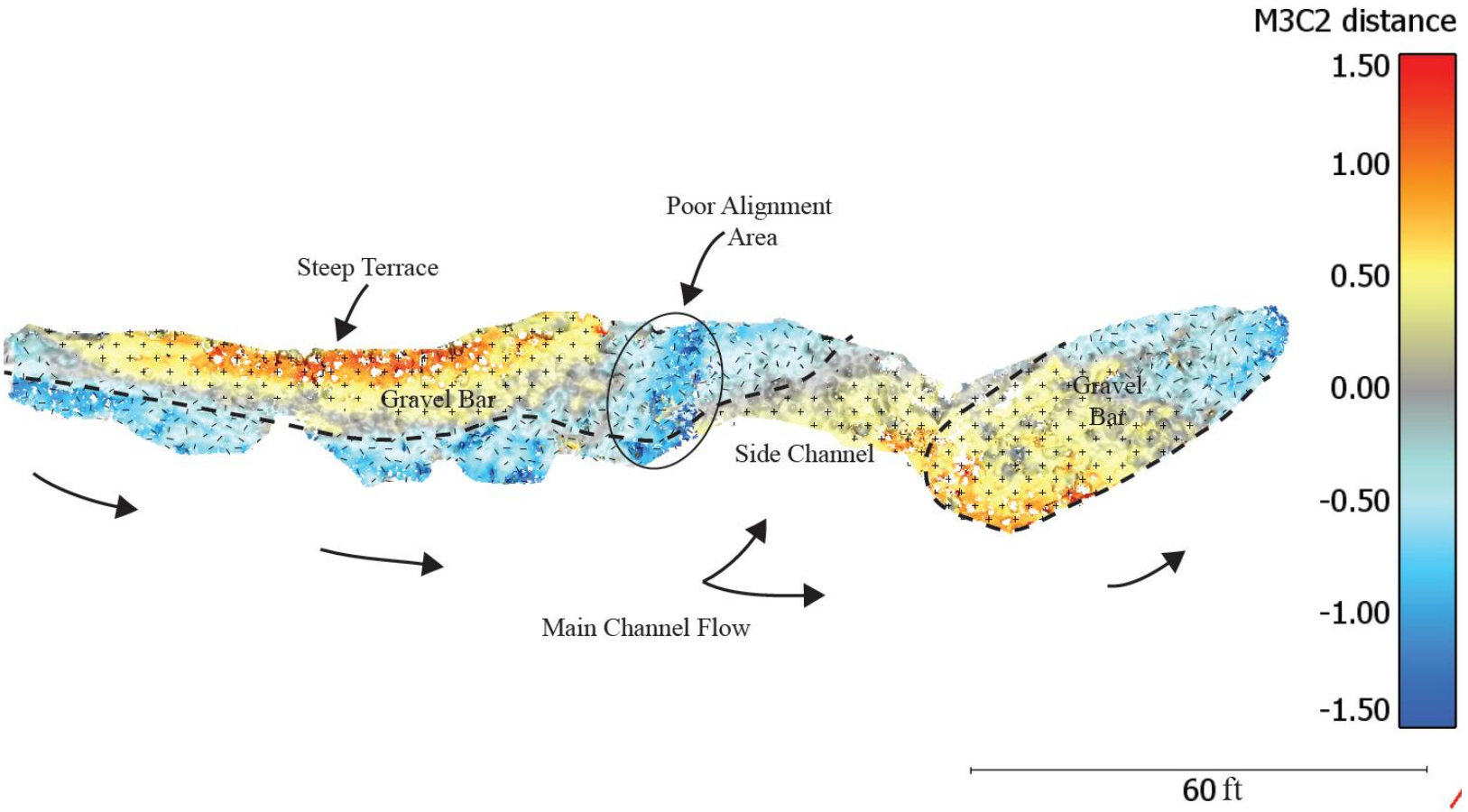

Figure 27. Site 2 differencing result. Warm colors are areas with deposition (plus symbol), grey is no change, and cool colors are areas of scour (minus symbol). The dashed line is the approximate edge of water at 100 cfs. Both scale bar units are feet.

Site 3. The photogrammetry analysis at Site 3 was more successful than Site 1 and 2. Dense clouds were built for both 2016 and 2017 (Figure 28). The range of change registered at Site 3 is small, varying from approximately -0.3 to 1.0 ft. The check point analysis on the 2017 dense cloud resulted in a RMSE of 0.14 ft for the entire site, with the error fairly evenly distributed between the checkpoints. Error within the water section of the site is not assessed because no check points were set. However, the clouds aligned well in the water section and the change registered is reasonable. The largest amount of change registered in the water section is at the most downstream end, which would be expected because the channel at this location is transitioning from a pool to a riffle crest so gravels being scoured out of the pool are being deposited on the riffle.

Table 2. Check Point Accuracy Assessment for Site 3.

Check Point	Measured Elevation	Model Elevation	Difference
Check Point # 4	1786.74 ft a.s.l.	1786.55 ft a.s.l.	0.19 ft
Check Point # 5	1787.56 ft a.s.l.	1787.67 ft a.s.l.	0.11 ft
Check Point # 6	1787.06 ft a.s.l.	1786.98 ft a.s.l.	0.08 ft
Check Point # 8	1786.44 ft a.s.l.	1786.27 ft a.s.l.	0.17 ft
Calculated RMSE			0.14 ft

If accounting for 0.05 ft as the registration error between the two clouds during alignment, then no change less than 0.05 ft is significant. The dominant pattern of deposition and scour at the site is what would be expected at a point bar, with the majority of the scour happening at the upstream end of the bar and majority of the deposition at the downstream end of the bar. Approximately 10% of the area registered as having no change.

The hill section of the site also registered change, following the same pattern of scour and deposition as the rest of the bar. This is because the hill section was most likely inundated like the rest of the bar during the peak flow of 1,080 cfs. Although no measured water surface elevation was taken at the site during the 1,080 cfs flow, the HEC-RAS model predicts a water surface elevation of 1,789 ft a.s.l. during that flow, and the top of hill section has an elevation of 1,790 ft a.s.l., meaning that the majority of the hill section would have been inundated. Altogether, the results at this site are representative of what can be expected for natural, year-to-year geomorphic change.

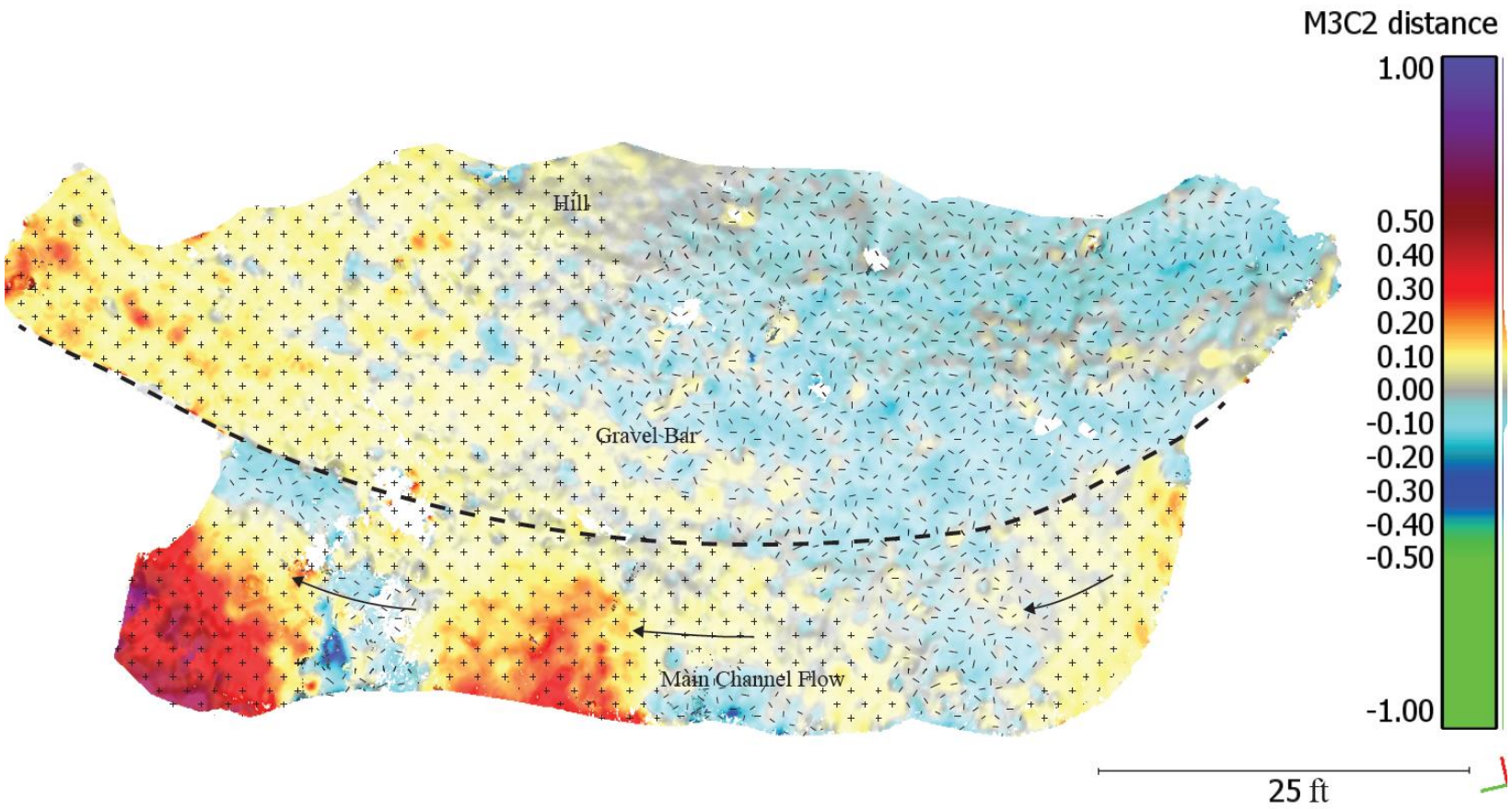

Figure 28. Result of differencing at Site 3. Warm colors are areas of deposition (plus symbol), grey is no change, and cool colors are areas of scour (minus symbol). The dashed line is the approximate edge of water at 100 cfs. Both scale bar units are feet.

Site 4. Site 4, the control bar, was the most successful of all sites for the photogrammetry analysis (Figure 29). Dense clouds for both 2016 and 2017 were successfully built. The 2017 check point analysis resulted in a RMSE of 0.05 ft. This site registered the least amount of change of any site with the majority of change falling between -0.3 and 0.3 ft. However, if we account for a 0.05 ft registration error between the 2016 and 2017 clouds, no change less than 0.05 ft is significant, which eliminates a large amount of the registered change on the bar. Unlike Site 3, this site has no discernable pattern for the registered change. However, the registered change near the water's edge shows large cobbles/small boulders that shifted slightly downstream.

Table 3. Check Point Accuracy Assessment for Site 4.

Check Point Name	Measured Elevation	Model Elevation	Difference
Check Point # 4	1714.87 ft a.s.l.	1714.93 ft a.s.l.	0.06 ft
Check Point # 5	1713.57 ft a.s.l.	1713.60 ft a.s.l.	0.03 ft
Check Point # 6	1714.07 ft a.s.l.	1714.15 ft a.s.l.	0.08 ft
Check Point # 8	1713.95 ft a.s.l.	1713.96 ft a.s.l.	0.01 ft
Calculated RMSE			0.05 ft

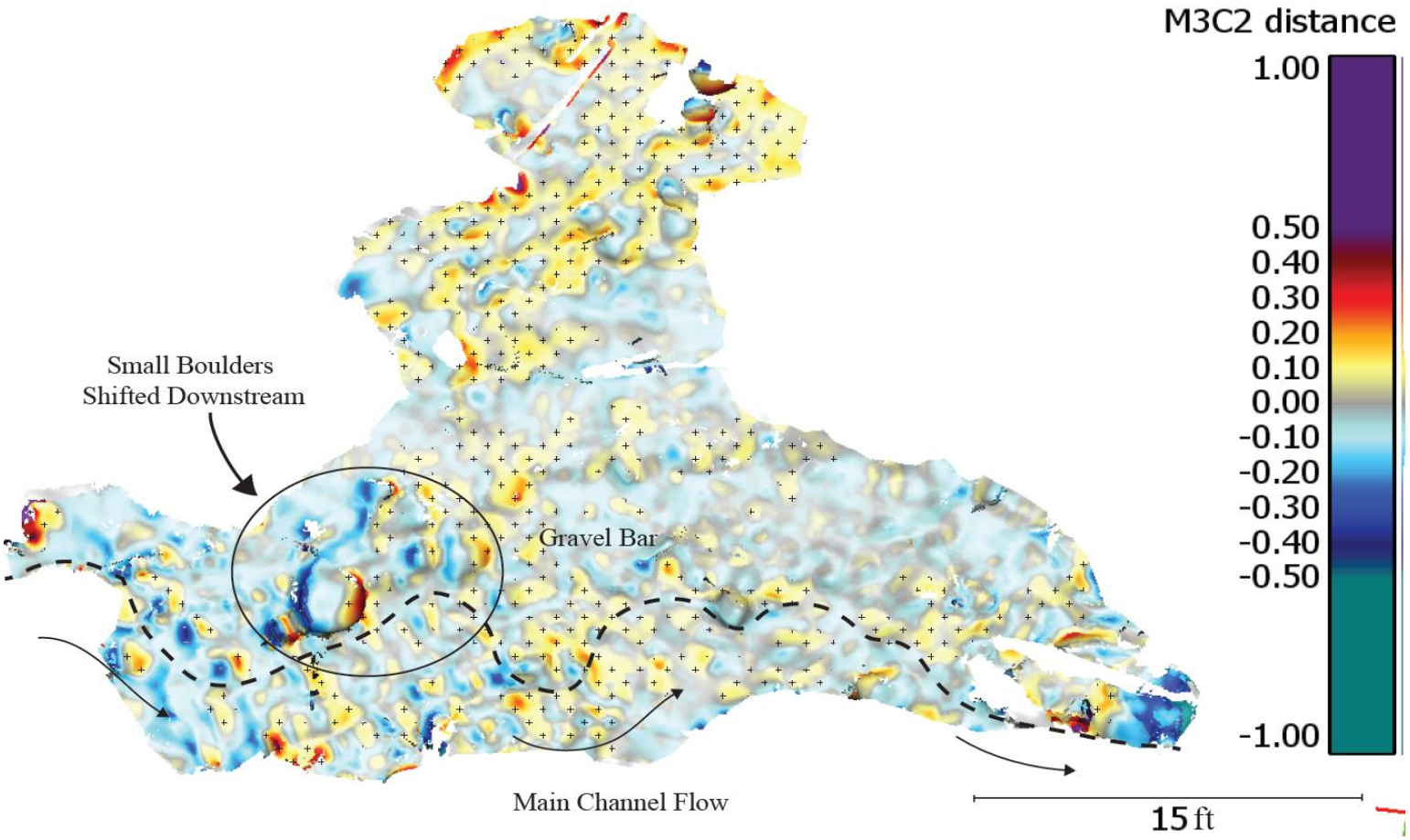

Figure 29. Result of differencing at Site 4. Warm colors are areas of deposition (plus symbol), grey is no change, and cool colors are areas of scour. Due to the irregular pattern only depositional areas were symbolized. The dashed line is the approximate edge of water at 100 cfs. Both scale bar units are feet.

Storage Capacity Volume Estimate Results

The volume estimate of void space that could be potentially filled with augmented gravels is approximately 800 tons of gravel for the entire thesis reach. This was quantified by first calculating the storage capacity of Site 2, by differencing the maximum elevations of gravels and minimum elevations of gravels to get a volume of void space that could be filled, and then extrapolating that volume over the area of the thesis reach. This volume is a rough estimate volume based on assumptions and averages that are discussed in the methods section.

The differencing analysis between the minimum and maximum elevation clouds returned a modal value of 0.10 ft, which I used to represent the height of empty space available on the gravel bar. By applying this height over the 3,200 ft^2 gravel bar area, the volume that could be lost to storage is equal to 288 ft^3, or approximately 10.5 yd^3. Using a density of 1.35 tons per yd^3, the storage capacity is equal to approximately 14 tons. If the thesis reach is on average 60 ft wide and is 4,000 ft long, then its area is 240,000 ft^2. This means that it is 75 times larger than Site 2, and could hold 75 times the amount of gravel, resulting in approximately 1,050 tons of gravel. However, we subtract 25% of that total to approximately account for bedrock sections that won't store gravel like alluvial sections, resulting in a final volume estimate of 790 (approximately 800) tons of gravel.

As stated before, this is an estimate based on assumptions and averaged data. Nonetheless, it provides an estimate of how much gravel could go into storage instead of immediately routing downstream. This does not mean that the gravel that goes into storage would stay there forever, rather satisfying the storage capacity will decrease the

void space in the channel and fine the bed, which in turn will increase bedload transport potential. The storage capacity estimate of 800 tons is interesting because it is close to the total amount of gravel that has been added thus far (250 tons in 2016 and 400 tons in 2017).

Photogrammetry Considerations

The four photogrammetry sites show almost no transport of the augmented gravels and very little natural geomorphic change occurs in this reach when flows are of the magnitudes and durations seen in water year 2017. Because the augmented gravels did not reach any of the sites, I was not able to determine if the sediment wave is propagating as a translational or stationary wave within the timeframe of this thesis. However, this method did capture natural geomorphic change that occurred with resolution better than 0.1 ft and accuracy ranging from 0.05 ft to 0.45 ft, which gives us confidence that the methodologies presented here could capture geomorphic change from gravel augmentation. Overall, it addresses the accuracy and applicability of using this technology in a river setting, the challenges of choosing and establishing appropriate sites, and provides a methodology for using photogrammetry in remote, steep, vegetated topography where GPS signals or high precision elevation instruments, such as RTK, are challenging to use.

The development of this methodology for using photogrammetry techniques within a river setting is a trial and error process. There are many factors to consider when choosing the site, establishing ground control points, and choosing the survey interval. Using a random site selection process is not a recommended approach. Ideally, subaerial

sites will have minimal vegetation, and wetted channel areas will fit within an acceptable depth range that does not limit sunlight.

If photographs are to be taken from above the water surface, flow needs to be as close to laminar as possible, with little to no aeration from turbulence or currents, and shallower than approximately 2.5 ft (if flow exceeds this depth then distortion becomes too great). Anytime photographs are taken above water, light refraction and distortion must be considered and acknowledged. Glare is another important factor when photographing from above the water surface. It is important to photograph a site from multiple angles to capture the 3D structure of the channel, but sun glare can make this impossible. If a site is photographed only from one angle, then distortion within the model is much more prominent and will cause a bowl shape effect of the point cloud. The addition of temporary GCPs within the channel area can help to eliminate this kind of distortion.

If photographs are to be taken underwater, with a regular camera, then the section must be shallower than six to eight ft (the depth at which red light is lost) but deeper than approximately three ft, or not enough distinguishable features are captured in each photograph for the program to align photos. The loss of red light decreases the likelihood of Agisoft Photoscan being able to align the photographs. Agisoft relies on distinct features and colors to align photographs, which is why irregular surfaces align better than smooth, homogenous surfaces. When red light is lost, the channel bed becomes one homogenous color (bluish green in this case) making it incredibly difficult to align

photos. Also, a uniform algae coat that covers the edges of rocks can eliminate distinct shapes, inhibiting the ability to align photographs.

Establishing GCPs in areas that fit the depth criteria is crucial to project success. For underwater areas that are captured from below the water surface, GCPs should be set between three ft in depth and six ft in depth so they can be captured and used within the photoset. Setting GCPs within this depth zone is a challenge and most likely will require a snorkeling or diving effort (hammering rebar post underwater requires a creative effort). In channel areas where photographs are taken from above the water surface, permanent GCPs should be set throughout the area, and temporary GCPs can be surveyed on distinguishable features to supplement control and help eliminate distortion. Permanent GCPs set on land should capture as much topographic difference as possible and should be clearly visible in the photographs. Permanent GCPs should be set in such a way that movement is extremely unlikely.

HEC-RAS Results and Discussion

In summary, the Ackers-White sediment transport function produced more stable model results than the Wilcock-Crowe function. This is most likely because the Wilcock-Crowe transport function is designed to model a range of particle sizes, including sand, which is rare in the thesis reach. It may also be because the Wilcock-Crowe function is designed for a fully alluvial channel, whereas the OGF is only a semi-alluvial channel with many bedrock sections. For these reasons, the remaining results, figures, and discussion will be regarding the model runs using the Ackers-White sediment transport

function.

HEC-RAS Overall Results

The HEC-RAS sediment transport modeling resulted in small changes in gravel storage and transport with the magnitude of flows seen in water years 2011, 2016, and 2017. The longitudinal profile results for these years show changes on the order of tenths of feet for some cross sections, but most cross sections showed changes less than one tenth of a foot (Figure 30). Water years 2011, 2016, and 2017 all have similar magnitude yearly peak flows of around 1,200 cfs. However, the water years were chosen because of differences in the structures of their hydrographs and not solely on peak flows. The purpose of choosing these water years was to explore the significance of the differences between the hydrographs and see if the yearly peak flows are the major driving forces of transport, or if other, smaller magnitude flows, are also contributing to transport. Because the most change was seen when modeling the 1996 hydrograph, the results suggest that large peak flows are the major driving factor of sediment transport and that summer baseflows, and even moderate long duration flows, are not major contributors. For the OGF gravel augmentation project, this means that receiving flows of the magnitudes seen in 2011, 2016, and 2017 will not result in transport downstream of Barrier Falls within the five-year time frame.

The modeling did result in more substantial changes in storage and erosion for water year 1996. There were two peak flow events with over double the magnitudes seen in the other water years. This resulted in deposition at some locations greater than 1 ft, and scour at some locations greater than 0.5 ft. The other water years show that small

amounts of transportation occurs (partial bed mobility) with flows at approximately 1,200 cfs, which means that in water year 1996 there would have been three peak flows capable of partially mobilizing the bed, two of which would have fully mobilized the bed. Model results from the 1996 model runs show deposition and scour occurring through the reach, suggesting that with multiple flows of such high magnitude, it could be possible to transport material long distances during a single water year.

Overall the sediment transport modeling results suggest that partial mobility of the bed occurs at approximately 1,200 cfs and the threshold for total bed mobility exists somewhere between 1,200 cfs and 3,000 cfs. Additional model runs are needed to narrow this zone. To estimate the time frame of which the augmented gravels will transport downstream of Barrier Falls, there must be a relation of transport of augmented gravels to the frequency of high peak flows (recurrence interval of flows). If the next five years produce hydrographs with more common recurrence interval peak flows such as those in 2011, 2016, and 2017 (approximately 1.5-year recurrence intervals), it is likely that we will continue to see small amounts of transport but not enough transport to pass downstream of Barrier Falls. If the next five years produce less frequent (high magnitude) peak flows such as those in 1996 (59-year recurrence interval), there is a higher likelihood of long distance transport, although it would likely take multiple of these events to reach Barrier Falls. If sediment transport modeling on the OGF is done in the future, I recommend modeling flows with recurrence intervals that vary between the flows modeled in this thesis, to better develop the relationship between flow magnitude and transport distance.

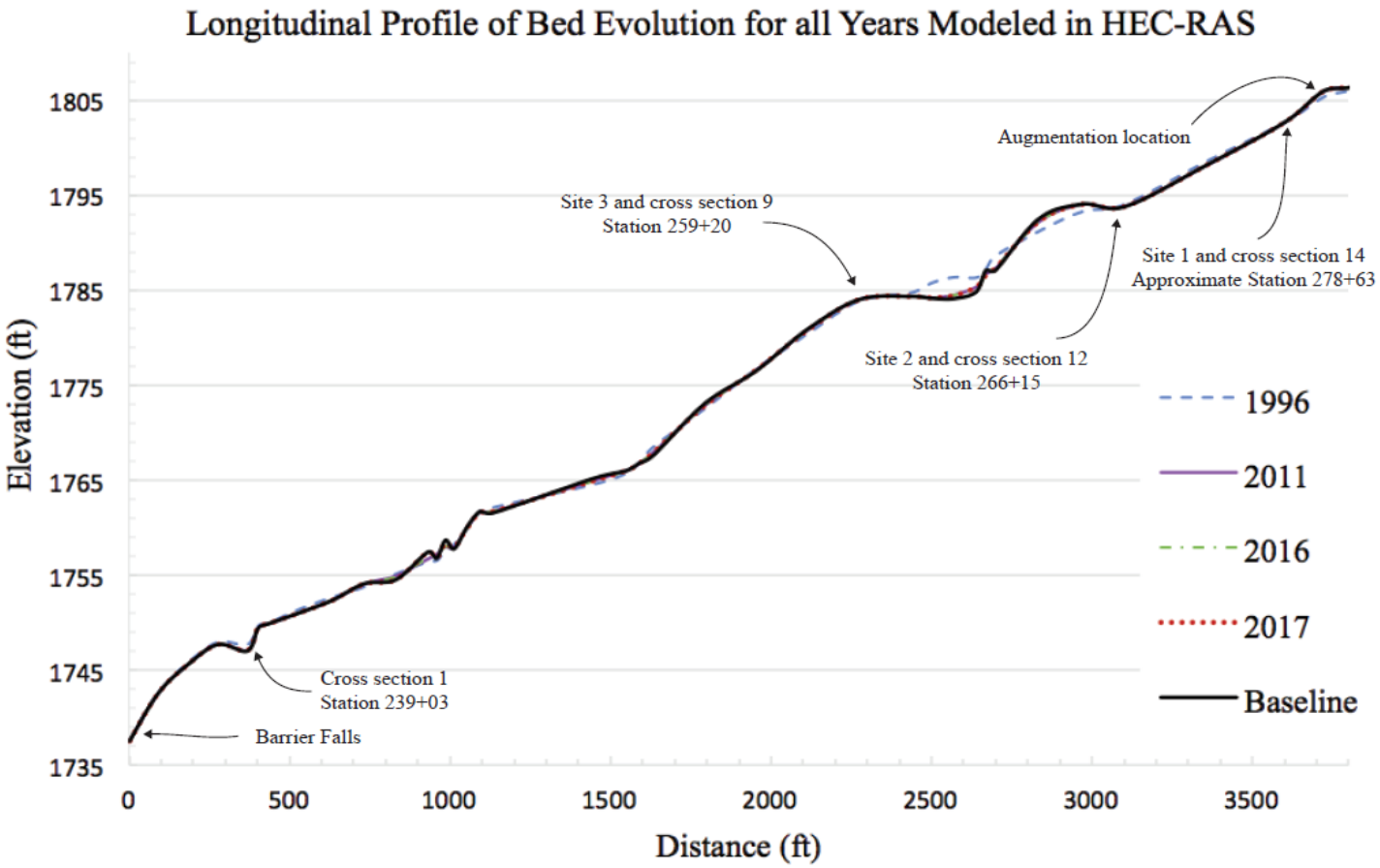

Figure 30. Longitudinal profile (baseline in black solid line), showing modeled bed evolution for all four water years. The 1996 water year shows the greatest deposition and erosion for all water years.

HEC-RAS Results Compared to Photogrammetry Results

The results of the HEC-RAS analysis generally agree with the photogrammetry analysis, and show that very little transport and storage of sediment occurred during the 2017 water year. The four cross sections that are closest to the photogrammetry sites (cross sections 14, 12, 9, and 1, see Figure 6) are looked at in detail below to compare the results of the HEC-RAS modeling and the photogrammetry.

Model output for cross section 14 predicted 0.1 ft of deposition during water years 2011, 2016, and 2017, and experienced 0.1 ft of scour during water year 1996 (Figure 31). The results predicted at this cross section for water years 2011, 2016, and 2017 were very similar. The photogrammetry results for Site 1, which is just upstream of cross section 14, show that augmented gravel did transport into the pool area of the site but did not make it downstream to the riffle crest where the cross section was measured. Although the cross section results show that 0.1 ft of deposition could have occurred during 2017, the difference between zero change measured from the photogrammetry analysis and the 0.1 ft measured in the HEC-RAS model is not significant enough to suggest if one method is more effective than the other in terms of capturing sediment wave propagation.

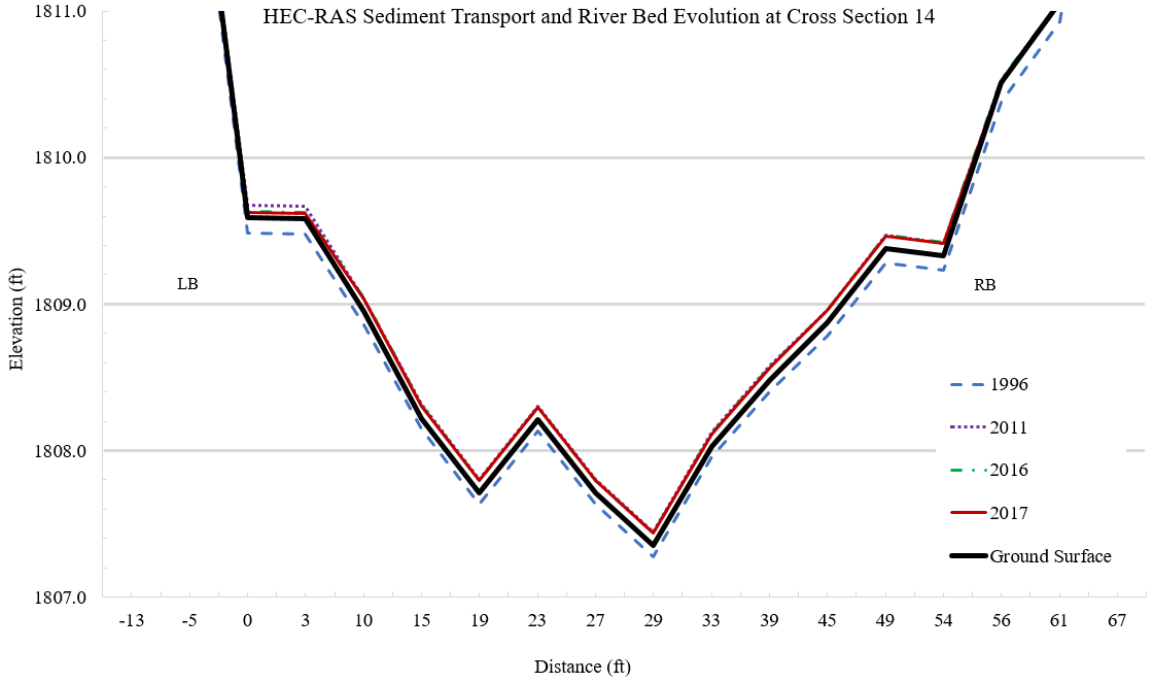

Figure 31. Bed evolution comparison at cross section 14 for all water years modeled.

Cross section 12 experienced 0.05 ft of deposition in some areas for 2011, 2016, and 2017 and up to 0.2 ft of deposition during water year 1996 (Figure 32). The results predicted at this cross section for water years 2011, 2016, and 2017 were very similar. The photogrammetry results for Site 2, which encompasses cross section 12, did show change, most of which was between -0.5 and 0.5 ft. The difference in reported values between the two methods could be a result of a few factors, the first being that much of the change reported using the photogrammetry method was downstream of the cross section location, in the side channel and downstream bar area, whereas the cross section is toward the upstream end of the photogrammetry site, where most of the photogrammetry change is attributed to material contributed from the terrace. The second factor being that the HEC-RAS model is only capturing one cross section within the

overall site, which results in a less detailed analysis, and the third reason being that there were some accuracy issues within the 2016 and 2017 dense clouds, which resulted in false change being reported.

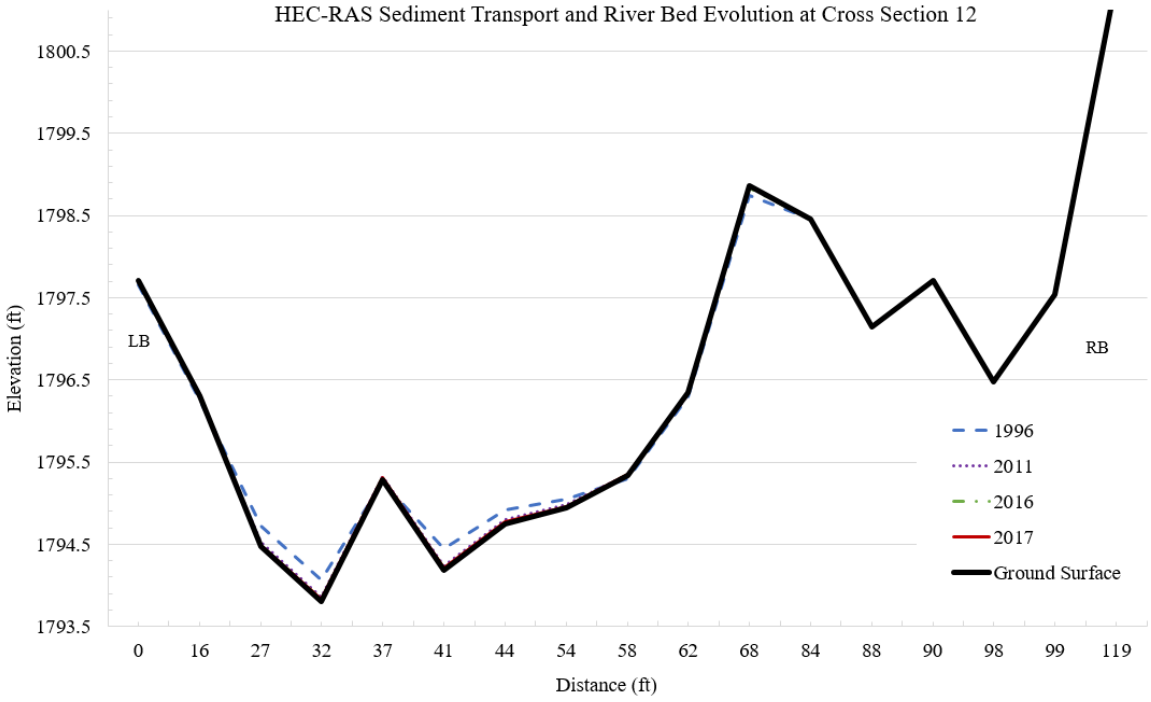

Figure 32. Bed evolution comparison at cross section 12 for all water years modeled.

Cross section 9 experienced no change during water years 2011, 2016, and 2017, and 0.5 ft of change during water year 1996 (Figure 33). The photogrammetry analysis for Site 3, which encompasses cross section 9, also showed very little change occurring during 2017 for the gravel bar and hill section. The photogrammetry analysis does show that up to 1 ft of accretion happened in the channel section, however the accuracy in the channel section was not measured during the checkpoint survey, so the change is unverified. Overall, results of the two methods support each other at this site.

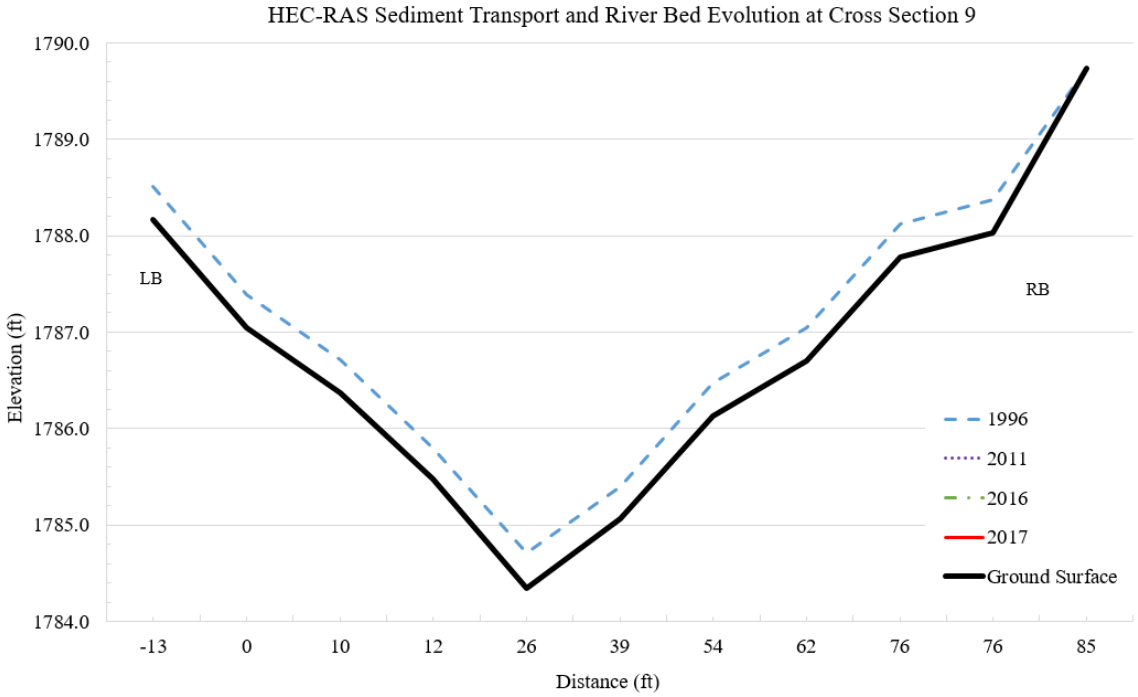

Figure 33. Bed evolution at cross section 9 for all water years modeled. 2011, 2016, and 2017 do not show up because there was no change from baseline condition.

Cross section 1 was chosen to compare to the control bar because it is the next closest cross section to the control bar besides cross section 0 (Figure 34). Cross section 0 was not chosen for comparison because it is the farthest downstream cross section and sets the boundary conditions for all upstream cross sections in the model. The cross sections that set the boundary conditions respond differently to change than the other cross sections; for example, the upstream cross section (cross section 15) has an equilibrium condition set where neither scour nor deposition can occur. Therefore, neither the upstream most or downstream most cross section was chosen to look at in detail. Cross section 1 experienced 0.05 ft of deposition during water years 2011, 2016, and 2017, and experienced 0.8 ft of deposition during water year 1996. The

photogrammetry results on the control bar agree with this magnitude of change for water year 2017.

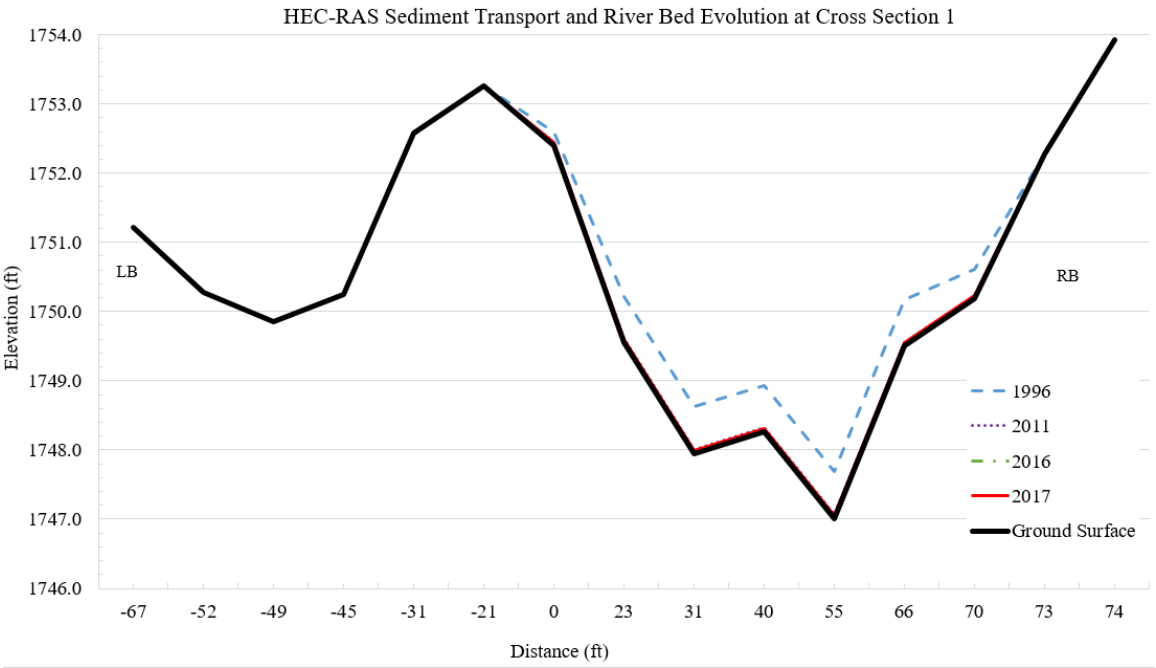

Figure 34. Bed evolution at cross section 1 for all water years modeled.

Overall the photogrammetry results and the HEC-RAS results are comparable for the four photogrammetry sites. The two methods together suggest that routing the augmented gravels downstream past Barrier Falls within a five-year time frame is unlikely to happen without receiving multiple 50 to 100-year flood events (e.g., flows exceeding 3,000 cfs). Because the augmented gravels did not fully reach photogrammetry Site 1 or cross section 14, it was not possible to investigate whether the sediment wave is translational or stationary. However, after comparing the results of the two methods it is clear, that if HEC-RAS is to be used to investigate wave propagation in parallel with photogrammetry, then the density of cross sections at each photogrammetry site should

be increased. This was most apparent with the Site 2 results, where the photogrammetry registered 0.5 ft more change than the HEC-RAS model. This difference could have been better understood if there were more than one measured cross section at the site.

HEC-RAS Considerations

This research shows that when designing a HEC-RAS sediment transport model, certain variables such as cross section density, transport function, and computation increment are highly sensitive input variables that can greatly impact the magnitude of erosion and deposition predictions. It is advised that multiple transport functions are studied and experimented with until one is found that doesn't result in model instabilities. The computation increment should be varied, with longer increments for low flows (i.e., stable), and shorter for high flows or rapidly changing flows.

The density of cross sections impacts how well the model calibrates to measured conditions. On long, straight sub-reaches where the hydraulics have small variances, the density of cross sections can be low (one cross section per 200-300 ft). On sub-reaches that have steep slope breaks, tight bends, or changes in bed material, the density of cross sections need to be increased (one cross section per 50-100 ft), to distribute the hydraulic changes. Overall, HEC-RAS operates best when there are gradual changes between cross sections. Because the density of measured cross sections was low for this thesis (mostly due to wading and access restrictions) the model relied on interpolated cross sections between measured cross sections to distribute hydraulic changes.

CONCLUSIONS AND RECOMMENDATIONS

The objectives of this thesis were to investigate sediment wave propagation, provide a timeline for full dispersal of the initial 250 tons of augmented gravels, explore the usefulness and accuracy associated with applying photogrammetry in a river setting, and provide an estimate of the volume of augmented gravels that may fill void space between particles on the existing, coarse bed.

As mentioned in the Results and Discussion section, studying the sediment wave propagation post-augmentation was not quantifiable because the gravel did not reach the first photogrammetry site or cross section within the lifetime of this MS thesis. However, the initial 250 tons transported downstream to the nearest pool, where it remained for the duration of this study. This indicates that there is indeed a significant storage capacity that must be filled before augmented gravels can route through the reach. There are also several other geomorphic features that represent potential storage sites (pools, coarse stream bed, and coarse gravel bars) that the gravel must route through before reaching Barrier Falls. The storage capacity estimate of 800 tons suggests that the initial 250 tons of gravel will be temporarily stored in void spaces.

The photogrammetry results and HEC-RAS modeling results show that very little geomorphic change is occurring throughout the reach with the magnitude of flows seen in 2017. The HEC-RAS results also suggest that partial mobility of the bed is achieved with a flow of approximately 1,200 cfs but full mobility is achieved at a flow somewhere between 1,200 cfs and 3,000 cfs. More model runs are needed to narrow this zone.

Therefore, an increase in peak flows over the next several winters is needed to route the material downstream past Barrier Falls before the end of the five-year time frame. Receiving multiple flood events such as the 3,900 cfs event in 1996 would greatly improve the likelihood of gravel routing past Barrier Falls by the end of year five. If the peak flows received in the next four years instead remain around the 1,200 cfs range such as in 2017, it is unlikely that the gravel will route past Barrier Falls by the end of year five.

Although I was not able to use photogrammetry during the thesis lifetime to study wave propagation, this thesis does demonstrate how photogrammetry can be used to create extremely high resolution DTMs. The photogrammetry effort resulted in DTMs that have resolution better than 0.1 ft and accuracy ranging from 0.45 ft to 0.05 ft, which demonstrates the capabilities of photogrammetry as a powerful tool to capture geomorphic change within a river setting. This is encouraging for future applications of photogrammetry in river settings, such as additional geomorphic change analysis, habitat mapping, storage capacity volume estimates, and studying sediment wave propagation. Photogrammetry provides the detailed analysis needed for a quantitative study at a cost affordable to most studies.

Using photogrammetry as a method to study geomorphic change in a river system does not come without challenges. Photogrammetry sites must be selected based on good conditions for photography. Underwater photography is highly limited by lighting conditions, and photographing through the water surface can introduce error into the model. Sometimes, even with an adequate geospatial distribution of GCPs, Agisoft

Photoscan has issues with photo alignment because of distortion. Using photogrammetry at such a close range limits the ability to use geotagged photographs because there is no significant difference in northing and easting between each photo (i.e., the same northing and easting is assigned to multiple photos). Photo alignment would be improved and processing time would decrease if the photographs could be geotagged. My overall recommendation for using photogrammetry in similar settings with similar equipment is to carefully choose sites based on optimal lighting conditions, use a high density of permanent and temporary GCPs, and achieve greater than 60% overlap between photographs.

My recommendations for future applications of these methods are to: 1) dedicate time at the beginning of the project for site visits to find ideal photogrammetry locations, 2) have an equal density of accuracy check points as GCPs, 4) if possible use geotagged photographs (this will decrease processing time, but is not possible if doing photogrammetry as close-range as this thesis) 3) if pairing photogrammetry and HEC-RAS, increase the density of cross sections for the HEC-RAS model through the photogrammetry sites (this will provide a more detailed comparison between the two methods, 4) when choosing locations for HEC-RAS cross sections capture entire geomorphic features; (i.e., capture the upstream end, middle, and downstream end of pools, riffles, and runs) this will better capture slope through the model and decrease the number of interpolated cross sections needed, 5) if possible extend the HEC-RAS modeling reach to capture all photogrammetry locations (provides a comparison and accuracy check between methods) .

This thesis used a necessary combination of software programs including Agisoft Photoscan, CloudCompare, ESRI ArcMap and ArcScene, AutoCAD, HEC-RAS, and Microsoft Excel. For the photogrammetry effort it was necessary to create the point clouds in Agisoft Photoscan and edit them in CloudCompare. Due to the rapid and recent development of photogrammetry technology, Agisoft Photoscan currently has only one competitor (Pix4D) that is also capable of generating point clouds from photographs. There are however, other cloud editing softwares available, including extensions in the ESRI suite, LAS Tools, and extensions in AutoCAD that could be used in place of CloudCompare. The advantage of using CloudCompare is that it has many tools for editing clouds, differencing clouds, and has an open online discussion forum.

Although ESRI ArcMap and ArcScene were used, they were used to create aesthetically pleasing finished results and were not actually used during cloud creation or analysis.

AutoCAD was extremely useful for both the photogrammetry effort and the HEC-RAS effort. AutoCAD was used to triangulate the true positions (northings and eastings) of GCPs and cross sections, which were otherwise unobtainable, and to measure downstream reach lengths needed for the HEC-RAS model. If available, an instrument such as a RTK could be used to collect GCP and cross section positions in place of AutoCAD.

Microsoft Excel was a critical data management component for the HEC-RAS model. Excel was used to organize cross section data, roughness values, northings and eastings, and pebble count data, that was later used as model inputs for the HEC-RAS

sediment transport model. Overall, HEC-RAS and CloudCompare are the most accessible (least expensive) of the software used in this study, and are open source programs available for download from the internet.

REFERENCES

Ackers, P., and White W. K. (1973). Sediment transport: New approach and analysis. *Journal of Hydrology*. Div., ASCE, Vol 95, No. HYll, 2041-2060.

Beechie, T. J., Sear, D. A., Olden, J. D., Pess, G. R., Buffington, J. M., Moir, H., & Pollock, M. M. (2010). Process-based principles for restoring river ecosystems. *BioScience,* Vol 60, No. 3, 209-222.

Bird S, Hogan D, Schwab J. (2010). Photogrammetric monitoring of small streams under a riparian forest canopy. *Earth Surface Processes and Landforms*, Vol 35, No. 8: 952–970.

Brodu, Nicolas. and Lague, Dimitri. (2012). Terrestrial lidar data classification of complex natural scenes using a multi-scale dimensionality criteria: applications in geomorphology. *Journal of Photogrammetry and Remote Sensing*, Vol 68: 121-134.

Brooks, H. C. (1963). Quicksilver in Oregon (No. 55). State of Oregon, Department of Geology and Mineral Industries.

Brunner, G. W. (2001). HEC-RAS river analysis system: User's manual. US Army Corps of Engineers, Institute for Water Resources, Hydrologic Engineering Center.

Buffington, J.M. and Montgomery, D.R. (1999). A procedure for classifying textural facies in gravel-bed rivers. *Water Resources Research*, Vol 3, No. 6: 1903-1914.

Butler, Justin., Lane, Stuart., Chandler, Jim. and Porfiri, Ekaterini. (2002). Through-water close range digital photogrammetry in flume and field environments. *The Photogrammetric Record*, Vol 17, No. 99: 419-439.

CALFED, Science Program and Ecosystem Restoration Program, Gravel Augmentation Panel. (2005). Key uncertainties in gravel augmentation: geomorphological and biological research needs for effective river restoration.

Chandler J, Ashmore P, Paola C, Gooch M, Varkaris F. (2002). Monitoring river-channel change using terrestrial oblique digital imagery and automated digital photogrammetry. *Annals of the Association of American Geographers*, Vol 92 No. 4: 631–644.

Chandler, Jim. (1999). TECHNICAL COMMUNICATIONS-Effective Application of Automated Digital Photogrammetry for Geomorphological Research. *Earth Surface Processes and Landforms*, Vol. 24 No. 1: 51-64.

Cui, Y., Parker, G., Lisle, T.E., Pizzuto, J.E. and Dodd, A.M. (2005). More on the evolution of bed material waves in alluvial rivers. *Earth surface processes and landforms*, Vol 30, No. 1:107-114.

Daniels, M.D. and McCusker, M.H. (2010). Operator bias characterizing stream substrates using Wolman pebble counts with a standard measurement template. *Geomorphology*, Vol 115 No. 1: 194-198.

Dietrich, J.T. (2016). Riverscape mapping with helicopter-based Structure-from-Motion photogrammetry. *Geomorphology*, Vol 252: 144-157.

Duda, J.J., Freilich, J.E. and Schreiner, E.G. (2008). Baseline studies in the Elwha River ecosystem prior to dam removal: introduction to the special issue.

Fonstad, M.A., Dietrich, J.T., Courville, B.C., Jensen, J.L. and Carbonneau, P.E. (2013). Topographic structure from motion: a new development in photogrammetric measurement. *Earth Surface Processes and Landforms*, Vol 38, No. 4: 421-430.

Gaeuman, D. (2014). High-flow gravel injection for constructing designed in-channel features. *River Research and Applications*, Vol 30 No. 6: 685-706.

Giménez, R., Marzolff, I., Campo, M.A., Seeger, M., Ries, J.B., Casalí, J. and Alvarez-Mozos, J. (2009). Accuracy of high-resolution photogrammetric measurements of gullies with contrasting morphology. *Earth Surface Processes and Landforms*, Vol 34, No. 14: 1915-1926.

Girardeau-Montaut, Daniel. (2015). Cloud-to-Cloud Distance. CloudCompare Documentation page for V2.6 and higher. Retrieved from CloudCompare Novemeber, 2016. http://cloudcompare.org

Graf, W. L. (1999). Dam nation: A geographic census of American dams and their large scale hydrologic impacts. *Water resources research*, Vol 35, No. 4: 1305-1311.

Grant, G. E. (1997). River Quality: Dynamics and Restoration: Chapter 7. A Geomorphic Basis for Interpreting the Hydrologic Behavior of Large River Basins. 105-117.

Hammond, P. E., Anderson, J. L., & Manning, K. J. (1980). Guide to the geology of the upper Clackamas and North Santiam Rivers area, northern Oregon Cascade Range. Geologic field trips in western Oregon and southwestern Washington: *Oregon Department of Geology and Mineral Industries Bulletin*, 101: 133-167.

Hart, D. D., Johnson, T. E., Bushaw-Newton, K. L., Horwitz, R. J., Bednarek, A. T., Charles, D. F., & Velinsky, D. J. (2002). Dam removal: challenges and opportunities for ecological research and river restoration. *BioScience*, Vol 52, No. 8: 669-682.

Javernick, L., Brasington, J. and Caruso, B. (2014). Modeling the topography of shallow braided rivers using Structure-from-Motion photogrammetry. *Geomorphology*, Vol 213: 166-182.

Kondolf, G. M., Gao, Y., Annandale, G. W., Morris, G. L., Jiang, E., Zhang, J., ... & Hotchkiss, R. (2014). Sustainable sediment management in reservoirs and regulated rivers: Experiences from five continents. *Earth's Future*, Vol 2, No. 5: 256-280.

Kondolf, G. M., Lisle, T. E. (2016a). Tools in fluvial geomorphology: Chapter 13. Measuring bed sediment. John Wiley & Sons, 283-293.

Kondolf, G. M., Piegay, H. (2016b). Tools in fluvial geomorphology: Chapter 5. System approaches in fluvial geomorphology. John Wiley & Sons, 79-83.

Kondolf, G.M., Lisle, T.E. and Wolman, G.M. (2003). Bed sediment measurement. Tools in fluvial geomorphology, pg: 347-395.

Lackey, R. T. (2003). Pacific Northwest salmon: forecasting their status in 2100. *Reviews in fisheries Science*, Vol 11, No. 1: 35-88.

Lague, Dimitri., et al. (2013). Accurate 3D comparison of complex topography with terrestrial laser scanner: Application to the Rangitikei canyon (NZ). ISPRS *Journal of Photogrammetry and Remote Sensing* 82: 10-26.

Leopold, L. B., Wolman, M. G., & Miller, J. P. (1964). Fluvial Processes in Geomorphology: Chapter 6. *Water and sediment in channels*. Dover Publications. 151-188.

Ligon, F.K., Dietrich, W.E. and Trush, W.J. (1995). Downstream ecological effects of dams. *BioScience*, Vol 45, No. 3: pp.183-192.

Lisle, T. E., Church, M. (2002). Sediment transport-storage relations for degrading gravel-bed channels, *Water Resources Research*, Vol 38, No. 11. doi:1210.1029/2001WR001086.

Lisle, T.E., Cui, Y., Parker, G., Pizzuto, J.E. and Dodd, A.M. (2001). The dominance of dispersion in the evolution of bed material waves in gravel‐bed rivers. *Earth Surface Processes and Landforms*, Vol 26, No. 13: 1409-1420.

Lisle, Thomas E. (1997). Understanding the role of sediment waves and channel conditions over time and space. *What is Watershed Stability*: 23-25.

Magilligan, F. J., & Nislow, K. H. (2005). Changes in hydraulic regimes by dams. *Geomorphology*, Vol 71, No. 1: 61-78.

Matthews, N. A. (2008). Aerial and close-range photogrammetric technology: providing resource documentation, interpretation, and preservation. Technical Note 428. U.S. Department of the Interior, Bureau of Land Management, National Operations Center, Denver, Colorado: 1-42.

McBain & Trush Inc. (2002). Sediment Yield Analysis for the Oak Grove Fork and Upper Mainstem Clackamas River above North Fork Reservoir. Clackamas River

Project (FERC: 135/2195). Prepared for the Clackamas River Hydroelectric Project Relicensing Fish and Aquatics Workgroup.

McBain & Trush Inc. (2004). Synthesis of Geomorphic, Vegetation, and Instream Flow Studies, Oak Grove Fork Project, Oak Grove Fork and Clackamas River Upstream from North Fork Reservoir. Prepared for Portland General Electric.

McBain & Trush Inc. (2002). Sediment Yield Analysis for the OGF and Upper Mainstem Clackamas River Above North Fork Reservoir. Prepared for Clackamas River Hydroelectric Project Relicensing Fish and Aquatics Workgroup.

McBain Associates, Portland General Electric Company. (2013). Mainstem Fish Habitat Enhancement Plan for the Oak Grove Fork of the Clackamas River. Clackamas River Project (FERC: 2195).

McCluney, K.E., Poff, N.L., Palmer, M.A., Thorp, J.H., Poole, G.C., Williams, B.S., Williams, M.R. and Baron, J.S. (2014). Riverine macrosystems ecology: sensitivity, resistance, and resilience of whole river basins with human alterations. *Frontiers in Ecology and the Environment*, Vol 12, No. 1: 48-58.

McCormick, S.D., Lerner, D.T., Monette, M.Y., Nieves-Puigdoller, K., Kelly, J.T. and Björnsson, B.T. (2009). Taking it with you when you go: how perturbations to the freshwater environment, including temperature, dams, and contaminants, affect marine survival of salmon. *In American Fisheries Society*, Vol 69: 195-214.

Nelson, J. M., McDonald, R. R., Shimizu, Y., Kimura, I., Nabi, M., & Asahi, K. (2016). Tools in fluvial geomorphology: Chapter 18. Modelling flow, sediment transport and morphodynamics in rivers. John Wiley & Sons, 422-426.

Ock, Giyoung., Gaeuman, David., Mcsloy, Jeanne., Kondolf, Mathias. (2015). Ecological functions of restored gravel bars, the Trinity River, California. *Ecological Engineering*, Vol 83.

Oregon Geospatial Data Clearinghouse. (2017). Oregon Spatial Data Library. Website partners are State of Oregon, Oregon State University, Oregon Explorer, and Institute for Natural Resources. http://spatialdata.oregonexplorer.info/geoportal/

Parker, Chris., Clifford, Nicholas J., Thorne, Colin R. (2011). Understanding the influence of slope on the threshold of coarse grain motion: Revisiting critical stream power. *Geomorphology*, Vol 126.

Peck, D. L., Griggs, A. B., Schlicker, H. G., Wells, F. G., & Dole, H. M. (1964). Geology of the central and northern parts of the western Cascade Range in Oregon (No. 449). *U.S. Geological Survey*. Government Printing Office.

Pess, G.R., McHenry, M.L., Beechie, T.J. and Davies, J. (2008). Biological impacts of the Elwha River dams and potential salmonid responses to dam removal.

Petit, Francois., Houbrechts, Geoffrey., Peeters, Alexandre., Hallot, Eric., Campenhout, Jean., Denis, Anne-Cecile. (2015). Dimensionless critical shear stress in gravel-bed rivers. *Geomorphology*, Vol 250.

Poff, N. L., & Hart, D. D. (2002). How dams vary and why it matters for the emerging science of dam removal. *BioScience*, Vol 52, No. 8: 659-668.

Portland General Electric. (1999). Initial Information Package for the Clackamas River Hydroelectric Project and Oak Grove Project-FERC No. 135 and North Fork Project-FERC No. 2195.

Portland General Electric. (2016). Fish Counts and Fish Runs: Clackamas Fish Runs. Webpage. https://www.portlandgeneral.com/corporate-responsibility/environmental-stewardship/water-quality-habitat-protection/fish-counts-fish-runs/clackamas-fish-runs.

Potyondy, J.P. and Hardy, T. (1994). Use of pebble counts to evaluate fine sediment increase in stream channels. JAWRA *Journal of the American Water Resources Association*, Vol 30, No. 3: 509-520.

Sherrod, D. R., & Scott, W. E. (1995). Preliminary geologic map of the Mount Hood 30-by 60-minute Quadrangle, [northern] Cascade Range, Oregon. *U.S. Geological Survey*.

Sims, A.J. and Rutherfurd, I.D. (2017). Management responses to pulses of bedload sediment in rivers. *Geomorphology*.

Sklar, L.S., Fadde, J., Venditti, J.G., Nelson, P., Wydzga, M.A., Cui, Y. and Dietrich, W.E. (2009). Translation and dispersion of sediment pulses in flume experiments simulating gravel augmentation below dams. *Water resources research*, Vol 45, No. 8.

Sloan, Jeff. and Joe. Adams. (2016). USGS Unmanned Aircraft Systems Data Post-Processing: Section 2- MicaSense 5-band Multispectral Imagery. UAS Mission Planning and Data Processing, U.S. Fish and Wildlife Service and National Park Service Geospatial Training Workshop, Shepherdstown, West Virginia.

Taylor, B. (1999). Salmon and steelhead runs and related events of the Clackamas River basin–a historical perspective. Prepared for Portland General Electric Company, Portland, Oregon.

U.S. Forest Service, Pacific Northwest Region. (1996). Oak Grove Watershed Analysis. Prepared for the U.S. Department of Agriculture, Washington DC.

Venditti, J.G., Dietrich, W.E., Nelson, P.A., Wydzga, M.A., Fadde, J. and Sklar, L., (2010). Mobilization of coarse surface layers in gravel ‐ bedded rivers by finer gravel bed load. *Water Resources Research*, Vol 46, No. 7.

Ward, J.V. and Stanford, J.A. (1995). Ecological connectivity in alluvial river ecosystems and its disruption by flow regulation. *River Research and Applications*, Vol 11, No. 1: 105-119.

Watershed Network Professionals. (2005). Clackamas Basin summary watershed overview. Prepared for Clackamas River Basin Council, Clackamas, Oregon.

Westaway, R.M., Lane, S.N. and Hicks, D.M. (2000). The development of an automated correction procedure for digital photogrammetry for the study of wide, shallow, gravel-bed rivers. *Earth Surface Processes and Landforms*, Vol 25, No. 2: 209-226.

Westaway, R.M., Lane, S.N. and Hicks, D.M. (2003). Remote survey of large-scale braided, gravel-bed rivers using digital photogrammetry and image analysis. *International Journal of Remote Sensing*, Vol 24, No. 4: 795-815.

Westoby, M. J., Brasington, J., Glasser, N. F., Hambrey, M. J., & Reynolds, J. M. (2012). 'Structure-from-Motion'photogrammetry: A low-cost, effective tool for geoscience applications. *Geomorphology*, Vol 179: 300-314.

Wheaton JM, Brasington J, Darby SE, Sear DA. (2010). Accounting for uncertainty in DEMs from repeat topographic surveys: improved sediment budgets. *Earth Surface Processes and* Landforms, Vol 35, No. 2: 136–156.

Wilcock, P.R. and Crowe, J.C. (2003). Surface-based transport model for mixed-size sediment. *Journal of Hydraulic Engineering*, Vol 129, No. 2: 120-128.

Yager, E. M., J. W. Kirchner, and W. E. Dietrich (2007a), Calculating bed load transport in steep boulder bed channels. *Water Resources Research*, Vol 43, doi:10.1029/2006WR005432.

Yager, E. M., W. E. Dietrich, J. W. Kirchner, and B. W. McArdell (2007b), Patch dynamics and stability in steep, rough streams. *Journal of Geophysical Research: Earth Surface*, Vol 117, No. F2, 2156-2202.

Yager, E. M., W. E. Dietrich, J. W. Kirchner, and B. W. McArdell (2012). Prediction of sediment transport in step-pool channels. *Water Resources Research*, Vol 48, No. 1, 10.1029/2011WR010829.

Zeug, S.C., Sellheim, K., Watry, C., Rook, B., Zimmerman, J., Hannon, J., Cox, D., Merz, J. (2013). Gravel augmentation increases spawning utilization by anadromous salmonids: A case study from California, USA. *River Research Applications*, Vol 30.

APPENDIX A

Cross Section Data Collection:					
XS 234+54	Streamflow = 100 cfs	7/25/2016			
Station	Foresight	Backsight	Notes	Height of Instrument	Elevation
(ft)	(ft)	(ft)		(ft a.s.l.)	(ft a.s.l.)
		1.48	BS	1745.99	1744.51
0.0	3.86		Top LBP	1745.99	1742.13
0.0	4.31		Base LBP	1745.99	1741.68
7.7	5.70		LEW	1745.99	1740.29
19.0	8.46		Thalweg	1745.99	1737.53
29.0	7.14			1745.99	1738.85
51.0	5.38		REW	1745.99	1740.61
57.5	3.52			1745.99	1742.47
65.0	3.18		Base RBP	1745.99	1742.81
65.0	2.63		Top RBP	1745.99	1743.36
74.0	4.97		Behind pin	1745.99	1741.02
80.0	3.90			1745.99	1742.09
88.0	2.22			1745.99	1743.77

Cross Section Data Collection:					
XS 239+03	Streamflow = 100 cfs	7/25/2016			
Station	Foresight	Backsight	Notes	Height of Instrument	Elevation
(ft)	(ft)	(ft)		(ft) a.s.l.	(ft) a.s.l.
		4.50	BS	1756.66	1752.16
-67.0	5.44			1756.65	1751.21
-52.0	6.39		LEW	1756.65	1750.26
-48.6	6.80		Thalweg	1756.65	1749.85
-44.6	6.41		REW	1756.65	1750.24
-31.0	4.09			1756.65	1752.56
-21.0	3.40		Terrace	1756.65	1753.25
0.0	3.33		LBP Top	1756.65	1753.32
0.0	4.27		LBP Base	1756.65	1752.38
23.30	7.11		LEW	1756.65	1749.54
31.3	8.71			1756.65	1747.94
40.0	8.40			1756.65	1748.25
55.0	9.65		Thalweg	1756.65	1747.00
66.0	7.16		REW	1756.65	1749.49
70.0	6.48			1756.65	1750.17
73.4	4.38		RBP Base	1756.65	1752.27
73.4	4.10		RBP Top	1756.65	1752.55
74.4	2.73			1756.65	1753.92

Cross Section Data Collection:					
XS 239+81	Streamflow = 100 cfs	7/25/2016			
Station	Foresight	Backsight	Notes	Height of Instrument	Elevation
(ft)	(ft)	(ft)		(ft) a.s.l.	(ft) a.s.l.
		5.71	BS		
-3.0	1.81			1757.86	1756.05
3.0	5.98			1757.86	1751.88
10.0	7.16			1757.86	1750.70
16.0	7.31		LEW	1757.86	1750.55
23.5	6.98		REW	1757.86	1750.88
34.0	2.88			1757.86	1754.98
47.0	3.48			1757.86	1754.38
70.0	6.08		Terrace	1757.86	1751.78
77.5	7.99		LEW	1757.86	1749.87
89.0	7.54		Thalweg	1757.86	1750.32
107.5	6.24		REW	1757.86	1751.62
118.0	3.15		Base of Cliff	1757.86	1754.71

Cross Section Data Collection:					
XS 244+38	Streamflow = 100 cfs	7/25/2016			
Station	Foresight	Backsight	Notes	Height of Instrument	Elevation
(ft)	(ft)	(ft)		(ft) a.s.l.	(ft) a.s.l.
		0.86	BS	1765.45	1764.59
21.0	1.70			1765.45	1763.75
12.0	-2.70		Top of Terrace	1765.45	1768.15
26.5	2.77			1765.45	1762.68
30.0	7.06			1765.45	1758.39
30.0	6.25		WSE	1765.45	1759.20
40.0	6.00		WSE	1765.45	1759.45
66.0	6.70			1765.45	1758.75
77.0	8.05		Thalweg	1765.45	1757.40
89.2	5.49		REW	1765.45	1759.96
100.0	0.37		Hillside	1765.45	1765.08

Cross Section Data Collection:					
XS 245+25	Streamflow = 100 cfs	7/25/2016			
Station	Foresight	Backsight	Notes	Height of Instrument	Elevation
(ft)	(ft)	(ft)		(ft) a.s.l.	(ft) a.s.l.
0.0		4.86	BS	1769.45	1764.59
-41.0	0.83		Terrace	1769.452	1768.622
-26.0	6.00		Top SC	1769.452	1763.452
-20.6	8.98			1769.452	1760.472
-12.5	8.84		Other EW	1769.452	1760.612
-7.0	6.73			1769.452	1762.722
0.0	5.41		Base LBP	1769.452	1764.042
8.0	6.98			1769.452	1762.472
13.7	8.51		LEW	1769.452	1760.942
27.0	10.29			1769.452	1759.162
41.0	11.69		Thalweg	1769.452	1757.762
51.2	8.56		REW	1769.452	1760.892
53.1	6.70		RBP	1769.452	1762.752
63.1	2.90		Base of cliff	1769.452	1766.552

Cross Section Data Collection:					
XS 246+42	Streamflow = 100 cfs	7/25/2016			
Station	Foresight	Backsight	Notes	Height of Instrument	Elevation
(ft)	(ft)	(ft)		(ft) a.s.l.	(ft) a.s.l.
		5.99	BS	1770.58	1764.59
-3.0	0.09			1770.582	1770.492
2.0	3.10			1770.582	1767.482
13.0	4.94			1770.582	1765.642
48.0	5.59			1770.582	1764.992
52.9	6.99		LEW	1770.582	1763.592
70.0	8.49			1770.582	1762.092
87.0	9.05		Thalweg	1770.582	1761.532
100.2	7.06		REW	1770.582	1763.522
107.0	3.06		RB	1770.582	1767.522

Cross Section Data Collection:					
XS 250+60	Streamflow = 100 cfs	7/26/2016			
Station	Foresight	Backsight	Notes	Height of Instrument	Elevation
(ft)	(ft)	(ft)		(ft) a.s.l.	(ft) a.s.l.
		3.94	BS	1775.70	1771.76
58.4	4.22		Top RBP	1775.70	1771.48
58.4	5.04		Base RBP	1775.70	1770.66
60.4	2.70			1775.70	1773.00
73.0	1.49			1775.70	1774.21
54.5	7.89		REW	1775.70	1767.81
51.3	8.15			1775.70	1767.55
46.0	9.62		Thalweg	1775.70	1766.08
39.0	9.75			1775.70	1765.95
32.0	9.22			1775.70	1766.48
22.0	8.89			1775.70	1766.81
18.0	7.75		Start boulders	1775.70	1767.95
14.4	7.72		WSE	1775.70	1767.98
7.5	4.09		Top boulders	1775.70	1771.61
3.3	3.66			1775.70	1772.04
0.0	2.86		Base LBP	1775.70	1772.84
0.0	2.50		Top LBP	1775.70	1773.20
-4.0	0.67		Behind LBP	1775.70	1775.03

Cross Section Data Collection:					
XS 251+44	Streamflow = 100 cfs	7/26/2016			
Station	Foresight	Backsight	Notes	Height of Instrument	Elevation
(ft)	(ft)	(ft)		(ft) a.s.l.	(ft) a.s.l.
		3.94	BS	1775.70	1771.76
LBP	2.19		Top of LBP	1775.70	1773.51
LBP	2.58		Base of LBP	1775.70	1773.12
BS		8.44	Moved level	1781.95	1773.51
0.0	8.85		Base of LBP	1781.95	1773.10
-5.4	7.77		LB	1781.95	1774.18
-5.8	6.05			1781.95	1775.9
-14.0	4.09			1781.95	1777.86
-27.0	2.12			1781.95	1779.83
6.0	9.76			1781.95	1772.19
12.0	7.66		Top boulders	1781.95	1774.29
16.8	12.52		LEW	1781.95	1769.43
21.0	14.05			1781.95	1767.90
28.0	13.89		boulders	1781.95	1768.06
29.3	12.20		On boulders	1781.95	1769.75
31.4	14.37			1781.95	1767.58
39.0	13.52			1781.95	1768.43
46.0	13.11			1781.95	1768.84
52.0	14.12			1781.95	1767.83
57.5	13.95		Thalweg	1781.95	1768.00
67.3	12.59		REW	1781.95	1769.36
69.0	9.88			1781.95	1772.07
72.9	8.83		RBP base	1781.95	1773.12
72.9	7.95		RBP top	1781.95	1774.00
87.0	6.04		RB	1781.95	1775.91
98.0	5.83			1781.95	1776.12

Cross Section Data Collection:					
XS 259+20	Streamflow = 100 cfs	7/26/2016			
Station	Foresight	Backsight	Notes	Height of Instrument	Elevation
(ft)	(ft)	(ft)		(ft) a.s.l.	(ft) a.s.l.
0.0		8.36	BS	1795.88	1787.52
0.0	8.83		Base LBP	1795.88	1787.05
-13.0	7.71		LB	1795.88	1788.17
9.8	9.51		LEW	1795.88	1786.37
12.3	10.40			1795.88	1785.48
26.2	11.54		Thalweg	1795.88	1784.34
38.8	10.81			1795.88	1785.07
54.0	9.75		REW	1795.88	1786.13
61.5	9.18			1795.88	1786.70
75.9	8.10		Base RBP	1795.88	1787.78
75.9	7.85		Top RBP	1795.88	1788.03
84.9	6.15		RB	1795.88	1789.73
No Stn	8.28		PPT RP	1795.88	1787.60

Cross Section Data Collection:					
XS 260+52	Streamflow = 100 cfs	7/26/2016			
Station	Foresight	Backsight	Notes	Height of Instrument	Elevation
(ft)	(ft)	(ft)		(ft) a.s.l.	(ft) a.s.l.
		5.93	BS	1793.45	1787.52
62.0	3.39		Base of cedar	1793.45	1790.06
45.9	6.84		REW	1793.45	1786.61
36.0	8.01			1793.45	1785.44
29.0	8.62			1793.45	1784.83
20.0	8.63			1793.45	1784.82
10.1	6.79		LEW	1793.45	1786.66
2.0	2.90			1793.45	1790.55
-9.0	1.95			1793.45	1791.50
-20.0	4.01			1793.45	1789.44
-39.0	7.10			1793.45	1786.35
3.5	3.50		H W Mark	1793.45	1789.95

Cross Section Data Collection:					
XS 261+95	Streamflow = 100 cfs	7/26/2016			
Station	Foresight	Backsight	Notes	Height of Instrument	Elevation
(ft)	(ft)	(ft)		(ft) a.s.l.	(ft) a.s.l.
		4.36	BS	1796.66	1792.30
0.0	4.81		Top LBP	1796.65	1791.84
0.0	4.64		Ground LBP	1796.65	1792.01
-13.0	5.20			1796.65	1791.45
-17.0	5.34		Base hillslope	1796.65	1791.31
-25.0	1.13			1796.65	1795.52
5.0	4.73		hillslope seep	1796.65	1791.92
7.0	5.54			1796.65	1791.11
12.4	6.16			1796.65	1790.49
20.2	7.37		LEW	1796.65	1789.28
26.0	8.00			1796.65	1788.65
31.0	8.25			1796.65	1788.40
38.0	8.53			1796.65	1788.12
43.0	9.20			1796.65	1787.45
47.0	9.55			1796.65	1787.10
54.0	8.63			1796.65	1788.02
59.0	7.24		REW	1796.65	1789.41
69.0	5.58			1796.65	1791.07
74.0	5.00			1796.65	1791.65
82.3	3.22		Top RBP	1796.65	1793.43
82.3	3.52		Base RBP	1796.65	1793.13
88.0	2.15		RB	1796.65	1794.50
	3.73		Top RBP of XS 261+75	1796.65	1792.92
	4.06		Base RBP XS 261+75	1796.65	1792.59

Cross Section Data Collection:					
XS 266+15	Streamflow = 100 cfs	7/26/2016			
Station	Foresight	Backsight	Notes	Height of Instrument	Elevation
(ft)	(ft)	(ft)		(ft) a.s.l.	(ft) a.s.l.
		4.19	BS=PPT	1803.68	1799.49
119.1	2.33		RB behind XS	1803.67	1801.34
99.1	5.07		Top RBP	1803.67	1798.60
99.1	6.14		Base RBP	1803.67	1797.53
97.5	7.20		side channel	1803.67	1796.47
90.3	5.97			1803.67	1797.70
87.5	6.53		side channel	1803.67	1797.14
84.0	5.22		Top of levee	1803.67	1798.45
68.0	4.82			1803.67	1798.85
61.8	7.34		REW	1803.67	1796.33
58.0	8.35			1803.67	1795.32
54.0	8.74			1803.67	1794.93
44.0	8.93			1803.67	1794.74
41.0	9.49			1803.67	1794.18
37.0	8.39			1803.67	1795.28
31.5	9.87		Thalweg	1803.67	1793.80
27.0	9.21		LEW	1803.67	1794.46
16.0	7.38			1803.67	1796.29
0.0	5.62		LBP Top	1803.67	1798.05
0.0	5.97		LBP Base	1803.67	1797.70

Cross Section Data Collection:					
XS 271+15	Streamflow = 100 cfs	7/26/2016			
Station	Foresight	Backsight	Notes	Height of Instrument	Elevation
(ft)	(ft)	(ft)		(ft) a.s.l.	(ft) a.s.l.
		3.27	BS	1809.73	1806.46
0.0	3.84		Top LBP	1809.72	1805.88
0.0	4.40		Base LBP	1809.72	1805.32
13.5	4.88		LEW	1809.72	1804.84
23.2	5.47			1809.72	1804.25
29.3	4.74		Top boulders	1809.72	1804.98
33.4	5.24			1809.72	1804.48
41.0	6.61			1809.72	1803.11
49.0	6.83			1809.72	1802.89
58.5	7.06		Thalweg	1809.72	1802.66
62.5	6.20			1809.72	1803.52
69.0	6.02			1809.72	1803.70
79.6	5.20		REW	1809.72	1804.52
82.0	4.45		boulders	1809.72	1805.27
84.0	2.92		Top RBP	1809.72	1806.80
84.0	3.33		Base RBP	1809.72	1806.39

Cross Section Data Collection:					
Approx. XS 278+63	Streamflow = 100 cfs	7/26/2016			
Station	Foresight	Backsight	Notes	Height of Instrument	Elevation
(ft)	(ft)	(ft)		(ft) a.s.l.	(ft) a.s.l.
		4.76	BS	1815.49	1810.73
0.0	5.16		Top LBP	1815.49	1810.33
0.0	5.90		Base LBP	1815.49	1809.59
-5.0	2.78		LB	1815.49	1812.71
-13.0	1.15			1815.49	1814.34
2.5	5.91		LEW	1815.49	1809.58
9.5	6.54			1815.49	1808.95
14.5	7.27		End boulders	1815.49	1808.22
19.0	7.78			1815.49	1807.71
23.0	7.28			1815.49	1808.21
27.0	7.78			1815.49	1807.71
28.5	8.14			1815.49	1807.35
33.0	7.46			1815.49	1808.03
39.0	7.01			1815.49	1808.48
45.0	6.62			1815.49	1808.87
48.8	6.11		REW	1815.49	1809.38
54.0	6.16			1815.49	1809.33
55.5	4.98			1815.49	1810.51
61.3	4.43		Base RBP	1815.49	1811.06
61.3	4.06		Top RBP	1815.49	1811.43
67.3	2.08			1815.49	1813.41

APPENDIX B

Initial GCP Setup Survey					
Photogrammetry Site 1	7/28/2016	Streamflow = 100 cfs			
Station	Foresight	Backsight	Notes	Height of Instrument	Elevation
(ft)	(ft)	(ft)		(ft) a.s.l.	(ft) a.s.l.
P-mag nail		5.29	B.S.	1816.02	1810.73
GCP 1	7.01			1816.023	1809.013
2.0	7.35			1816.023	1808.673
A	5.73			1816.023	1810.293
B	6.09			1816.023	1809.933
C	5.85			1816.023	1810.173
3.0	7.75			1816.023	1808.273
4.0	7.15			1816.023	1808.873
5.0	7.44			1816.023	1808.583
6.0	5.57			1816.023	1810.453
7.0	5.87			1816.023	1810.153

Initial GCP Setup Survey					
Photogrammetry Site 2	7/28/2016	Streamflow = 100 cfs			
Station	Foresight	Backsight	Notes	Height of Instrument	Elevation
(ft)	(ft)	(ft)		(ft) a.s.l.	(ft) a.s.l.
RP 266+15		3.30	BS	1799.98	1796.68
GCP 5	2.61			1799.976	1797.366
6.0	3.83			1799.976	1796.146
4.0	2.90			1799.976	1797.076
7.0	3.84			1799.976	1796.136
3.0	3.42			1799.976	1796.556
8.0	4.01			1799.976	1795.966
2.0	4.13			1799.976	1795.846
9.0	4.10			1799.976	1795.876
10=X	4.16			1799.976	1795.816
1.0	4.03			1799.976	1795.946
XI=11	4.61			1799.976	1795.366
XII=12	5.92			1799.976	1794.056

Initial GCP Setup Survey					
Photogrammetry Site 3	7/27/2016	Streamflow = 100 cfs			
Station	Foresight	Backsight	Notes	Height of Instrument	Elevation
(ft)	(ft)	(ft)		(ft) a.s.l.	(ft) a.s.l.
LBP		5.56	BS	1793.08	1787.52
LBP	6.03		LBP	1793.08	1787.052
PPT RP	5.61		PPT RP 259+20	1793.08	1787.472
T.S.pin	6.13		T.S pin	1793.08	1786.952
GCP1	5.71			1793.08	1787.372
2.0	6.50			1793.08	1786.582
3.0	7.08			1793.08	1786.002
4.0	5.89			1793.08	1787.192
5.0	6.52			1793.08	1786.562
6.0	7.14			1793.08	1785.942
7.0	5.91			1793.08	1787.172
X=10	5.83			1793.08	1787.252
XI=11	6.52			1793.08	1786.562
LBP		3.98	Moved level.	1791.50	1787.52
LBP	4.45		Base	1791.50	1787.05
GCP8	4.49			1791.50	1787.01
9.0	5.55			1791.50	1785.95

Initial GCP Setup Survey					
Photogrammetry Site 4	7/27/2016	Streamflow = 100 cfs			
Station	Foresight	Backsight	Notes	Height of Instrument	Elevation
(ft)	(ft)	(ft)		(ft) a.s.l.	(ft) a.s.l.
T.S pin		6.48	BS	1718.06	1711.58
PPT LB	2.28			1718.057	1715.777
GCP6	3.57			1718.057	1714.487
5.0	3.43			1718.057	1714.627
1.0	3.97			1718.057	1714.087
2.0	4.10			1718.057	1713.957
A	4.07			1718.057	1713.987
3.0	4.06			1718.057	1713.997
B	3.52			1718.057	1714.537
4.0	3.99			1718.057	1714.067
PPT RP	4.21			1718.057	1713.847

APPENDIX C

Camera Specifications	
Name	Olympus Stylus TG-4 Tough
Number of effective pixels on camera	16 million dots
Image sensor	1/2.3-inch CMOS sensor
Lens construction	7 groups, 9 elements
Focal Length (35 mm equivalent)	4.5 to 18.0 mm (25 to 100 mm)
Maximum aperture	W2.0 to T4.9
Magnification	Optical zoom: 4x super resolution, 8x digital zoom
Recording format	JPEG, Raw, DPOF compatible, Exif 2.3, PRINT Image Matching III
Number of recorded pixels (at 4.3)	16M, 8M, 3M, VGA
Aspect ratio	4:3, 3:2, 16:9, 1:1
Movie recording	High-speed moving, Time lapse
Number of recorded pixels	1080 P
Internal memory	55 MB
Supported memory	SD/SDHC/SDXS cards
Shooting modes	Scene modes, underwater modes, microscope modes, picture mode
Shutter speed	1/2 to 1/2000 sec.
Self-timer	Yes
Flash	Yes
Waterproof	Yes
Dustproof	Yes
Supported smartphone apps	Wi-Fi connection to Olympus Image Share
Power supply	AC adapter and battery
Size	111.5 mm x 65.9 mm x 31.2 mm
Weight	247 g

APPENDIX D

Computer	Dell Precision
Operating System	Windows 10
Amount of Ready Access Memory (RAM)	64 GB
Number of Core Processing Units (CPUs)	6 units
Number of Graphic Cards or Graphic Processing Units (GPUs)	2 units
Photogrammetry Software	
Point Cloud Generation Software	Agisoft Photoscan Professional
Version	1.3.3 Windows 64-bit
Point Cloud Editing Software	Cloud Compare
Version	2.8.1 (Hogfather) Windows 64-bit
Digital Terrain Model Generation Software	ESRI ArcMap and ArcScene
Version	10.1
Additional Software Name	AutoCAD
Version	AutoCAD 2017
Additional Software Name	Microsoft Excel
Version	Excel 2016
Sediment Transport Model Software	
Name	HEC-RAS
Version	HEC-RAS 5.0.3